FLORIDA INTERNATIONAL UNIVERSITY

Miami, Florida

# SELF-INTERFERENCE CANCELLATION (SIC) FOR SIMULTANEOUS TRANSMIT AND RECEIVE

A dissertation submitted in partial fulfillment of the

requirements for the degree of

DOCTOR OF PHILOSOPHY

in

ELECTRICAL AND COMPUTER ENGINEERING

by

Md Nurul Anwar Tarek

2023

To: Dean John L. Volakis
College of Engineering and Computing

This dissertation, written by Md Nurul Anwar Tarek , and entitled Self-Interference Cancellation (SIC) for Simultaneous Transmit and Receive, having been approved in respect to style and intellectual content, is referred to you for judgment.

We have read this dissertation and recommend that it be approved.

Jean H. Andrian

Shubhendu Bhardwaj

Stephen Secules

Elias Alwan, Major Professor

Date of Defense: June 12, 2023

The dissertation of Md Nurul Anwar Tarek is approved.

Dean John L. Volakis
College of Engineering and Computing

Andrés G. Gil
Vice President for Research and Economic Development
and Dean of the University Graduate School

Florida International University, 2023

DEDICATION

To my parents and all my respected teachers.

ACKNOWLEDGMENTS

I want to express my gratitude to my advisor, Dr. Elias Alwan, for providing me with the incredible opportunity to work under his guidance and supervision. I am truly thankful for his support and mentorship throughout my journey. I am also thankful to all my committee members for their guidance and suggestions during my Ph.D. journey. I would also like to extend my immense appreciation to Sandhiya Govindaraj, Rimon Hokayem, Asif Hassan, Khadimul Islam, Md Nazim Uddin, Marisol Roman Guerra, Anthony Nunez for their invaluable contributions and for creating such a fantastic working environment. You all have been amazing co-partners who have made my work much easier. Words alone cannot adequately express my gratitude towards each of you.

I would also like to extend my gratitude to my parents, who have constantly supported and encouraged me. Their unwavering faith in me and my abilities has been a driving force in my success.

I am also thankful to my loved one and dear brother Zobaier for being a constant source of encouragement throughout my journey.

I am deeply thankful to all my respected teachers for their exceptional guidance and support throughout my academic journey. I would also like to express my gratitude to my mentor, Mr. Mir Ahmed Sir, whose guidance and support have been invaluable.

Finally, I would like to thank all my well-wishers for their constant support and encouragement. Your kind words and gestures have kept me motivated throughout my Ph.D. journey.

ABSTRACT OF THE DISSERTATION

SELF-INTERFERENCE CANCELLATION (SIC) FOR SIMULTANEOUS TRANSMIT AND RECEIVE

by

Md Nurul Anwar Tarek

Florida International University, 2023

Miami, Florida

Professor Elias Alwan, Major Professor

Microwave communication requires simultaneous transmit and receive (STAR) systems, but isolating the transmit and receive radio chains can be challenging. The most common practice is using a single antenna and a circulator, which provides insufficient isolation for full-duplex communication. Practical STAR systems need additional cancellation stages to prevent receiver desensitization caused by high-power transmit signals.

To address this challenge, a novel STAR system that includes two circulators, a hybrid coupler, and a self-interference cancellation (SIC) circuit based on a Finite Impulse Response (FIR) topology was developed. This design achieved an average Tx/Rx port isolation of about 37 dB over a 25 MHz bandwidth in simulations. A prototype was fabricated and tested, showing an average cancellation of 36 dB with a cancellation range of 33 dB to 42 dB and good agreement with the simulations.

In-band full-duplex (IBFD) systems can double spectral efficiency by enabling simultaneous transmission and reception within the same band. However, SI suppression becomes more challenging across broader bandwidths, and conventional SIC circuits require a filter bank with at least two FIR filters to achieve wide bandwidths. A wideband and low-profile SIC circuit based on a hybrid FIR and resonator filter topology has been developed to address this challenge. The design achieved

an average cancellation of 22 dB across 800 MHz in the L-band, with simulations showing a minimum cancellation of 15 dB and a maximum cancellation of 45 dB. A prototype was fabricated and tested, offering an average of around 20 dB cancellation, with a minimum cancellation of 15 dB and maximum cancellation of 27 dB.

A two-stage SIC system has been developed that includes transmit and receive antenna isolation and RFSIC filter stages. The isolation between the transmit and receive antennas is based on a novel symmetric suppression technique, and the RFSIC filter is based on a hybrid FIR filter and resonator architecture. The design achieved an average isolation of around 52 dB across a 500 MHz bandwidth, with simulations showing a minimum cancellation of 41 dB and a maximum cancellation of 65 dB. A prototype was fabricated and tested, showing an average of around 44 dB cancellation, with good agreement with the simulations.

These novel STAR and SIC systems offer practical solutions for full duplex communication and SI suppression, enabling enhanced spectrum access and doubled spectral efficiency. These advancements can improve the efficiency of microwave communication systems and open up new possibilities for communication technology.

TABLE OF CONTENTS

LIST OF FIGURES

CHAPTER 1

# INTRODUCTION

The development of broadband technologies is essential to enable high-speed data transfer, excellent service quality, and uninterrupted connectivity in the future of wireless communication. We require an *enhanced radio spectrum* to meet this demand, increasing the radio frequency (RF) spectrum accessible for wireless communication. As the RF spectrum is limited, it is essential to make the most efficient use of the available spectrum and find ways to expand it. A necessary aspect of this effort is the successful design of RF transceivers, which form the foundation of wireless communication. An effective RF transceiver must improve the spectrum capacity, deal with large amounts of data quickly and effectively, maintain signal quality, and reduce interference. A visual representation shown in Fig. 1.1 displays different applications of wireless communication systems.

## 1.1 Statistics of Wireless Communication

The statistics show that only 740 million mobile subscriptions were available globally in 2000. There were 6.38 billion active smartphone subscriptions as of 2021; by 2026, that number is projected to rise to 7.52 billion. The implementation of 5G technology is expanding quickly. By 2030, the market for 5G technology alone is predicted to be worth 620 billion US dollars [sta]. By 2035, the global GDP is anticipated to increase by 1.3 trillion dollars due to the use of 5G in industries such as healthcare, smart utilities, consumer goods, and media. Simultaneously, the 5G value chain is anticipated to create close to 23 million new jobs. In 2028, 5G will be the only source of mobile data traffic increase as 4G traffic is expected to stagnate. By the end of 2028, it is predicted that the average monthly usage per smartphone will have increased to 46 GB from 19 GB today [eri, sta].


Figure 1.1: Multiple use cases or functions of wireless communication systems [nag].

## 1.2 Challenges of Wireless Communication

The swift growth of wireless communication systems encounters obstacles such as insufficient bandwidth, restricted frequency bands, and ineffective utilization of frequency and time resources. The issues related to narrow bandwidth are as follows-

- Restricted bandwidth: The quantity of data that can be transferred at a given time is constrained. These poor data transfer rates are challenging for applications that need real-time data transfer or high-speed networking.
- Susceptibility to interference: Limited bandwidth also makes transmission more vulnerable to interference from other sources. For instance, a nearby signal operating at the same frequency as the transmitted signal may interfere with the desired received signal and degrade the received signal's quality.

- Restrict the signal range: Low bandwidth also restricts the signal's range of coverage. For example, this can be difficult for wireless or satellite transmissions, where a wider coverage area is necessary.
- Limited Interoperability across various devices and systems: Limited bandwidth might also result in problems with interoperability across various systems and devices. For instance, a device that works at a particular frequency range could not be compatible with a different frequency range system.

### 1.2.1 Time Division Duplexing

A technique known as time division duplexing (TDD), shown in Fig. 1.2, can be used to accomplish full-duplex communication. With the help of this method, the transmitter and receiver can utilize the same frequency range for data transmission and reception at different times. Even while time division duplexing allows for full duplex, there are still several issues, namely:

- Latency: As information can only be transferred when a channel becomes available, latency is the fundamental disadvantage of TDD.
- Required strict phase/time synchronization: TDD relies on allotted time slots for operation. Hence, strict phase/time synchronization is necessary to prevent interference between Uplink and downlink transmissions.
- Interference: Uplink and downlink communications use the same carrier frequency at different times. As a result of their shared frequency, the uplink and downlink channels cause interference.

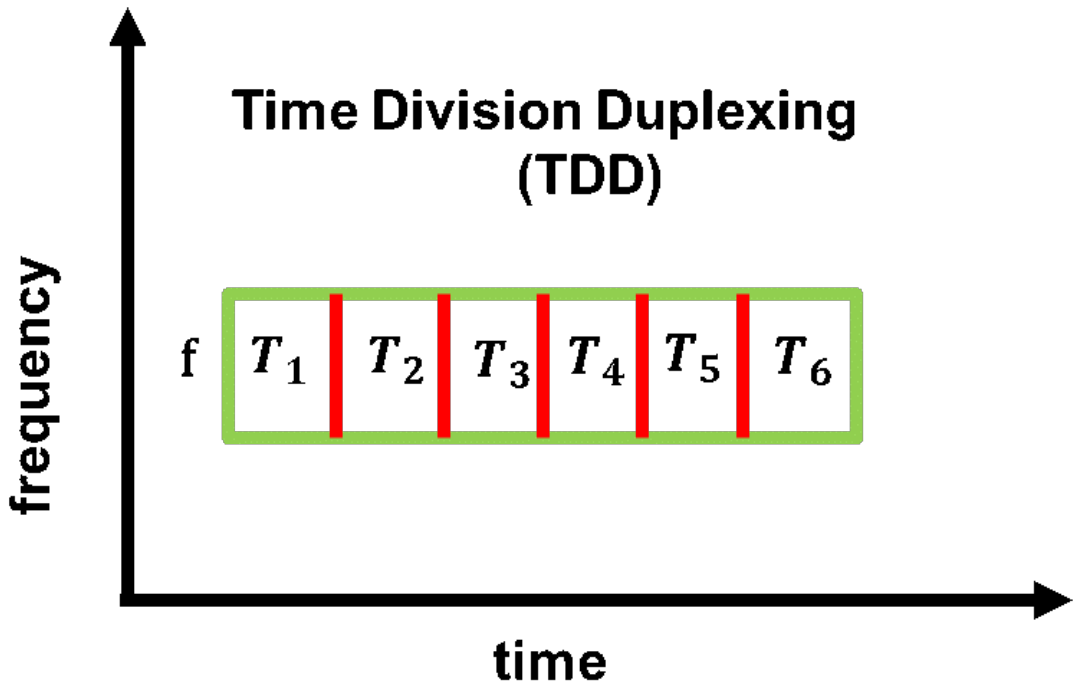


Figure 1.2: Use of time and frequency resources by a wireless system using the TDD approach

### 1.2.2 Frequency Division Duplexing

In frequency-division duplexing (FDD), as shown in Fig. 1.3, customers are given access to two distinct frequency bands for transmission and reception. Each user is given two separate carrier frequencies, one for upstream transmission and one for downstream reception, to facilitate communication in FDD. The user transmits data using the upstream frequency and receives data using the downstream frequency. The two frequencies are normally chosen from different frequency ranges to prevent interference and maximize the available bandwidth for each user. Although FDD is likewise full-duplex, it also has several disadvantages.

- Wastage of Frequency resources: The frequencies for the uplink and downlink are different in FDD. The primary disadvantage of FDD is the waste of

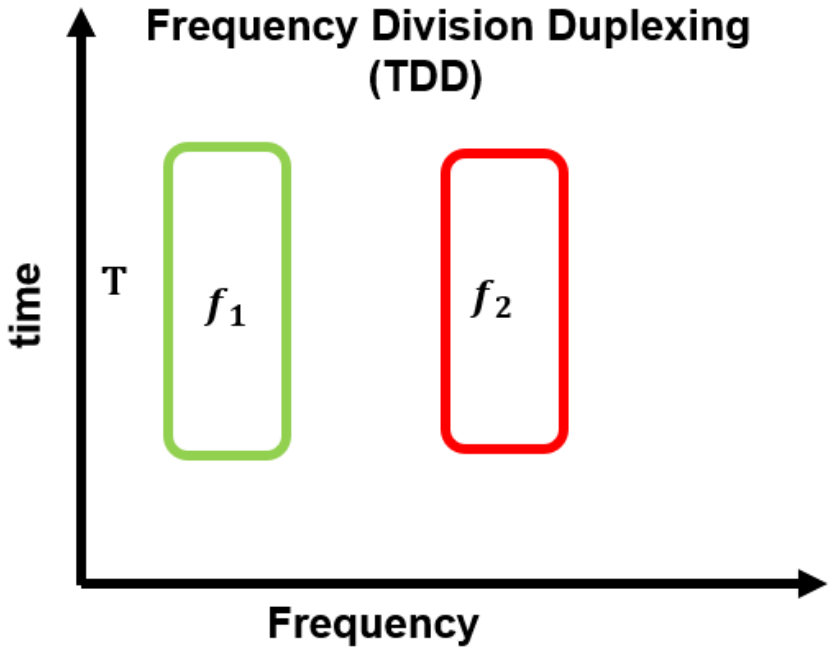


Figure 1.3: Use of time and frequency resources by a wireless system using the FDD approach

frequency resources.

- Larger form factor: FDD-based multiband communication systems require numerous adjustable duplexers, which demand a complex RF architecture and larger form factors.
- Paired Spectrum: FDD requires two paired spectrums with a sufficient gap between them to function.

### 1.2.3 Code Division Duplexing (CDD)

Another full-duplex technology that enables simultaneous transmissions simultaneously and on the same frequency is Code division duplexing (CDD). This method can be thought of as combining time division multiplexing and frequency division multiplexing. As depicted in Fig. 1.4, each user in code division duplexing (CDD) has a unique code sequence allocated to them (or waveform). Yet, this method has the following issues:

- Cautious code selection: The CDD mandates careful code selection because a poor choice could result in delays.
- Limited network capacity: Two considerations constrain a CDD system's network capacity. The length of the code word, which can only accommodate a certain number of orthogonal codes, is the first determining factor. The greatest power that a sender can transmit is the second factor. Moreover, a receiver interprets other users' transmissions as background noise.
- Near Far effect: The "near-far" effect is a drawback of the CDD approach. This effect occurs when the interference transmitter is significantly closer to the receiver than the intended transmitter.

## 1.3 In Band Full Duplex System

The need for an "in-band full duplex communication system," also known as a simultaneous transmit and receive (STAR) system, arises from the drawbacks above. This system effectively preserves time and frequency resources, resulting in improved spectral efficiency and substantial cost reductions in spectrum licensing. However, a significant challenge occurs when the high-power signal transmitted from the Tx

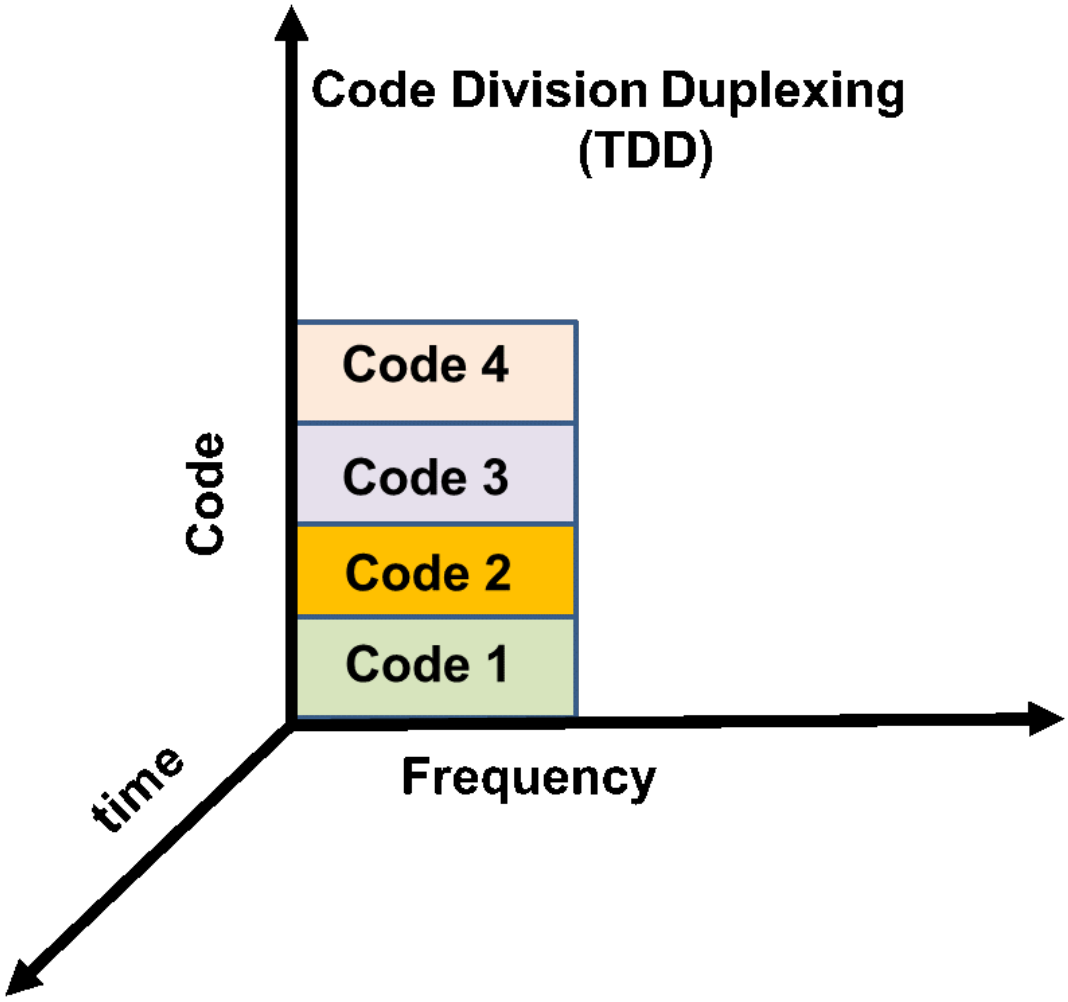


Figure 1.4: Use of time and frequency resources by a wireless system using the CDD approach

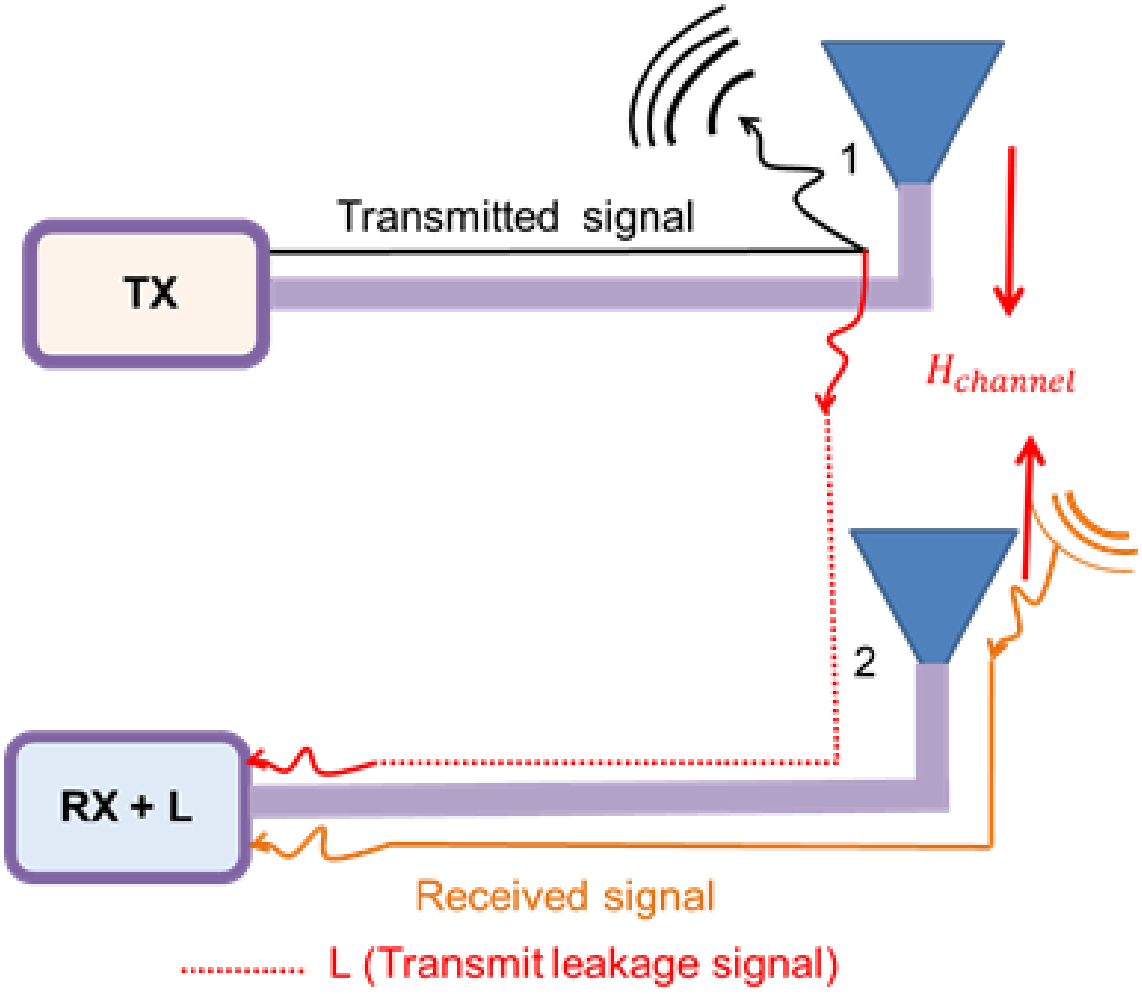


Figure 1.5: Configuration of a simultaneous transmit and receive system

antenna interferes with the Rx antenna, causing complete receiver desensitization, as depicted in Fig. 1.5.

## 1.4 Self Interference Cancellation in STAR

Therefore, to effectively utilize the spectrum, we must suppress self-interference (SI) caused by coupling between the transmitter and receiver. To achieve this isolation, a self-interference cancellation (SIC) filter has been inserted between the Tx and

Rx modules, as shown in Fig. 1.6. Both monostatic and bistatic STAR systems are possible. Early STAR system architectures used two interference cancellation stages to achieve up to 80dB cancellation for very narrowband signals (5 MHz): 1) antenna isolation and 2) analog post-processing [KGK11a, DS10b]. For up to 110dB cancellations, other STAR implementations added a stage of digital baseband cancellations [CJS+10, JCK+11]. All of these narrowband methods fell short of the necessary isolation. In addition, Wideband cancellation is one of the major bottlenecks that this effort advances new paradigms for handling.

This dissertation presents a wide-band self-interference cancellation (SIC) technique for a simultaneous transmit and receive system. We aim to 1) design and implement a wideband self-interference cancellation (SIC) circuit, 2) design and implement a dual-stage monostatic system, and 3) design and implement a dual-stage bistatic system.

## 1.5 Monostatic STAR system

The transmitter and receiver coupling is achieved through direct or scattered near-field coupling or a beamforming network. With a circulator configuration, a monostatic system can be implemented. Since the passive antenna is used for both Tx and Rx, its characteristics, such as impedance and pattern, are identical as long as the antenna is made of reciprocal materials. In [EEF15a], a novel four-arm spiral-helix antenna-based circularly polarized monostatic STAR system is described. The four-arm spiral is designed so that two arms are used for Tx and the other two arms for Rx. The helix termination is used to improve the low-end gain of the spirals. With realistic components and hybrid imbalances, isolation levels greater than 39.6-50 dB over multiple octaves are achieved, as shown in Fig. 1.7. How-

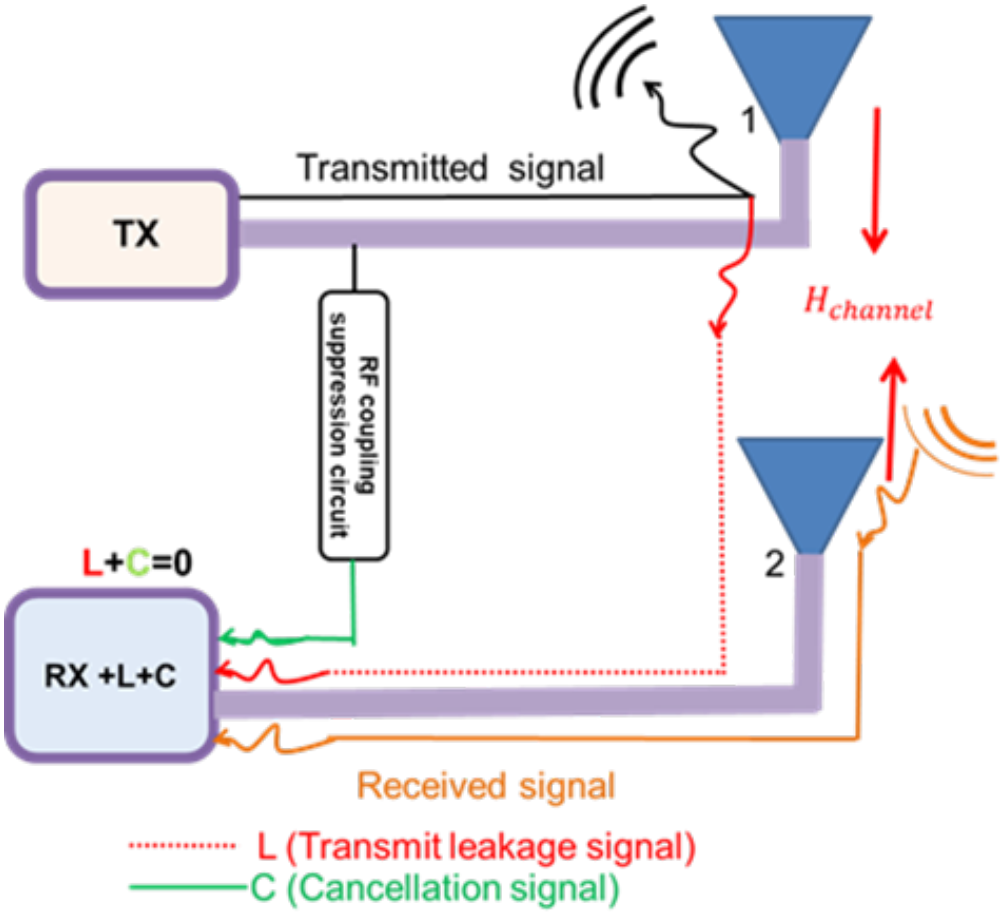


Figure 1.6: Configuration of a simultaneous transmit and receive system with Self Interference cancellation filter

ever, to improve the performance of the hybrid imbalances and simplify the feeding network, this method also employs microstrip feeders with impedance transformers to feed the two two-arm spirals, eliminating the need for 180° hybrids. However, the isolation was decreased to 36 dB over an 8:1 bandwidth using the microstrip feeding technique. In another study [EEF16a], a novel eight-arm equiangular spiral aperture-based wideband monostatic STAR antenna is shown in Fig. 1.8. Four of the eight arms of the STAR spiral's configuration are used for Tx, while the other four arms are used for Rx. It has a large geometric structure because the Tx and Rx arms have been doubled compared to the prior study [EEF15a]. The architec-

ture is also complicated due to the numerous hybrids used. For various modes of operation, system isolation ∼40 dB is achieved over an 8:1 bandwidth while maintaining comparable high-quality TX and RX radiation characteristics. In another monostatic system for achieving high isolation, a four-arm spiral, its beam forming network (BFN), and circulators are used [EEF17]. The configuration shown in Fig. 1.9 comprises a single four-arm spiral and two analog circuit layers designed to provide maximum isolation between the Tx and Rx channels. The first layer includes two butler matrix BFNs, one for TX and another for RX. The second layer incorporates four circulators, ideally phase-matched, between the spiral arms and the BFNs. However, this technique achieved isolation ranging from 23 to 38 dB for various mode arrangements. Another study [HEVPF17] introduces a monostatic, dual-CP STAR antenna system composed of two butler matrix BFNs and a sequential rotating array (SRA). A BFN feeds four dual-polarized antenna elements arranged in a sequential rotation array. The coupling from the Tx to Rx ports is canceled at the BFN's Rx port. This study achieved the measured isolation of 47dB across 2.40–2.49 GHz. In [SAF17], a single reflectarray and feed system benefits the monostatic configuration. However, this monostatic configuration transmit (Tx) and receive (Rx) ports are isolated by 41 dB at 5.8 GHz, as shown in Fig. 1.10. In [YF21], a quasi-monostatic setup in which the footprints of the Tx and Rx antennas coincide. An eight-arm (octafilar) helix is presented as the configuration for the quasi-monostatic STAR system, which involves two identical quadrifilar helices that are coaxially oriented. The excellent Tx-Rx pattern symmetry is one advantage of utilizing quadrifilar helices as the Tx and Rx elements. However, the bandwidth is constrained because the quadrifilar helix is a resonant structure by design. On the other hand, the beam-forming network ensures a high level of Tx-Rx isolation (∼65 dB). In another research, from 27-29 GHz frequency range, a

co-polarized, co-channel simultaneous transmit and receive (STAR) antenna system utilizing a two-layer spherically stratified lens is demonstrated [HBE+21]. A WR28 waveguide-implemented balanced circulator BFN is used to operate the STAR system. This study uses two 90° hybrids, two circulators, and antenna symmetry to cancel circulator leakages. The SI cancellations of 30 and 34 dB are attained with and without the spherical lens, respectively. However, it has an acceptable lens impact on the system isolation.

Recent studies have showcased the successful demonstration of active electronic and photonic circulators [CA11, KCHG00]. These advancements have led to a photonic circulator with a remarkable decade bandwidth and isolation exceeding 40 dB. However, it is essential to acknowledge certain limitations associated with both photonic and active circulators. These drawbacks encompass factors such as complexity, restricted power handling capacity, linearity concerns, larger physical size, and higher overall cost

Therefore, the inclusion of a beamformer and additional hybrid couplers in the monostatic system results in increased complexity. While these components enhance the system's capabilities, they also introduce additional complexity.

Furthermore, the far-field performance of the STAR spiral is compromised at lower frequencies when compared to a conventional spiral. Parasitic arms primarily cause this degradation in performance within the STAR spiral's structure.

In response, we have developed a novel system that overcomes this limitation.

Remarkably, our technique is simple and highly effective, utilizing just two circulators, a hybrid coupler, and an FIR filter circuit. This streamlined design offers a significant advantage in terms of power efficiency. Given the costly nature of RF power, our novel design maximizes transmission efficiency, thereby optimizing power consumption.

Additionally, our new system tackles the problematic magnetic effects by reducing the number of circulators employed. Instead, we have introduced a novel SIC circuit that effectively replaces the reduced circulator, enhancing the system's overall performance.

## 1.6 Bistatic STAR system

A bistatic configuration offers more flexibility in structure design and placement than a monostatic configuration, where the isolation is highly dependent on the symmetry of the structure. In addition, compared to monostatic systems, bistatic systems do not require a less complex beamforming network, which lowers the overall system's complexity and cost [PEF17]. In a dual-polarized configuration, a bistatic system can process both polarizations simultaneously over the same frequency, enhancing system performance and enabling more effective STAR operation. As a result, the bistatic STAR system has been the subject of extensive research. For STAR applications shown in Fig. 1.11, a T/R antenna is combined with a wideband SIC feature in which the receive antenna has an additional cross-polarized port. Conversely, this work achieves 50 dB isolation in a 300 MHz bandwidth [DK15]. Polarization diversity is only applicable in systems with a single type of polarization. Another study [KHFP12] employed an 8-element transmit ring array antenna on a circular ground plane and a raised receive element. As displayed in Fig. 1.12, a beamformer with opposing elements phased 180 degrees apart was also used to provide the array with linear progressive phase shifts. This study showed 55 dB of isolation across 100MHz bandwidth. Another study [WC12] showed a tiny three-element linear planar array that was made specifically to achieve high isolation between elements for STAR applications. They used tunable resonators to regulate the array's near fields,

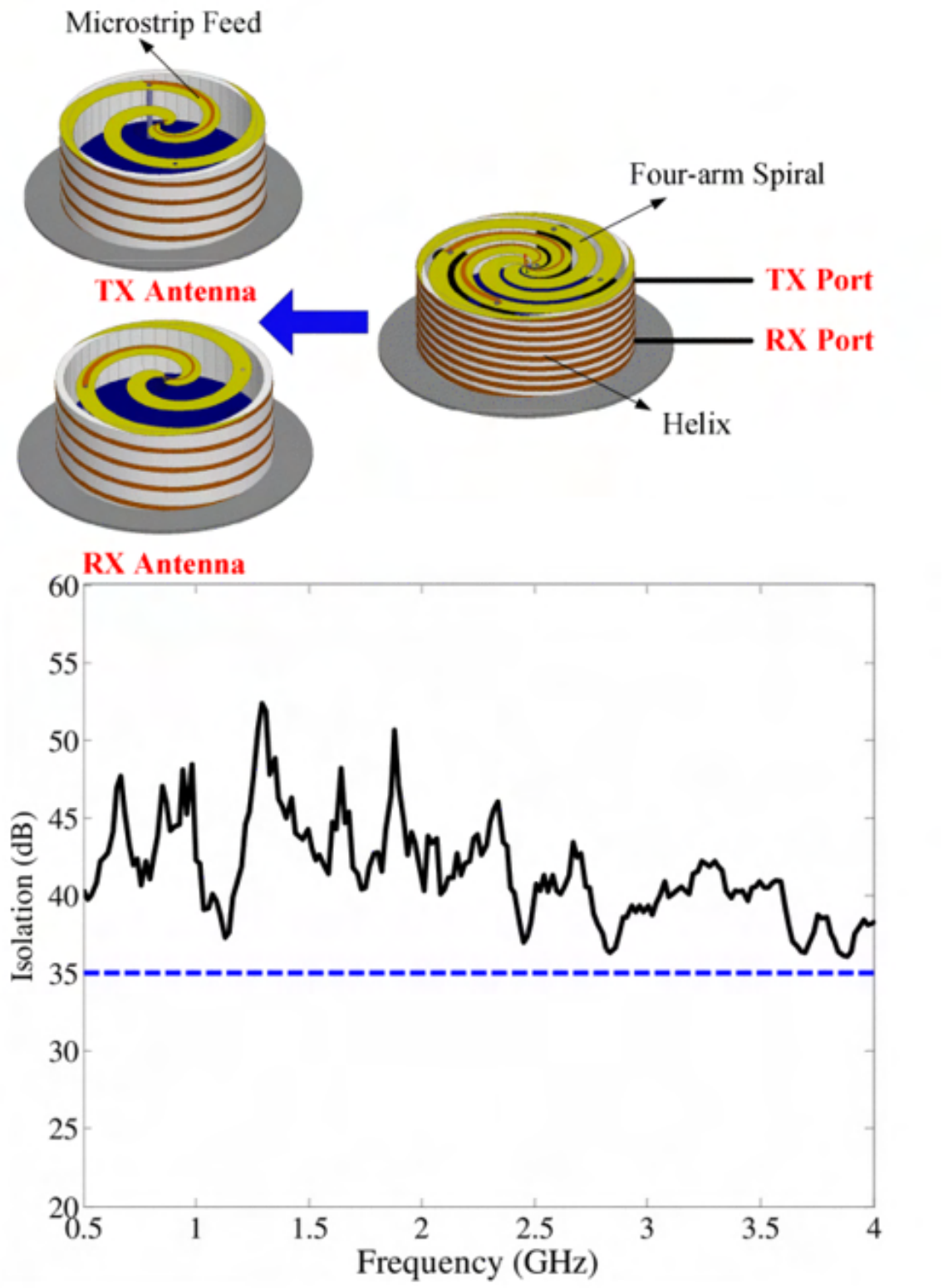


Figure 1.7: Spiral-helix STAR is capable of achieving isolation between the transmit (Tx) and receive (Rx) chains [EEF15a]

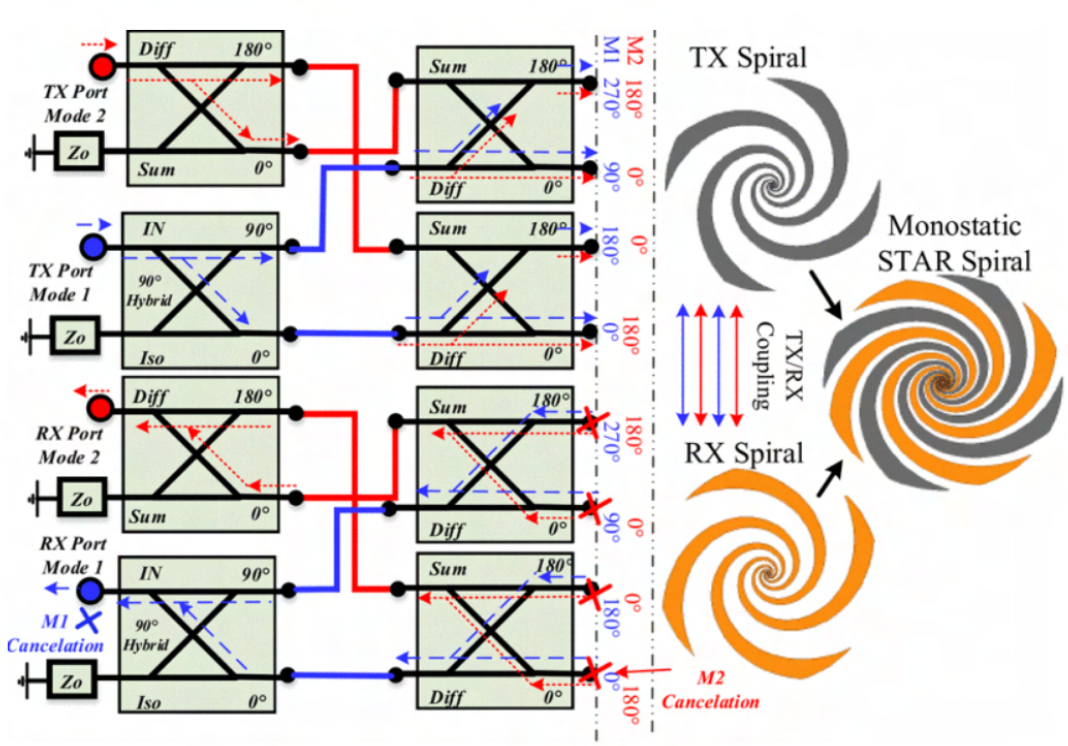


Figure 1.8: Eight-arms dual-mode spiral monostatic STAR antenna system [EEF16a].

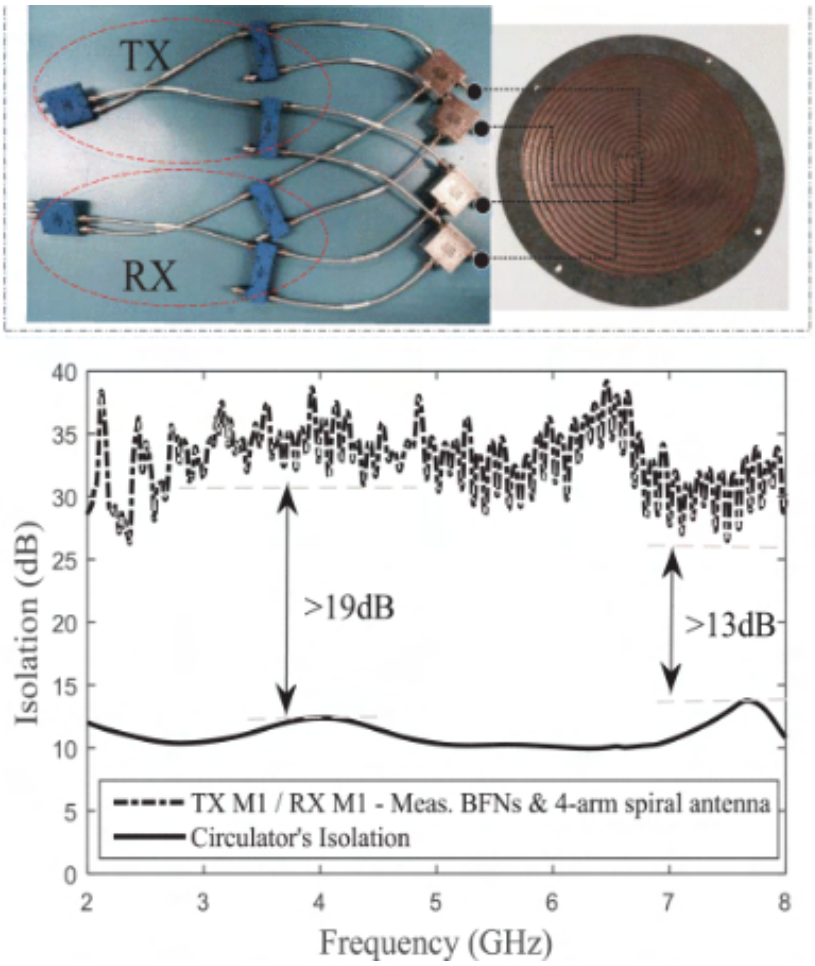


Figure 1.9: Measured isolation between the TX/RX BFN's ports compared with one of the four used circulators [EEF17].

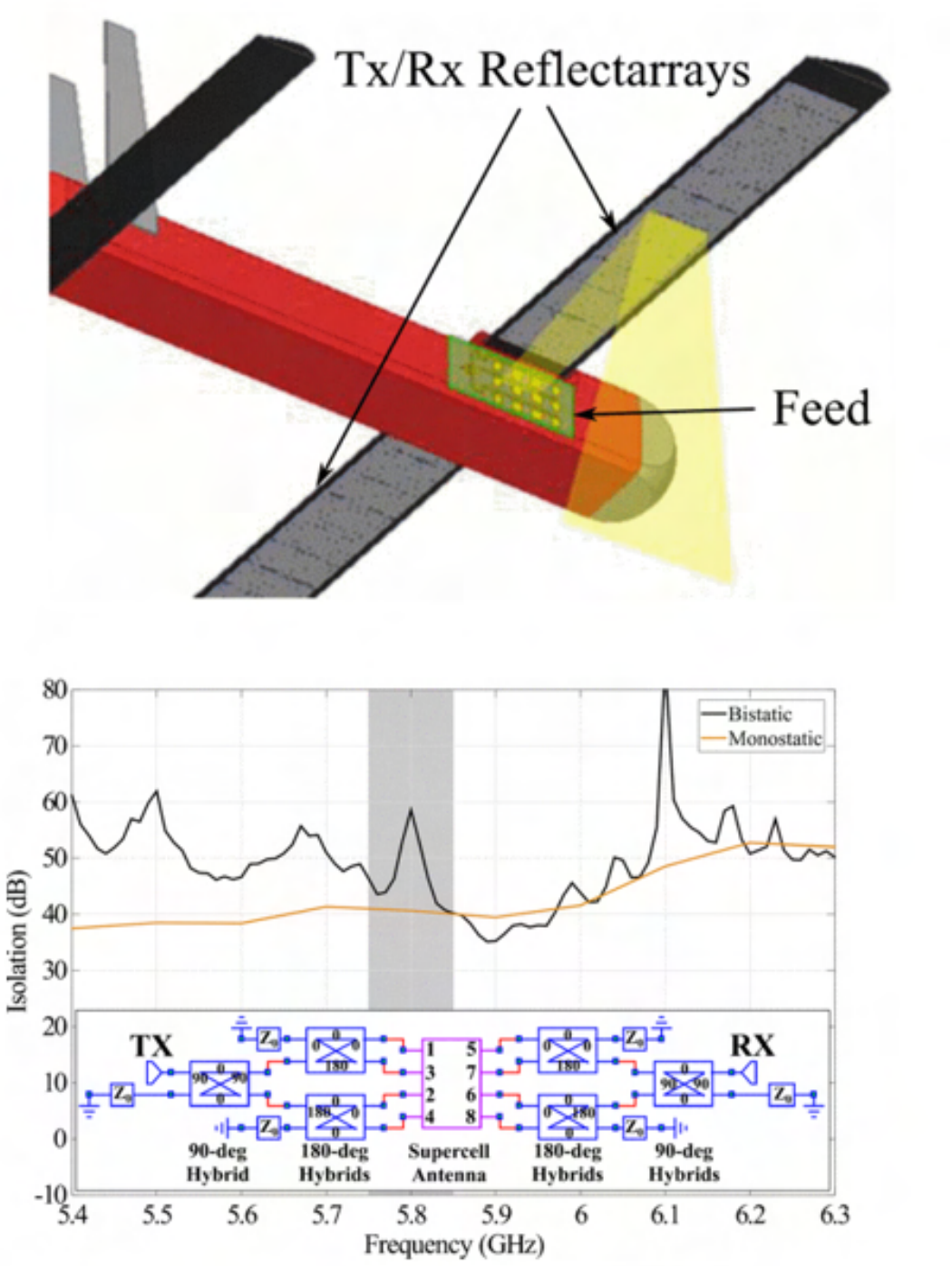


Figure 1.10: Reflectarray antennas are capable of achieving isolation between the transmit (Tx) and receive (Rx) chains [SAF17].

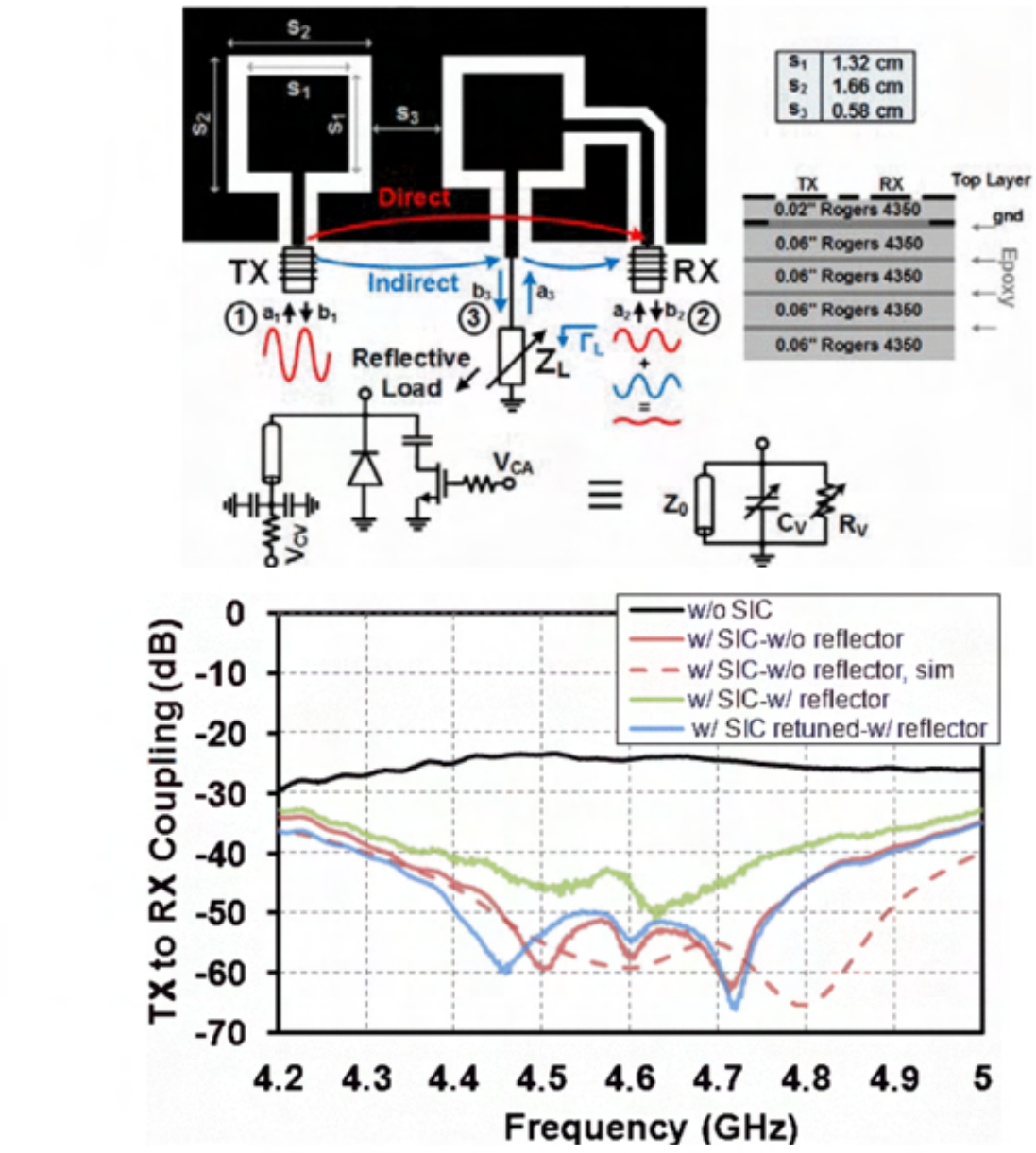


Figure 1.11: S21 measurement provided the level of coupling between the transmit and receive chains of the system under test [DK15].

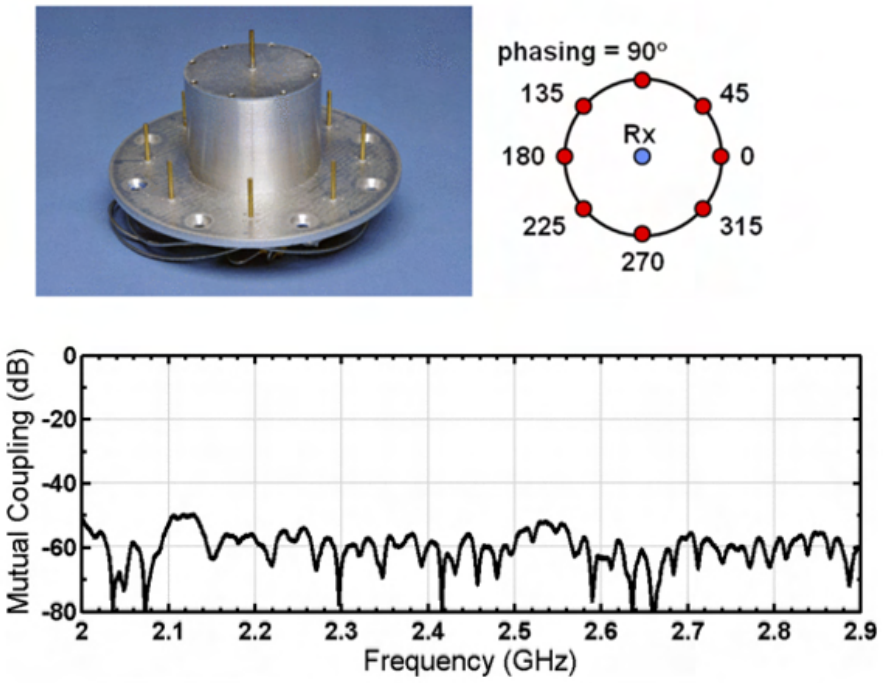


Figure 1.12: Antenna coupling measurement between Tx and Rx antenna [KHFP12]

as shown in Fig. 1.13. At 3.3 GHz, the study was able to isolate signals by 51 dB. This shows that the near-field cancellation approach requires a complex beamforming network and is sensitive to electrical and geometrical symmetries, whereas the null placement technique is restricted to narrowband applications.

Researchers have recently focused on developing fully integrated RFIC (Radio Frequency Integrated Circuit) solutions incorporating self-interference cancellation (SIC) for the STAR system. One study implemented a multiple-stage bandpass filter (BPF) using nanoscale CMOS technology to enable SI cancellation in the RF domain [ZCDK15]. This CMOS implementation offers desirable features such as tunability, reconfigurability, and high-quality factor (Q). However, this technique achieves a maximum of 20 dB of SIC across a 20 MHz bandwidth.

Another research effort utilized a 65 nm CMOS platform to design a seven-tap

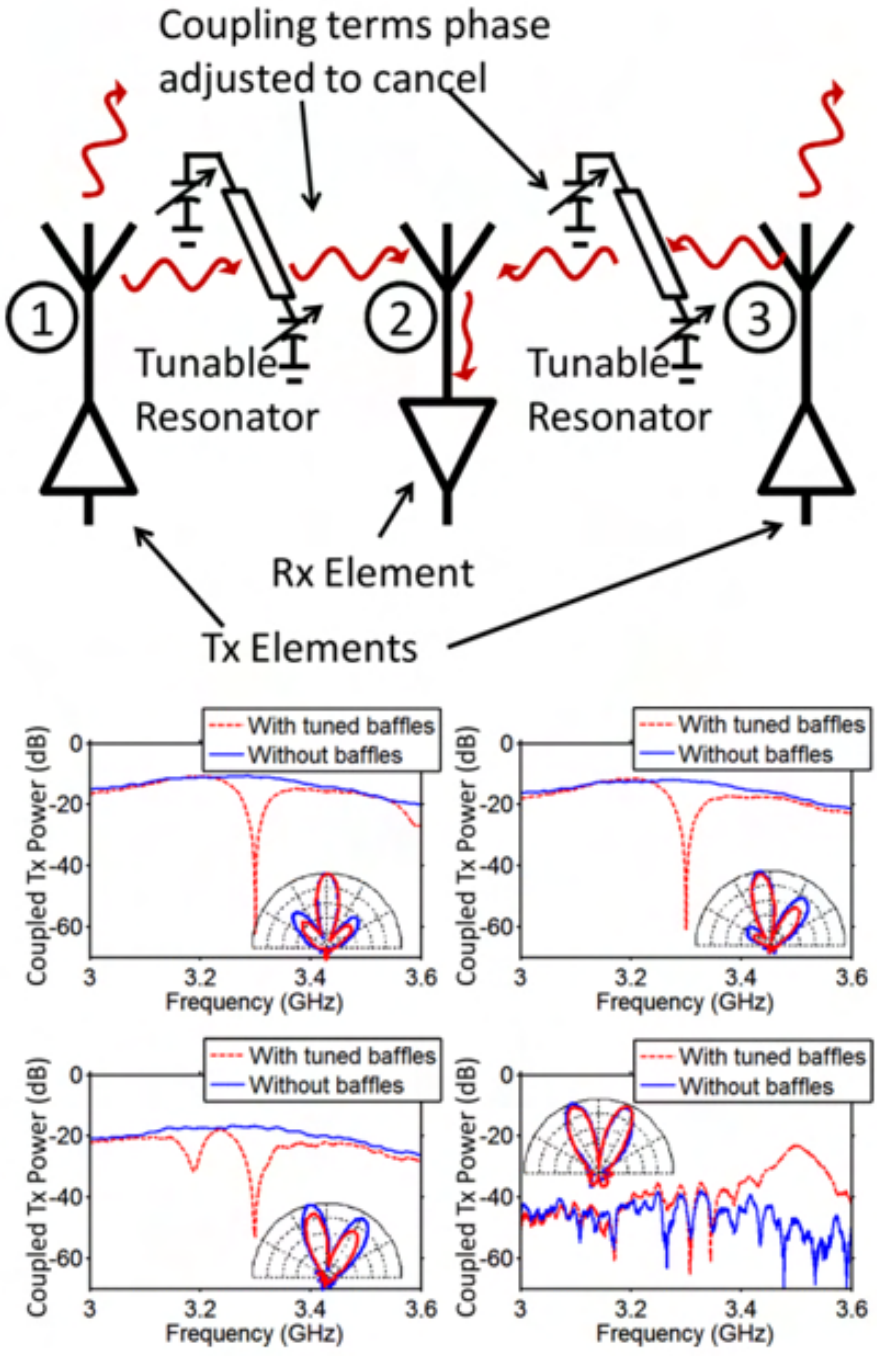


Figure 1.13: The cancellation and antenna patterns were measured at different angles of scanning, specifically at a frequency of 3.3 GHz, which was the frequency where the cancellation was optimized to achieve the highest level [WC12].

RF canceller with time-interleaved switched capacitor delays [NGA+21]. While operating within a narrow bandwidth, this technique provides an average cancellation of 32.5 dB across a 20 MHz bandwidth. These studies have explored various RFIC implementations for SIC in the STAR system, leveraging nanoscale CMOS technology and advanced circuit designs. However, the achieved cancellation levels and bandwidths are very limited.

Multi-tap FIR filters have been employed for self-interference cancellation (SIC) purposes. For instance, [LSYB17], a 16-tap FIR filter was implemented, resulting in 47 dB cancellation across a narrow bandwidth of 80 MHz. The implementation involved multiple attenuators, specifically 16, which introduced additional complexity to the optimization algorithm.

Another study in [KMP16] demonstrated a time-domain narrowband cancellation technique using a four-tap delay line and attenuators, achieving 30 dB cancellation across a bandwidth of 30 MHz. Additionally, some multi-stage STAR implementations have incorporated a stage of digital baseband cancellations, leading to cancellation levels of 60-80 dB [JCK+11].

Recognizing that the aforementioned systems are primarily designed for narrowband applications, we have expanded our research to develop a wideband SIC circuit capable of operating across a bandwidth exceeding 500 MHz. This novel circuit offers substantial advancements in the field of STAR systems, addressing the need for effective self-interference cancellation across wider frequency ranges.

## 1.7 Research Purpose

This study aims to develop a novel wideband SIC cancellation technique for simultaneous transmission and reception to improve spectral efficiency. The objective of

this dissertation is to:

### 1.7.1 Achieve a Power Efficient Analog Monostatic STAR Architecture

- Designing a power-efficient STAR system using two circulators and an FIR filter.
- Using symmetrical design in the RF monostatic system and placing an FIR circuit with two circulators to provide up to 42 dB of isolation.
- Leveraging the second circulator and FIR filter to create a quasi-replica of the leaked transmitted signal for achieving passive cancellation.

### 1.7.2 Design and Implement a Wideband Self-Interference Cancellation circuit

- Designing a low profile and wideband SIC circuit that uses a hybrid topology of finite impulse response (FIR) and resonator filter.
- Introducing resonator in the SIC circuit to provide more flexibility and enable changes in the FIR responses for achieving wideband cancellation.

### 1.7.3 Design and Implement a Bistatic Wide band Cancellation Architecture

- Create a small and symmetrical analog RF cancellation system with a three-element antenna array (one for Tx and two for Rx), two SIC circuits, three power splitters, and one power combiner.

- Utilize two custom SIC circuits with a passive symmetric cancellation technique.

## 1.8 Outline of the Dissertation

Chapter 2 outlines the design and measurements of a monostatic STAR system implemented on a single-layer substrate. This STAR system includes two circulators, a hybrid coupler, and a SIC circuit based on an FIR topology, achieving an average Tx/Rx port isolation of approximately 37 dB over a 25 MHz bandwidth (2.395-2.42 GHz) in simulation. The minimum and maximum cancellations are 35 dB and 41 dB, respectively. The RF self-interference cancellation (SIC) is implemented using a low-cost, single-layer PC. Chapter 3 discusses developing and testing a wideband self-interference cancellation circuit that combines FIR and resonator design. The chapter also discusses improving self-interference cancellation across an 800 MHz bandwidth. Chapter 4 presents the design and measurements of a novel analog RF self-interference cancellation system with bistatic architecture. The system uses two customized SIC circuits to enhance symmetric isolation between the antenna arrays and integrate a hybrid coupler for additional isolation. The technique provides high isolation of over 52 dB across a bandwidth of 500 MHz. The chapter discusses the details of the design and measurement results. Chapter 5 summarizes this dissertation with proposed future work. It also discusses the different techniques to reduce self-interference in the STAR system.

CHAPTER 2

# MONO STATIC SIMULTANEOUS TRANSMIT AND RECEIVE SYSTEM

Current communication systems have operated in a mutually exclusive manner, requiring either two frequency bands to operate simultaneously (i.e., Frequency Division Duplexing, FDD) or two-time slots to operate on the same band (i.e., Time Division Duplexing, TDD) [PS98, Don07]. In contrast, full-duplex (FD) systems present an efficient use of time-frequency resources by enabling simultaneous transmission (Tx) and reception (Rx) in the same frequency band. The successful operation of the FD system requires high isolation between the Tx and Rx chains to avoid high-power Tx signals from leaking into the receiver and desensitizing it. However, with the rise and development of 5G and 6G technologies [SBL$^+$17, UC20, sam], systems able to simultaneously transmit and receive, and hence double the spectral efficiency, have become a necessity with the remarkably congested Radio Frequency (RF) spectrum. As such, STAR systems with high Tx/Rx isolation [THG$^+$22] is a challenge that must be tackled swiftly to alleviate the overcrowded RF spectrum. A failure to do so implies an increased spectral vulnerability to signal fratricide and interference and falling short of accommodating the growing number of users of humans and connected machines. Foremost, FD designs can be classified into two categories, monostatic or bistatic [EEF15b, VAV18, TNA20]. The monostatic designs share an antenna for both transmitting and receiving. Ultimately, this configuration relies on circulators and antennas with high isolation capabilities to cancel out the self-interference (SI). On the other hand, bistatic designs require separate antennas for transmitting and receiving. Given the need for multiple antennas, bistatic designs achieve the cancellation of the coupling through spacing, polarization, beam squint diversity, and other techniques. Nevertheless, several re-

search publications indicate that multiple cancellation stages must be implemented in the analog and digital domains to target SI and achieve the desired isolation levels [KPH19, BMK13, HSNS16] for both monostatic and bistatic FD designs. In fact, across the STAR literature, most works, [CD12, GRT$^+$19], have recognized the following as the main stages for SIC: (1) the antenna stage, which involves making space or design modifications to the physical antenna to reduce the coupling between the transmit and receive antennas; (2) the RF stage, which involves implementing RF SIC circuits; and (3) the digital stage, which involves the use of probabilistic channel models.

As mentioned, bistatic designs require at least one Rx antenna and one Tx antenna to achieve a higher isolation level by adjusting the spacing between these antennas. As a result, this method often demands a significant distance between the Tx and Rx antennas. Therefore, it is impractical for many applications, such as the sub-6 GHz range or higher frequencies, where the space is limited [FEB21]. For instance, in [KMP16], an 8-element Tx ring antenna array, with an elevated Rx element on the circular ground plane, is designed. The system's Rx and Tx antennas achieve 55 dB of isolation, along with an omnidirectional pattern, from 2.4 to 2.5 GHz through the use of a beamformer that phases the opposing parts 180° apart. However, this multi-in, multi-out approach is constrained by the available space and leads to overall unstable system efficiency. Additionally, as the number of Tx components rises, the beamformer network becomes more complicated and sensitive to feeding network flaws and size.

Other techniques applied to bistatic designs include the placement of tunable resonators between the Tx and Rx antennas to reduce coupling, as shown in [LM15]. However, this approach also requires significant separation, which is unfeasible for many applications with small spaces. A polarization multiplexing method also en-

ables the co-location of Tx and Rx antennas. For instance, [DK15] demonstrates a wideband SIC cancellation system using a Tx/Rx antenna pair with orthogonal linear polarization. When the SIC circuit is turned on, it produces 50 dB isolation across a 300 MHz bandwidth centered at 4.6 GHz. Using polarization orthogonality is acceptable for commercial purposes. However, it is unsuitable when full polarization diversity is required, such as in military radios, including evaluating electronic warfare engagements. Bistatic FD systems generally require a considerable separation distance between the Tx and Rx antennas to provide high isolation levels. On that account, monostatic FD systems are the most suited design for applications with space limits.

Despite being favorable for applications with small-sized devices, the reliance of monostatic systems on circulators and other components produces different drawbacks. These components have internal leakage and power losses, leading to inadequate isolation and increased power consumption. For example, in [MDTE20], a wideband monostatic setup incorporates a Wilkinson power divider, two circulators, and a balun. This setup provides 45 dB isolation in the 2-4 GHz frequency range. Even though acceptable isolation is achieved across a wide bandwidth, half of the Tx signal is lost when creating the equivalent leaking signal for cancellation. Similarly, the circulator-free design accomplished with a 180° coupler and power splitters presented in [DSPV$^+$20] results in half the Tx power loss. In [ZNSR17], a two-point SIC system is introduced, reducing the interference between the Tx and Rx in FD radios. This research provided 50 dB of SIC across 42 MHz of bandwidth. However, this cancellation shows high power loss at the Tx chain. In addition, due to the use of a 19-tap filtering technique, the SIC circuit is complex. In another study, an integrated six-port beam forming network (BFN) achieves 40 dB cancellation across 107 MHz. Since a BFN Network requires two 180° hybrid couplers, one 90° hybrid

coupler, and one Wilkinson power divider, a 3 dB power loss is observed at the Tx chain [WLX+22]. In another research [WSWL20], a monastic circularly polarized antenna system is presented to provide 40 dB of cancellation across 100 MHz. In this work, the feeding technique requires several Wilkinson power dividers implying high power loss at the Tx and Rx Chains. In [HEPF17], a BFN butter matrix is introduced in the Tx and Rx chains of a monostatic dual-polarized STAR antenna system. This study achieved 47 dB of isolation across a 100 MHz bandwidth. It should be noted that the butter matrix is implemented with three hybrid couplers, resulting in high power loss at both the Tx and Rx chains. Similarly, in [CHWC10], three quadrature hybrids were used to achieve 35 dB of isolation across a large bandwidth of 2.6 GHz. This method shows a 4.5 dB insertion loss in both Tx and Rx chains. Another study [JKY10] implemented an impedance tuning circuit at the coupling port of a directional coupler. This design achieved 65 dB of carrier leakage cancellation across a 100 MHz frequency band. However, because a directional coupler is used, a significant amount of Tx power is lost. Furthermore, tuning circuits are difficult to implement at high frequencies.

Alternatively, even with the implementation of an electrically balanced duplexer, as done in [MvLC+14, LBMH14], there is still a significant amount of Tx insertion loss that results in a half power loss of the Tx signal. In [GRT+19], a quadrature balanced power amplifier (QBPA) is used as an SIC canceller to improve Tx and Rx losses. However, this improvement was achieved at the cost of additional power amplifiers and hybrid couplers, implying increased hardware complexity.

Furthermore, the simple circulators structure realized in [Kno12] achieved isolation greater than 60 dB from 902-928 MHz with a circularly polarized patch antenna, a simple balanced feed network, and a second layer of analog feed-forward cancellation circuitry. However, there is Tx loss when feeding the circulator. Another work

using a circulator has reported 40 dB cancellation across 65 MHz of bandwidth [KFSE18]. However, because the structure uses inductors and capacitors, components with a low-quality factor, it needs an impedance matching terminal, which is challenging to implement at higher frequencies [KFSE18]. In [CA11], a new photonic circulator with Tx/Rx isolation greater than 39.6 dB across a 10:1 bandwidth is presented. However, its performance rapidly degrades when the antenna is poorly matched. In addition, one of the potential drawbacks of photonic circulators is their lower power handling compared to the fertile circulator.

This chapter presents a monostatic STAR architecture, as shown in Fig. 2.1. This work extends our previous research published in [TRA21] based solely on simulation. In contrast, this paper features a fabricated prototype and brings forward several novelties, among them:

1. The RF-SIC system is power efficient as it achieves high isolation with a minimal power loss of the Tx signal. In contrast, other designs lose an additional 3dB at both the Tx and Rx signal. In our design, there is no requirement for splitting the Tx signal.
2. The symmetrical design is simple yet novel as it only requires two circulators and finite impulse response (FIR) circuit topology to provide up to 42 dB in isolation across the operational bandwidth. The placement of the FIR circuit brings passive cancellation at the Rx chain, whereas other research requires active circuits such as IMT [KFSE18].
3. The second circulator and the FIR filter enable the creation of a quasi-replica of the leaked transmitted signal for passive symmetric cancellation.
4. The addition of an FIR filter between the two circulators improves the secondary matching to approximate the channel coupling for further SIC.

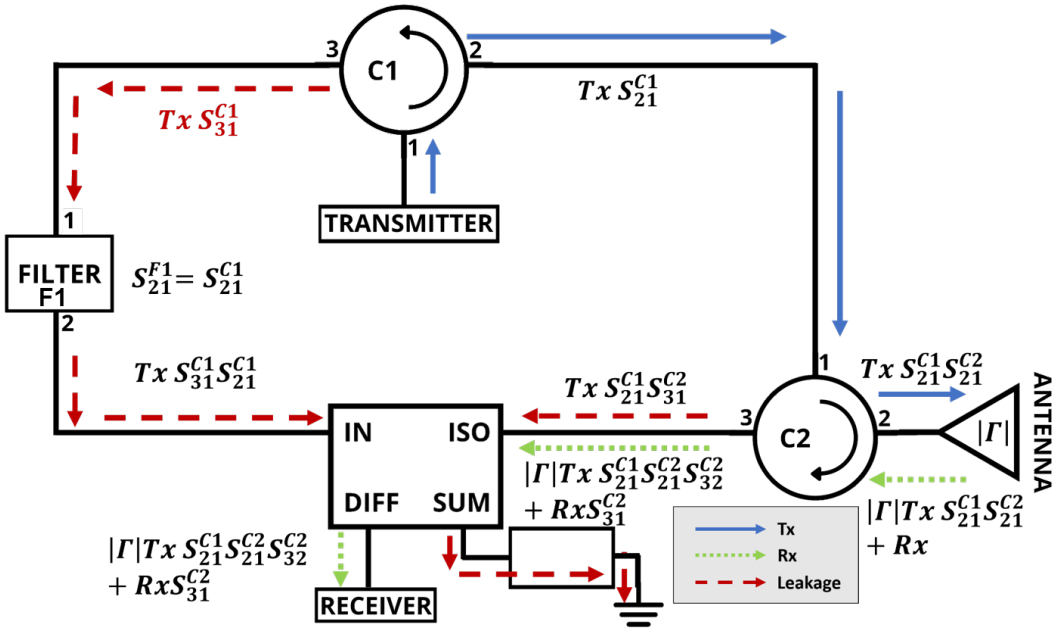


Figure 2.1: A monostatic dual circulator STAR system operating across 25MHz. The architecture comprises two circulators, an FIR filter, and a hybrid coupler to achieve up to 42 dB of self-interference cancellation.

5. Implementing a differential evolution algorithm (DE) to optimize the FIR filter. This algorithm was selected because optimizing the FIR filter in the analog domain requires a highly tuned solution and no initial guess. Moreover, DE is a population-based optimizer for finding the best solution to a problem; in its most basic form, it is the process of adding the weighted difference between two population vectors to a third vector.

Consequently, our improved STAR architecture achieved a minimum isolation of 35 dB and a maximum isolation of 41 dB in simulation. Similarly, the measurements of the fabricated prototype reached isolation of 33 dB and 42 dB, respectively, between the Tx and the Rx ports across 2.395-2.420 GHz.

## 2.1 Analysis of the Symmetric Coupling Cancellation for the RF Stage

The STAR configuration, shown in Fig. 2.1, has most of the Tx signal going through the first circulator, C1, as $TxS_{21}^{C1}$, while a small fraction leaks, $TxS_{31}^{C1}$, due to the circulator's mismatches. Simultaneously, the leaked signal passes through the filter, F1, on the system's left side. Notably, the filter design is based on an FIR circuit, which collectively behaves as follows:

$$S_{21}^{F1} = S_{21}^{C1}. \tag{2.1}$$

Therefore, at the output of the filter, the signal becomes:

$$TxS_{31}^{C1}S_{21}^{F1} = TxS_{31}^{C1}S_{21}^{C1}. \tag{2.2}$$

Moreover, on the right portion of the system, the Tx signal, $TxS_{21}^{C1}$, is sent out to the antenna via C2. Meanwhile, a part of the Tx signal leaks through port 3 of C2, adding to the incoming Rx signal and making the total signal:

$$y = TxS_{21}^{C1}S_{31}^{C2} + RxS_{32}^{C2}. \tag{2.3}$$

It should be noted that both circulators are equivalent, as shown below:

$$S_{31}^{C1} = S_{31}^{C2}. \tag{2.4}$$

Therefore, the leaked Tx signals on the left and right sides are identical. As a result, the received signal,

$$RxS_{32}^{C2}, \tag{2.5}$$

is isolated at the difference port of the 180° hybrid coupler, where $TxS_{21}^{C1}S_{31}^{C2}$ cancels out with the filtered quasi-replica, $TxS_{31}^{C1}S_{21}^{C1}$.

Table 2.1: Performance comparison with current state-of-the-art implementations of STAR systems.

| **Reference** | **Bandwidth** | **Tx-Rx Isolation** | **Signal loss** | **Technology** |
|---|---|---|---|---|
| [GRT+19] | 80 MHz | 50-56 dB | Low (.25 dB) | Tx and Rx loss improves at the cost of additional use of PA and hybrid couplers in the RF domain. |
| [MDTE20] | 2 GHz | 45 dB | High (3 dB) | Two circulators, a balun, and a power divider are combined, but half of Tx power is lost. |
| [DSPV+20] | 300 MHz | 55 dB | High (3 dB) | No circulator needed, but half of Tx power is wasted. |
| [ZNSR17] | 42 MHz | 50 dB | High | 19 taps filtering technique and a local oscillator were used for SIC cancellation. |
| [WSWL20] | 107 MHz | 40 dB | High (>3 dB) | An integrated six-port beamforming network (BFN) is used. More than half of the power is lost. |
| [WSWL20] | 100 MHz | 40 dB | High (>3dB) | Three Wilkinson power dividers and phase delay lines were used. A high amount of power is lost. |
| [HEPF17] | 100 MHz | 47 dB | High | Dual polarized antenna elements fed by two modified Butler matrices. Half of the power is lost. |
| [CHWC10] | 20 MHz | 35 dB | High (4.5 dB) | Three quadrature hybrids were used to create quasi-circulators. |
| [JKY10] | 100 MHz | 65 dB | High | A directional coupler and tuning circuits are used, causing Tx power loss. |
| [MvLC+14] | single freq. | 45 dB | High | Electrical duplexer implemented with Tx insertion loss. |
| [Kno12] | 26 MHz | 60 dB | High | Balanced feed network, but showed Tx insertion loss. |
| [KFSE18] | 65 MHz | 40 dB | High | A single circulator is used, but implementing the IMT at high frequencies is challenging. |
| [CA11] | 10:1 | 39.6 dB | N/A | Photonic circulator requires perfect antenna matching for SIC cancellation. |
| This work | 25 MHz | 37 dB | low(1.7 dB) | Symmetrical configuration realized with two circulators and an FIR circuit cause minimal loss. |

Our method avoids the 3dB loss in the Tx signal, allowing us to maintain a satisfactory power level. Ideally, typical values of circulator/ isolator insertion loss are of the order 0.2 to 0.4 dB. It is important to note that since we have used commercially off-the-shelf (COTS) components, the insertion loss is 0.707 dB at the first circulator's output. At the output of the second circulator, the insertion loss for the Tx power is 1 dB. Therefore, the total insertion loss for the Tx power is 1.7 dB. Conversely, other designs show a 3 dB insertion loss.

## 2.2 Segments of the Single Antenna STAR System

### 2.2.1 Circulators

Within the framework of our topology, we have implemented two circulators, which resulted in a symmetrical design. Ideally, these two circulators' responses should be identical because they are the same component. However, the measured responses of the two circulators varied. Therefore, since the isolation in monostatic systems will be limited by the performance of the circuit components, we must minimize the losses by reducing the number of components and picking high-performing options.

For this reason, we are only using two circulators from RFCI (component number CR5863). These circulators have an operating frequency range between 2.365-2.435 GHz. According to our measurements, the circulators have an isolation level of 15.5 dB at 2.41 GHz across all ports. Each circulator's two key S-parameters, isolation and transmission, were measured and shown in Fig. 2.2. Moreover, Fig. 2.3 shows the measured return loss at every port of the two circulators.

### 2.2.2 Antenna

A planar patch antenna was designed to test the antenna port and its corresponding leakage cancellation. We selected a patch as the most suitable design because it could be easily scaled to different bandwidths for testing and still shows a good match. Moreover, this antenna's characteristics, such as light-weight, low-profile, portable, and fabrication-flexible, were advantageous for fabrication and measurement setup.

The circulators operate from 2.365 to 2.435GHz GHz, so the antenna was designed for 2.4 GHz. Foremost, this cup-like antenna originally consisted of a rectangular $58.48 \times 36.60$ mm$^2$ patch. However, an arc-shaped transition, with a radius

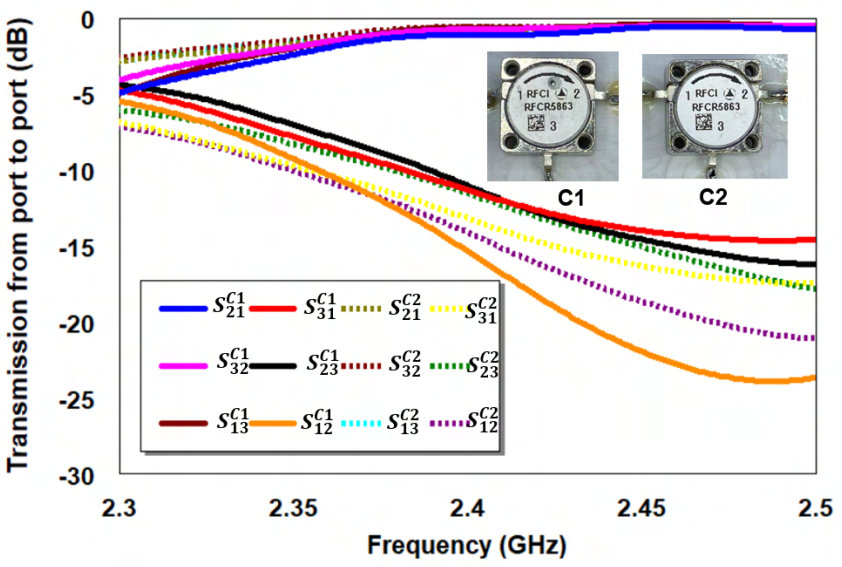


Figure 2.2: Transmission and isolation at the different ports for circulators C1 and C2.

of 32.9 mm, between the bottom half edges of the patch and the feed was added. The created round edges allow smoother current flow and better matching across a wide bandwidth. Similarly, the antenna has a reduced ground plane, 39.55 mm long, with a notch, 5.95 mm deep, parallel to the feed, to reduce the Q-factor and achieve wideband operation. This prototype was printed on the RT/Duroid 5880 substrate ($\epsilon_r$ = 2.2 and tan$\delta$ = 0.009) with a 1.575 mm thickness. The antenna, displayed in Fig. 2.4, is 73.2×98.7 mm$^2$. Notably, the antenna design results taken with the Vector Network Analyzer (VNA), shown in Fig. 2.5, demonstrate a good match with the full-wave simulation, as shown in Fig. 2.6.

### 2.2.3 FIR Circuit

The physical architecture of the FIR filter is depicted in Fig. 2.7. For ease of fabrication, we designed a $2^{nd}$ order FIR filter. Since the order of the filter is

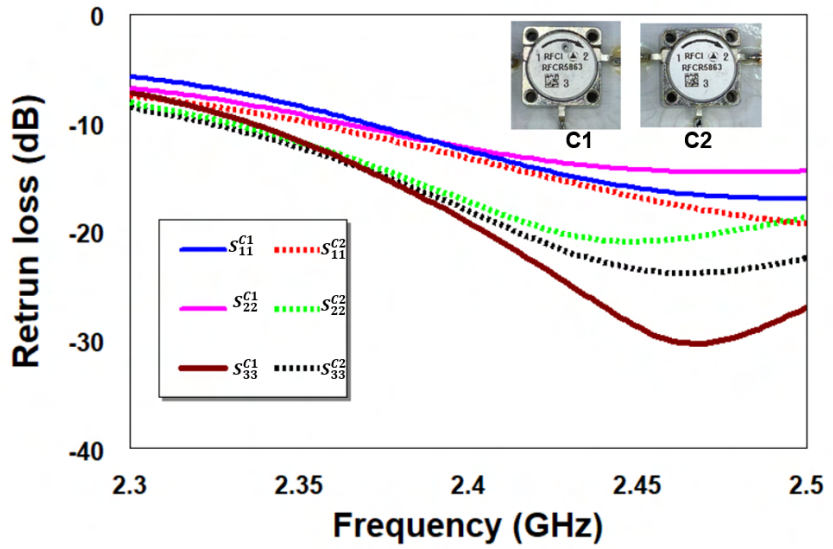


Figure 2.3: Return loss measurements of the circulators C1 and C2.

determined by the number of taps, this filter consists of a two-tapped FIR circuit that also includes delay lines and attenuators.

## 2.3 Self-Interference Cancellation Circuit Design

This section investigates the two-tap FIR arrangement, which mimics the behavior of the circulator C1 transmission from port 1 to port 2. Considering the identical operation of the two circulators, the transmission of C1 should satisfy (3) in an ideal situation. In reality, there is a slight variation in the responses of the two circulators, as seen in Fig. 2.2. One of the advantages of using an FIR circuit is that it can compensate for these slight circulator mismatches to achieve the desired level of cancellation. Notably, we present a simple FIR circuit with a two-tap topology. The latter offers three degrees of freedom, one of which is the delay line, while the other two are the attenuators. As such, by varying these 3 degrees of freedom, we can match the leakage and modify possible frequency response discrepancies of the

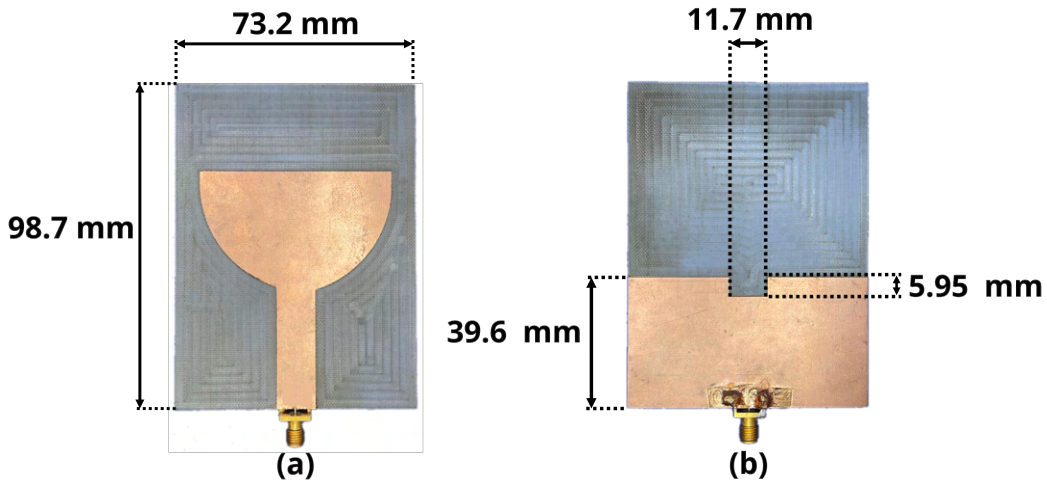


Figure 2.4: Geometry of the planar patch antenna. (a) Top view. (b) Bottom view.

circuit components. As a result, this freedom allows the circuit to accomplish the required cancellation.

Fig. 2.7 shows the schematic of the presented FIR circuit with one delay line and two-tap coefficients. Each tap consists of one attenuator. In the analog domain, the tap delays are represented by microstrip lines, and the tap coefficients are realized with attenuators. The width and length of the delay lines and attenuators are optimized to achieve a transfer function matched to the Tx signal passed by circulator C1. It must be noted that the FIR circuit is also a function of C2, given that it is the same as C1. Overall, the FIR circuit response design considers both circulators' responses.

Our architecture's electromagnetic (EM) layout is depicted in Fig. 2.8. The delay lines and attenuators were optimized to achieve a filter response that satisfied (2.2) and (2.3). In other words, the FIR circuit played a crucial role in capturing the dual circulator effect by adjusting the gain delay of the attenuators and the transmission lines (copper traced) across the desired frequency band of 2.395-2.42 GHz.

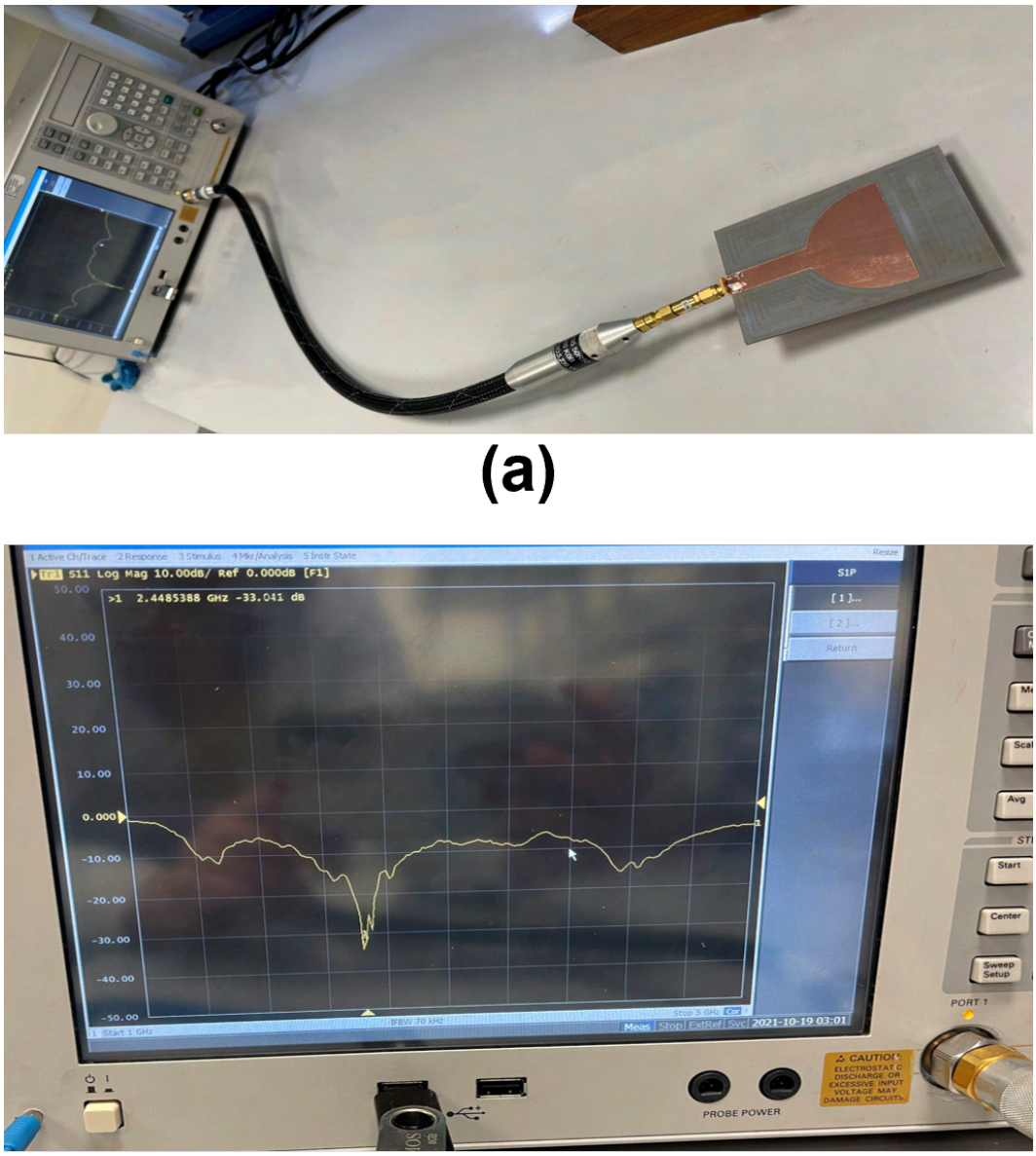


Figure 2.5: Measurement setup for the antenna. (a) VNA and the antenna. (b) Close-up of the VNA results.

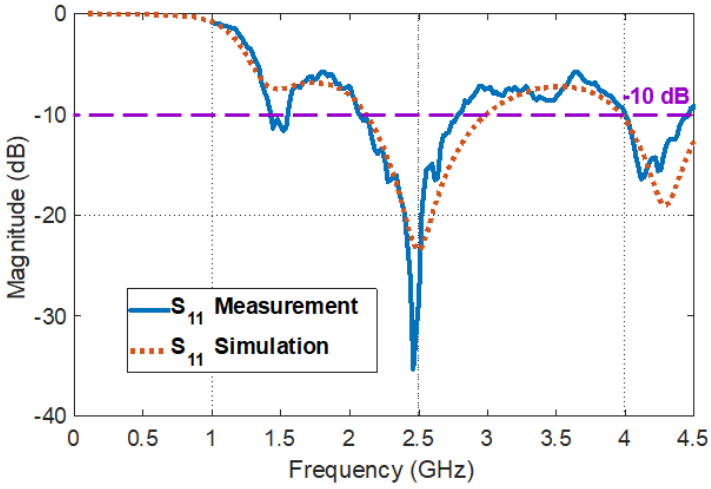


Figure 2.6: Simulated and measured $S_{11}$ of the antenna shown in Fig. 2.4.

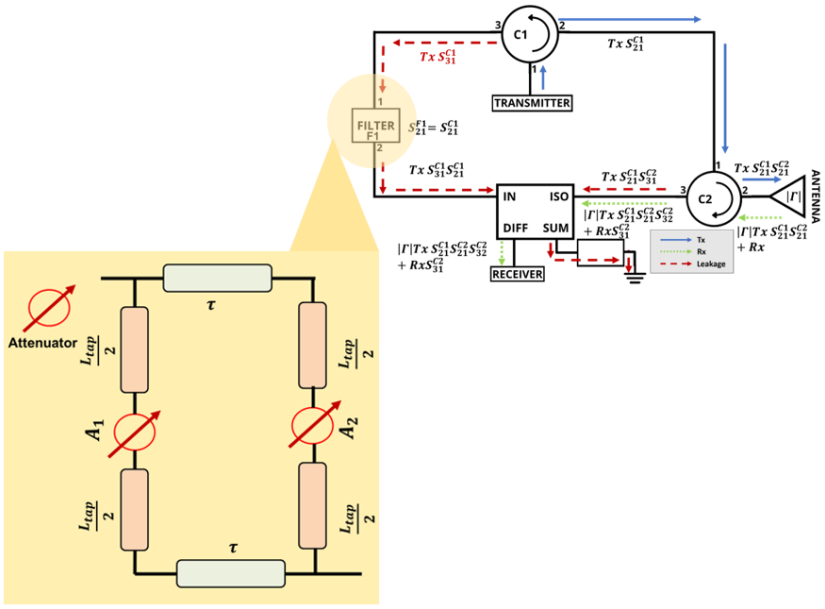


Figure 2.7: A Two-tap FIR circuit with delay lines and attenuators.

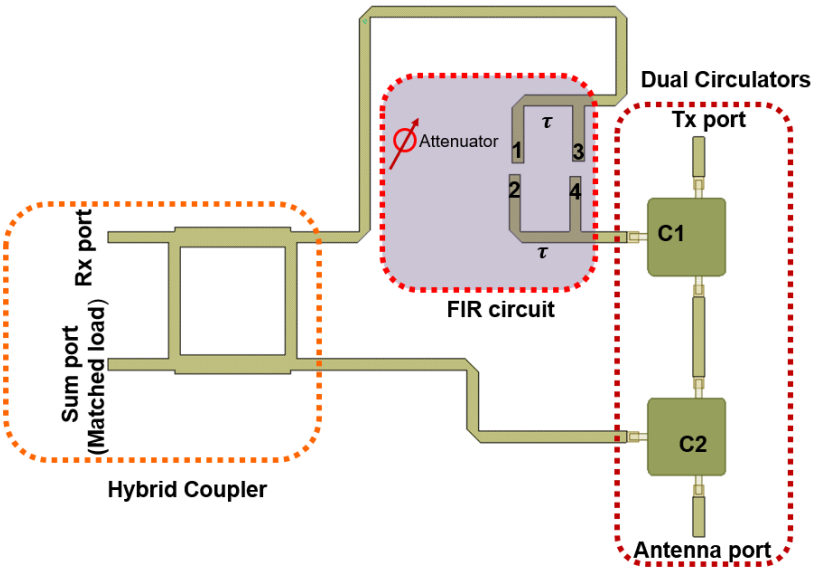


Figure 2.8: EM layout of the FIR circuit. Here is noted that the attenuator is a lumped component. One attenuator is later placed between ports 1 and 2 and the other between ports 3 and 4.

From the primary network, we note that the passive multi-port networks corresponding to the circulator leakage effect contain transfer functions (TFs) with both zeros and poles in their integer-order polynomial representations. The approximation of such coupling functions using an FIR circuit is possible. Our architecture was fabricated on a microstrip substrate to keep the circuit low profile. To reproduce this network's unit impulse response, an FIR filter would need to sample it at close intervals of time and use the sampled values as weights (*viz.* taps) for the FIR realization. The TF of the FIR filter can be represented using circuit taps, which are implemented using tap delay lines and tap coefficients. In this two-tapped FIR circuit, each tapped length is 24 mm. The form factor of this FIR circuit is 16 mm×24 mm.

More in detail, we designed a $2^{th}$ order circuit (*viz.* 2 taps). This topology is passive, as it only consists of passive elements: delay lines and attenuators. The width and length of the delay lines and attenuators are optimized to achieve a TF

that is conjugately matched to the channel's TF (leakage from both circulators). The delay spread, and filter coefficients are obtained using a DE algorithm. The specific filter taps are weighted filter coefficients with values {2,2}, and the delay spread is {0.042} ns at the center frequency. For optimization, we have considered several factors. A general rule for determining the population size is multiplying the number of parameters that can be optimized by five until the maximum number of parameters is reached (15 in this case). Smaller populations get results faster but are more likely to get stuck in a local optimum. No matter how many parameters there are, population sizes of more than 60 are generally unsuitable. When we tuned our circuit to imitate the coupling response, the size of our population was always less than 60.

We used the greedy technique in our SIC design since it yields results the quickest. With a first estimate, the problem becomes more manageable. We decided to choose a more significant cross-over probability as a result. The usual range of values is 0.0 to 1.0. The cross-over probability in our scenario is 0.9. Using this algorithm, we first performed a circuit simulation to get the optimum weights of the circuit elements. The simulated performance is shown in Fig. 2.9. Our design achieves an average Tx/Rx port isolation of ∼37 dB across a 25 MHz bandwidth (*viz.* 2.395-2.42 GHz). We also perform the simulation of our RFSIC system with three-tap FIR circuits. As can be seen, an additional 9 dB cancellation is achieved across 50 MHz. However, the three-tap FIR circuit incorporates an extra delay line and attenuator to achieve more excellent cancellation.

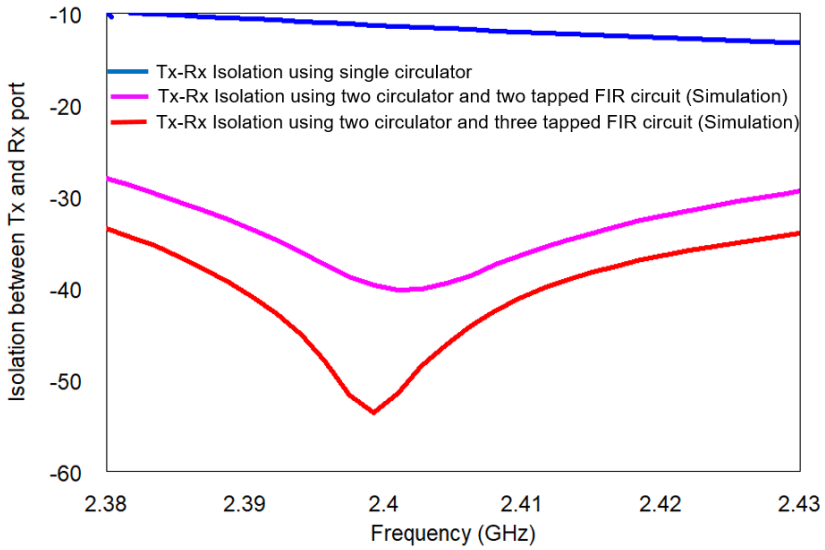


Figure 2.9: Monostatic STAR system simulation results. Our design achieves an average Tx/Rx port isolation of ∼37 dB across a 25 MHz bandwidth (*viz.* 2.395-2.42 GHz).

## 2.4 Self-interference Cancellation Circuit Fabrication

The monostatic SIC system was fabricated on a 0.8182 mm thick Rogers 4003C substrate ($\epsilon_r$ = 3.38 and tan$\delta$ = 0.0027). The final prototype is shown in Fig. 2.10. Foremost, to evaluate the overall performance of the presented single-antenna FD system, the achieved SI cancellation was tested by measuring the amount of the Tx signal leaked to the receiver ($S_{31}$). To reduce the amount of reflection, we enclosed the antenna with absorbers, as depicted in Fig. 2.11. The system's average measured cancellation is 36 dB across a BW of 25 MHz, which is displayed in Fig. 4.10. It is worth mentioning that the accuracy of the measurements is contingent on the accuracy of the attenuator values and hybrid coupler losses.

To evaluate our system in an active environment, we fed the Tx port with a 200 MHz modulated signal with with a 200 MHz modulated signal with a power level of 0 dBm. The measurement setup is shown in Fig. 2.13 and its respective results

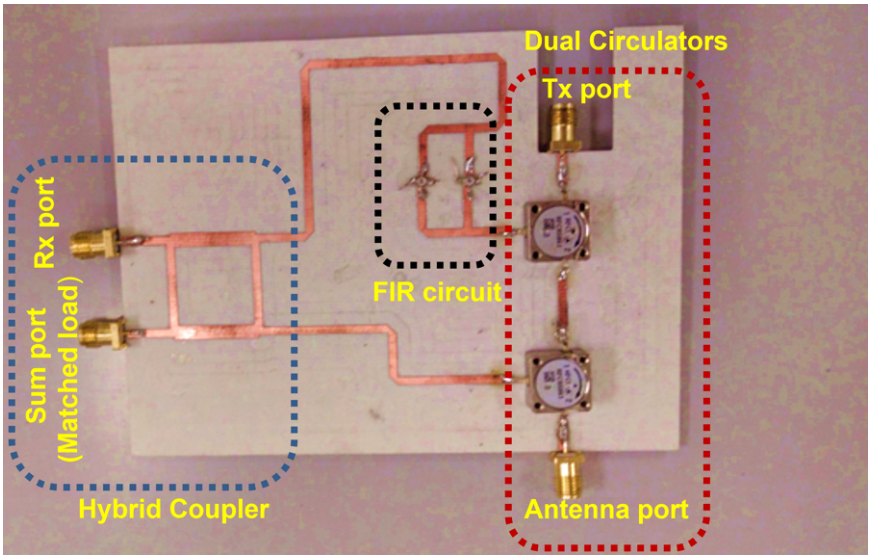


Figure 2.10: Fabricated prototype of the monostatic STAR system.

in Fig. 2.14. These measurements indicate an average isolation of 36 dB across 25 MHz. Since our circulator operates from 2.365 to 2.435 GHz, we have designed our filter and other circuit components across these operating frequencies. We measured a maximum Tx/Rx port isolation of 42dB and a minimum of 33 dB (on average, Tx/Rx port isolation of ∼37 dB is achieved from 2.395-2.42 GHz). Therefore, our system will work with any M-ary modulation with a bandwidth of up to 200MHz.

## 2.5 Comparison with Other State-of-Art STAR System

Table 2.1 compares the performance of our monostatic-stage STAR implementation with other state-of-the-art systems presented in the literature. Early monostatic STAR topologies initially used circulators to accomplish high isolation [MDTE20]. The most significant drawback of this approach is the loss of the Tx signal caused by the component's internal leakage. When no circulator is involved, other monostatic STAR implementations can achieve an isolation level of up to 55 dB [DSPV$^+$20]. For instance, by using an electrical duplex to substitute a circulator, these systems can

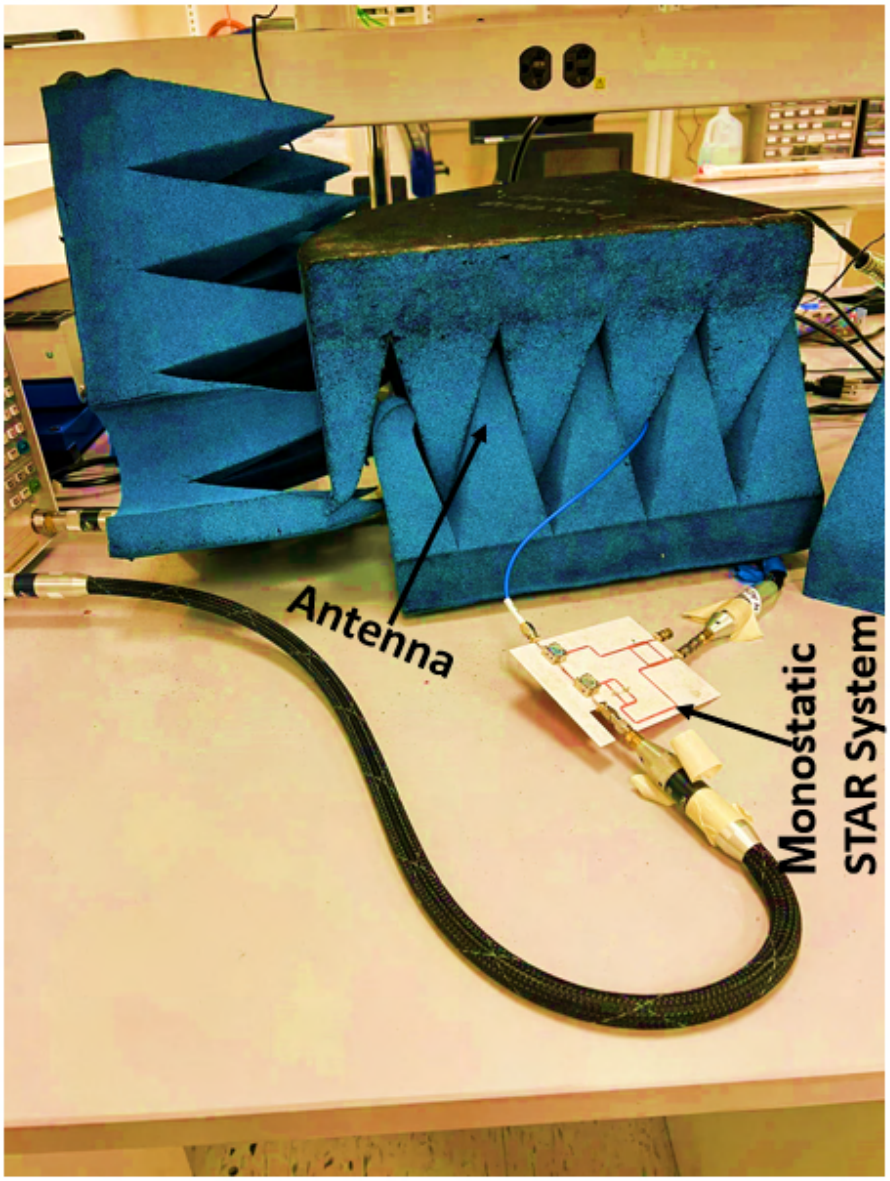


Figure 2.11: Measurement setup for testing the monostatic STAR system.

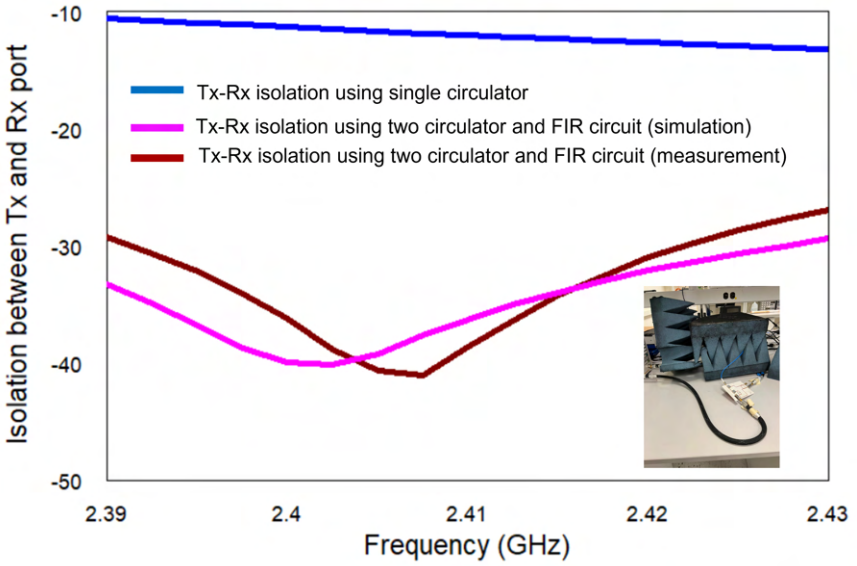


Figure 2.12: Measured vs. Simulated Tx-Rx isolation of the overall dual circulator and FIR architecture.

Figure 2.13: Tx-Rx isolation testing with active measurement.

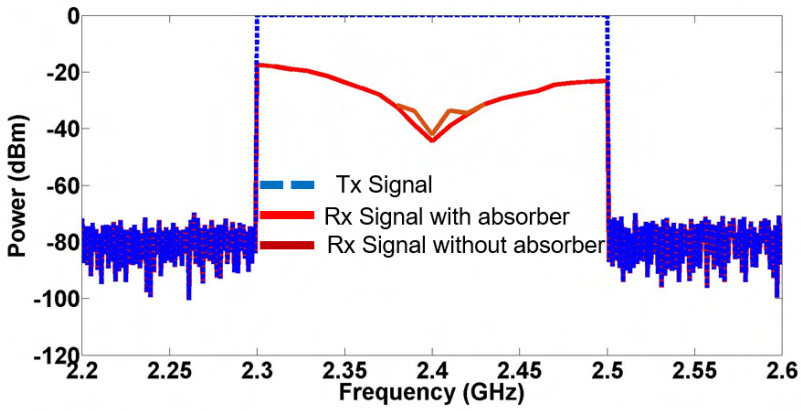


Figure 2.14: Tx-Rx signal in the monostatic STAR system showing a reduction by 36dB across 25MHz.

attain an isolation level of 60 dB across 26 MHz, as seen in [Kno12]. However, a considerable amount of Tx will be lost using this approach. Another technique for monostatic systems with high isolation is beamforming. However, this beam-informing approach results in significant Tx and Rx power loss [Kno12, HEPF17]. Alternatively, an impedance matching terminal (IMT) circuit, like the one in [KFSE18], can also be used, and it is constructed by employing the secondary signal to cancel the primary SI. While this work achieves 40 dB of isolation across a 65 MHz bandwidth, it must be noted that the IMT circuit requires a capacitor or an inductor, both impractical components for the higher frequencies. On the other hand, we have developed and implemented a monostatic cancellation system that uses the symmetric coupling cancellation technique while limiting the losses typically associated with circulator-based designs. This architecture marks the first time symmetry has been implemented utilizing several circuits, such as the two circulators and the FIR filter. Additionally, our FIR circuit offers low-profile characteristics as it was fabricated on a microstrip. Overall, our design can attain an average isolation of 36 dB, with a minimum of 33 dB and a maximum of 42 dB.

## 2.6 Conclusion

A power-efficient, monostatic RF-SIC system based on two circulators and a filter architecture is presented. This design operates across a 25 MHz bandwidth and achieves a coupling suppression between the transmit and receive ports of 37 dB (with a minimum of 35 dB and a maximum of 41 dB). While the two circulators offered isolation equal to 12 dB, the system's overall isolation was improved by implementing a symmetrical arrangement consisting of a two-tap FIR circuit and a second circulator placed in the middle. The second circulator with the filter allows for creating a quasi-replica of the leaked transmitted signal, resulting in sufficient isolation, high power efficiency, and a minimal power loss of the Tx signal. As a result, this setup brings the overall isolation up to 41 dB, which is a significant gain. Moreover, after experimental verification, our system achieved a cancellation that was measured to be 36 dB (with a minimum of 33 dB and a maximum of 42 dB). The disparity between simulation and measurement results is primarily attributable to the fabrication tolerance, exact phase balance of the hybrid coupler, and several other factors. Undoubtedly, this ground-breaking monostatic STAR system is a significant contender for the next generation of 5G connectivity.

CHAPTER 3

# WIDE BAND SELF INTERFERENCE CANCELLATION CIRCUIT

In the currently congested spectrum, in-band full-duplex (IBFD) wireless communication, also known as simultaneous transmit and receive (STAR), extends its benefits for spectrum allocation and reuse [Lar14, HBC+14, VAV18, SBL+17]. Indeed, an IBFD system can double the spectral efficiency by allowing concurrent transmission and reception at the same operational frequency. The implementation of the IBFD system is extremely challenging because of the strong self-interference (SI) that leaks from the transmitting to the receiving chains[LYJ+15, SGE17, WAKV15]. In many cases, the SI is $\sim$ 60–90dB stronger than the desired received signal [Ale19]. Typically, the SI includes coupled direct, noise, and reflected/multipath signals, in addition to harmonics from the power amplifier (PA). Therefore, it is very challenging to predict and suppress the SI below the receiver's noise floor [PEF17, KHFP12, HBC+14]. For instance, the noise floor for WiFi applications is about -90dBm. If the transmit power is 10dBm, then at least 100dB of self-interference cancellation (SIC) is necessary for the successful implementation of the IBFD communication system.

To achieve such a high SIC level, coupling suppression circuits are required at the transceiver's front-end, as depicted in Fig. 3.1. SIC circuits have been typically designed to achieve 1) passive antenna cancellation, 2) radio frequency (RF) cancellation, and/or 3) digital cancellation. Examples of passive cancellation techniques employ decoupling circuits between antenna elements[PEF17, HAV20, EEF16b], beamforming architectures [KHFP12, SSE+20], or circulators [KFSE18, Kno12, TRA21]. Typically, the first two techniques employ multiple antenna elements, implying increased hardware complexity. Alternatively, a single antenna is used in STAR systems using a circulator between the transmit and receive chains. However, commer-

cially available circulators have a limited port-to-port isolation of 25dB[Kno12]. In our previous work, we used a combination of two circulators and an SIC circuit. The topology yielded an average isolation of 55dB across a 20MHz bandwidth [TRA21].

Larger SIC has been reported across much smaller bandwidths. In [CJS+10], researchers implemented a multi-antenna system with 60dB isolation over 5MHz of bandwidth. In [BJK14], a 16-tap filter consisting of multiple fixed delay lines and an attenuator are used to achieve 47dB SI cancellation across a narrow band of 80MHz. A time-domain narrowband cancellation employing a filter with four tap delay lines and attenuators was able to show 30dB of cancellation over a bandwidth of 30MHz in [KMP16]. In [Weg14], a 30dB decrease in Tx/Rx coupling over 110MHz was achieved using two narrow-band tunable resonators in the antenna array's near-field. A finite impulse response (FIR) filter was used in another STAR design to provide 25dB of cancellation across 500MHz [VAV18]. The bandwidth of this device was eventually increased to 1GHz by cascading multiple FIR filters[VHAV19]. However, this cascading technique requires more space and increased hardware complexity. In another study [RBVV21], a filter bank concept is introduced in the design of the ultra-wideband (UWB) RF-SIC filter to produce 20dB of cancellation across a 1GHz bandwidth. However, using a filter bank implies increased coupling and hence less isolation.

In our previous study, we developed a novel hybrid 6-tap FIR and resonator design to achieve >25dB cancellation across 500MHz [THG+22]. In this chapter, we extend the design of our FIR-resonator circuit [THG+22], depicted in Fig. 3.2, to operate across 800MHz bandwidth. A prototype is fabricated and tested from 1GHz to 1.8GHz, for L-band applications [WLK11, vNDRB+03]. Notably, the L-band is used for satellite navigation, mobile service, aircraft surveillance, as well as digital audio and multimedia broadcasting. In our study, we used a single FIR resonator

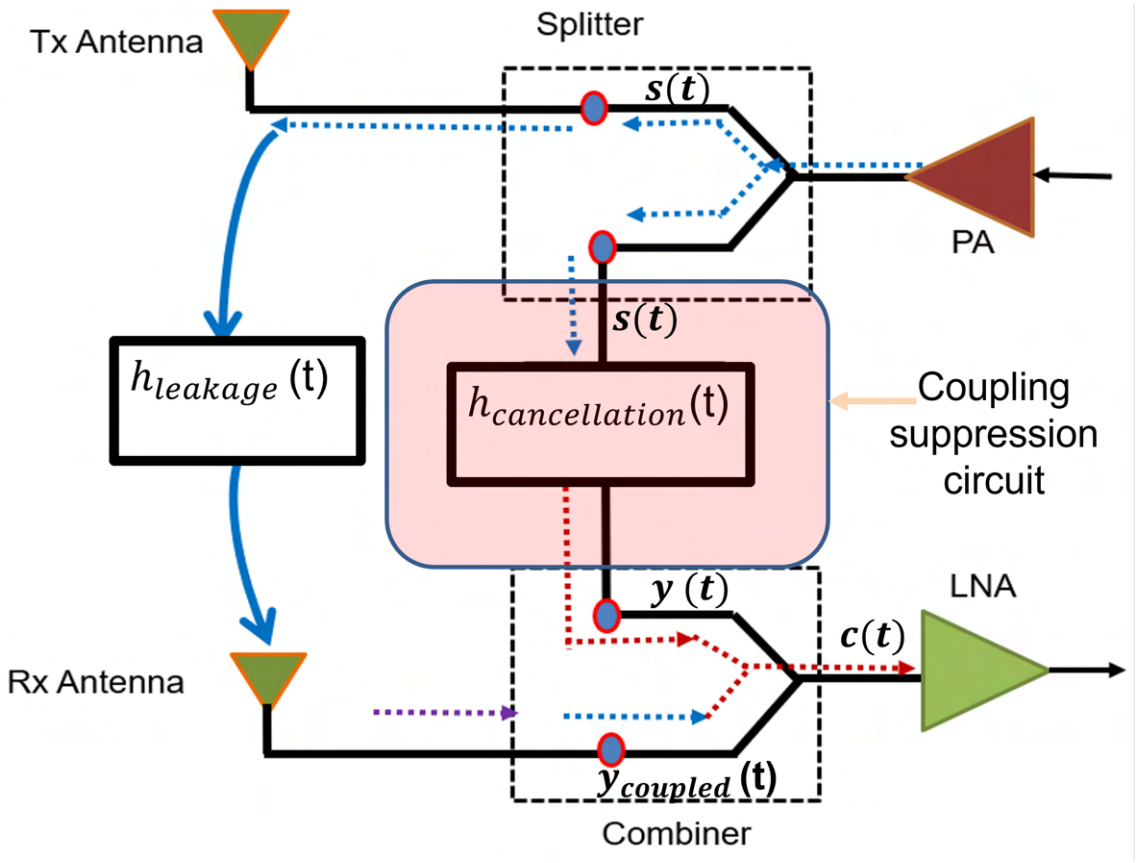


Figure 3.1: A bi-static STAR system with a cancellation filter implemented at the analog stage.

that achieved a minimum of 15dB to a maximum of 27dB cancellation. To our best knowledge, this is the first SIC circuit based on an FIR resonator topology to cover such a large bandwidth using a simple and low-cost design.

## 3.1 Channel Modeling and RF coupling Suppression Technique

The analog SIC stage, shown in Fig. 3.1, consists of a power splitter at the transmitter, an RF-SIC circuit, and a power combiner at the receiver. As such, the transmit (Tx) signal is equally split into two signals, both denoted as $s(t)$, where

one signal is fed to the Tx antenna and the other one is fed to the cancellation circuit. Notably, the RF-SIC circuit is designed and optimized to have an impulse response $h_{cancellation}(t)$ that conjugately matches the impulse response $h_{leakage}(t)$ of the coupling channel between the Tx and receive (Rx) antenna. Since the scattering parameters are related to the channel impulse response, using [3]:

$$h_{leakage}(t) = \frac{S(2,1)(1-\Gamma_L)(1-\Gamma_S)}{(1-S(1,1)\Gamma_L)(1-S(2,2)\Gamma_S) - S(2,1)\Gamma_L S(1,2)\Gamma_S} \tag{3.1}$$

Where $\Gamma_L$ and $\Gamma_S$ are the reflection at the source and load of the two-port network formed by the Tx and Rx ports. Under matching conditions, $\Gamma_L = \Gamma_S = S(1,1) = S(2,2) = 0$. Hence, (3.1) become

$$h_{leakage}(t) = S(2,1) \tag{3.2}$$

The coupled signal $y_{coupled}(t)$ at the Rx antenna is expressed as,

$$y_{coupled}(t) = s(t) * h_{leakage}(t) \tag{3.3}$$

Similarly, the signal $y(t)$ at the output of the RF-SIC circuit is expressed as,

$$y(t) = s(t) * h_{cancellation}(t) \tag{3.4}$$

Hence, at the combiner output of the receiver chain, we get

$$c(t) = s(t) * h_{leakage}(t) + s(t) * h_{cancellation}(t) \tag{3.5}$$

which can be rearranged such as

$$c(t) = s(t) * (h_{leakage}(t) + h_{cancellation}(t)) \tag{3.6}$$

To achieve maximum suppression of the coupled signal, we need to minimize $c(t)$. Ideally, we need $c(t) \approx 0$. That is,

$$h_{leakage}(t) + h_{cancellation}(t) = 0 \tag{3.7}$$

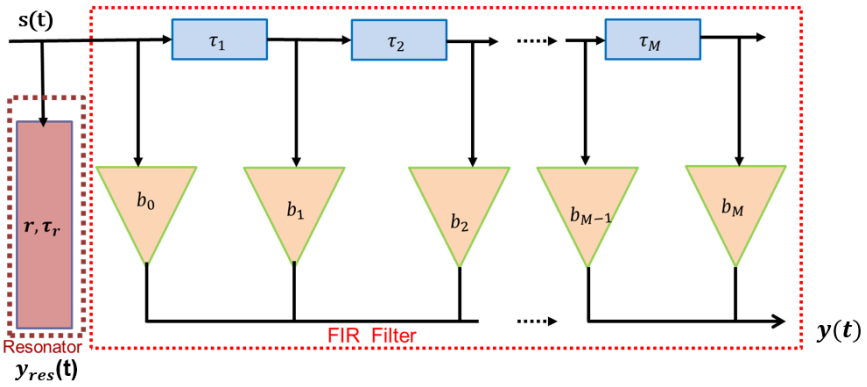


Figure 3.2: A multi-tap FIR-resonator circuit for wideband RF coupling suppression.

or

$$h_{leakage}(t) = -h_{cancellation}(t) \tag{3.8}$$

By taking the Fourier Transform (FT) [Bra12] of (3.8), we obtain,

$$\int_{w_{low}}^{w_{high}} h_{cancellation}(t)e^{-j\omega t}dw = -\int_{w_{low}}^{w_{high}} h_{leakage}(t)e^{-j\omega t}dw \tag{3.9}$$

Hence,

$$H_{cancellation}(j\omega) = -H_{leakage}(j\omega) \tag{3.10}$$

From (3.10), we conclude:

$$\mid H_{cancellation}(j\omega) \mid = \mid H_{leakage}(j\omega) \mid \tag{3.11}$$

and

$$\angle H_{cancellation}(j\omega) = 180^\circ + \angle H_{leakage}(j\omega) \tag{3.12}$$

In this chapter, we present a novel RF-SIC circuit based on a series combination of FIR circuit taps and a stub resonator with a frequency response $H_{cancellation}(j\omega)$ that satisfies (3.11) and (3.12). We note that, in the digital domain, the FIR filter is realized by a series of delays lines $(\tau_1, \tau_2, ....\tau_M)$ and tap coefficients $(b_0, b_1, ...b_M)$ [Bra12]. In the analog domain, RF microstrip delay lines and attenuators realize

tap delays and coefficients, respectively. A microstrip open stub acts as a resonator with an impulse response:

$$h_{resonator}(t) = r\delta(t - \tau_r) \tag{3.13}$$

where $r$ and $\tau_r$ are the coefficient and time delay of the resonator filter, respectively. Hence, referring to Fig. 3.2, at the output of the resonator filter, the signal is:

$$y_{res}(t) = s(t) * h_{resonator}(t) = rs(t - \tau_r) \tag{3.14}$$

The cascade impulse response of the hybrid FIR resonator can be expressed as

$$h_{cancellation}(t) = rb_0\delta(t - \tau_r) + rb_1\delta(t - \tau_1 - \tau_r) + ..... + rb_M\delta(t - \tau_M - \tau_r) \tag{3.15}$$

Hence, the filter signal $y(t)$ at the output of the FIR, the resonator can be written as:

$$y(t) = s(t)*h_{cancellation}(t) = rb_0s(t - \tau_r)+rb_1s(t - \tau_1-\tau_r)+.....+rb_Ms(t - \tau_M - \tau_r) \tag{3.16}$$

or

$$y(t) = rb_0s(t - \tau_r) + \sum_{k=1}^{M} rb_ks(t - \tau_k - \tau_r) \tag{3.17}$$

The transfer function of the FIR resonator is computed using the Fourier transform [Bra12] of its impulse response given by (3.17):

$$H_{FIR-Resonator}(j\omega) = re^{-j\omega\tau_r}(b_0 + \sum_{k=1}^{M} b_ke^{-j\omega\tau_k}) \tag{3.18}$$

Using an additional resonator within the FIR topology fundamentally changes how the FIR filter behaves across a wide bandwidth. (3.18) shows how the addition of the resonator affects the FIR response and introduces additional degrees of freedom for the approximation of the signal to be canceled across a wider bandwidth.

The innovation comes from a filter bank having individual FIR responses, which are superimposed with one another. At the same time, an FIR resonator accomplishes better performance with a single FIR response, including the resonator's contribution, as shown in (3.18).

The goal is to find the solution for the delay taps $(\tau_1, \tau_2, ....\tau_M)$, tap coefficients $(b_0, b_1, ...b_M)$, and the resonator parameter $(r,\ \tau_r)$ in such a way that the FIR resonator response conjugately matches the channel response (SI coupling response) to achieve maximum SIC cancellation.

The SIC is computed as follows [VAV18].

$$SIC_{dB} = 20\log_{10}[\frac{1}{2 \mid H_{leakage}(j\omega) \mid^2}(\mid H_{leakage}(j\omega) \mid^2 + \mid H_{cancellation}(j\omega) \mid^2 +2 \mid H_{leakage}(j\omega) \mid \times \mid H_{cancellation}(j\omega) \mid \cos(\angle H_{cancellation}(j\omega) - \angle H_{leakage}(j\omega)))]^{\frac{1}{2}} \tag{3.19}$$

## 3.2 Analog Stage Architecture for RF Coupling Suppression

### 3.2.1 Antenna Design

This chapter considers a two-element monopole antenna, one for Tx and another for Rx, as depicted in Fig. 3.3. Details of the antenna design, fabrication, and testing are provided in our previous work[THG+22]. Figs. 3.4 and 3.5 show the channel coupling response (*viz.* magnitude and phase of the transmission coefficient $S_{21}$) between the Tx and Rx antennas measured from 1 to 1.8GHz. The goal is to design an SIC FIR resonator filter with a frequency response that conjugately matches the

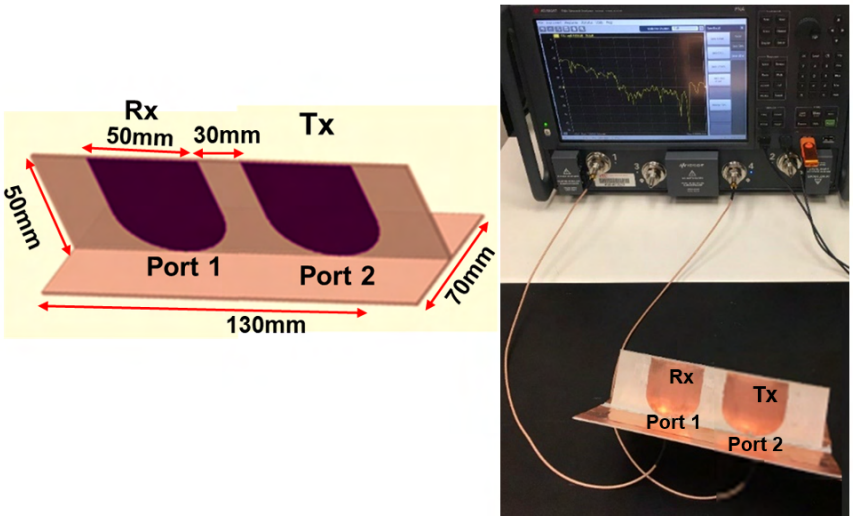


Figure 3.3: Fabricated prototype and two-port measurement setup of the two-element monopole array [THG+22].

channel coupling response of the antennas by optimizing the coefficients and delays in (3.17) or (3.18).

### 3.2.2 Filter Stage

The antenna response determines how the filter step will be implemented. An antenna's response can be weakly linear or completely non-linear. We can conduct regression analysis in a manner that is determined by the behavior of the antenna response. Both linear and non-linear approaches may be used using regression analysis. In this particular instance, the antenna's behavior is weakly linear in character. For this reason, we have performed a linear regression analysis [RBVV21]. The antenna response and the first and second-order errors are shown in Fig. 3.6. The divergence of the antenna response from the linear phase approximation is referred to as first and second-order errors. The second-order divergence in linear regression determines the filter stage [RBVV21]. As observed, to achieve SIC cancellation

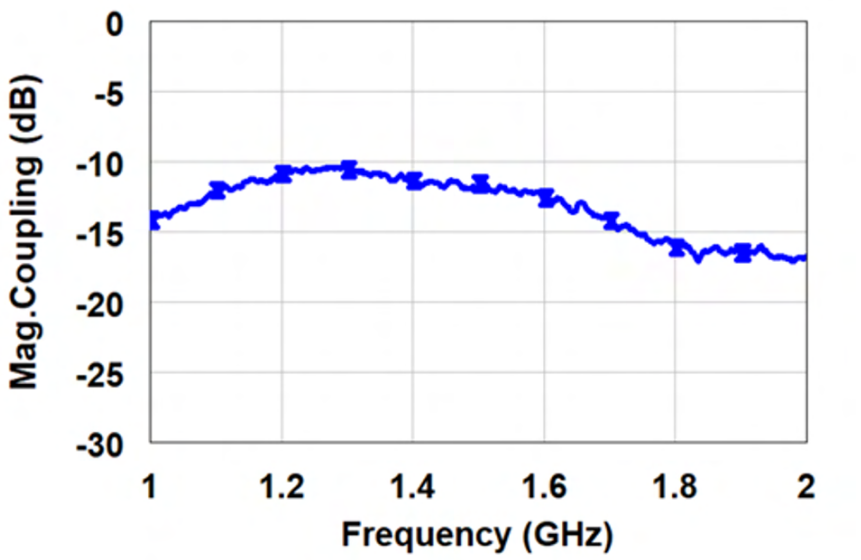


Figure 3.4: Measured magnitude of the coupling channel ($S_{21}$) between the Tx and Rx antennas [THG+22].

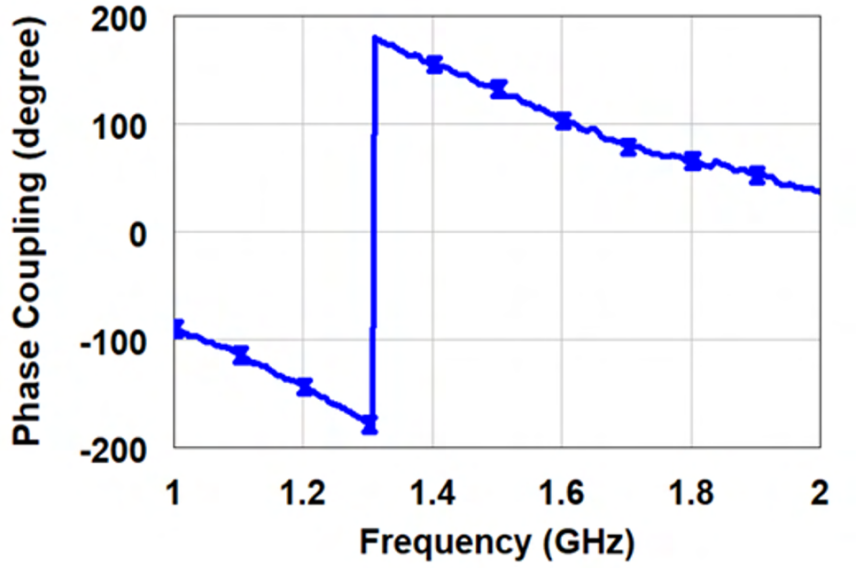


Figure 3.5: Measured phase of the coupling ($S_{21}$) between Tx and Rx antenna [THG+22].

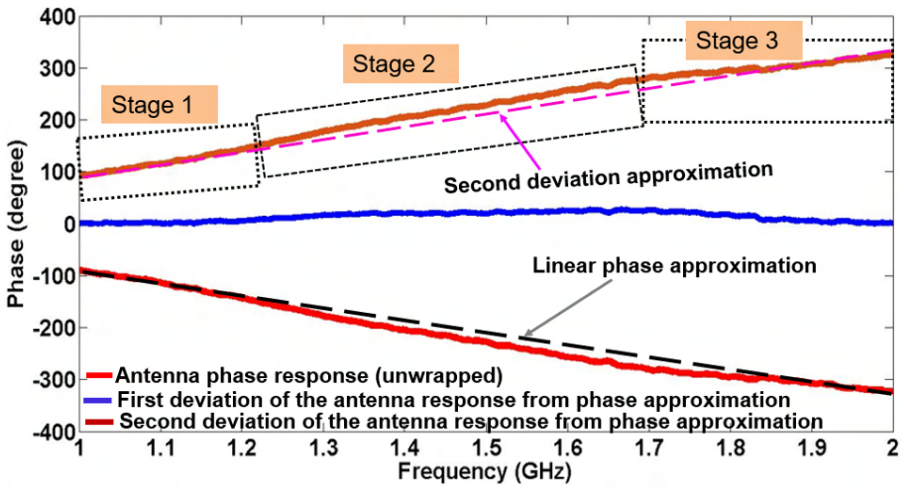


Figure 3.6: Estimation of the filter stage from regression analysis.

throughout 800MHz, we need a filter with three stages. However, we conducted broadband cancellation in this investigation by substituting the filter bank with an FIR resonator. It is also important to note that the assessment of cancellation is necessary since we do broadband cancellations. As illustrated in Fig. 3.7, the amplitude and phase matches between the FIR resonator response and that of the antenna coupling need to be within 1.57dB and 5.27°, respectively, to obtain a cancellation level of 21dB over a broad bandwidth.

### 3.2.3 Circuit Optimization of the FIR-Resonator Filter

We considered a 6-tap FIR-resonator filter (see Fig. 3.2 for the circuit and Fig. 3.8 for the microstrip layout). In this section, we only considered the circuit layout and used the Differential Evolution (DE) optimization algorithm. Notably, DE performs well with multi-variable optimization if the specified problems have a well-tuned solution and there is no need for an initial estimate [DS10a]. Optimization was conducted from 1 to 1.8GHz. The filter taps weighted coefficients were found to be $b_k = \{0, 12, 7, 12, 5, 3\}$dB with time delay values $\tau_k = \{15, 109, 10.3, 10.6, 5\}$ps

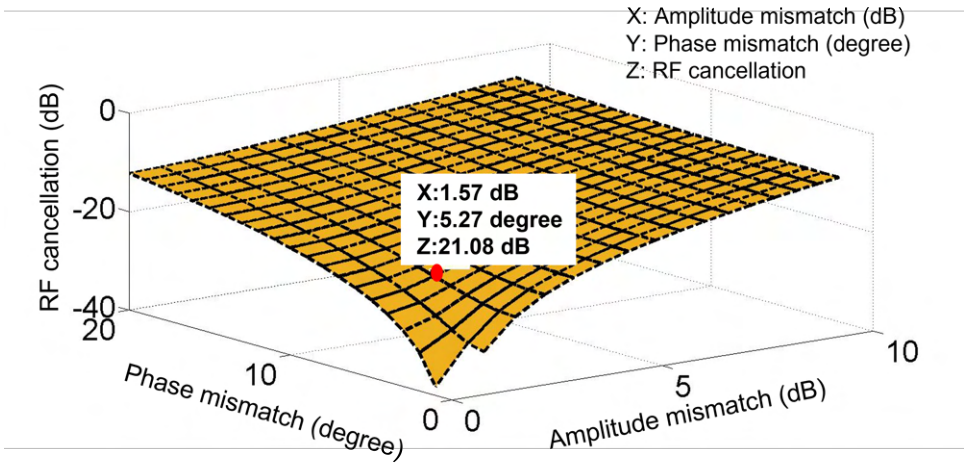


Figure 3.7: Estimation of the RF-SIC cancellation.

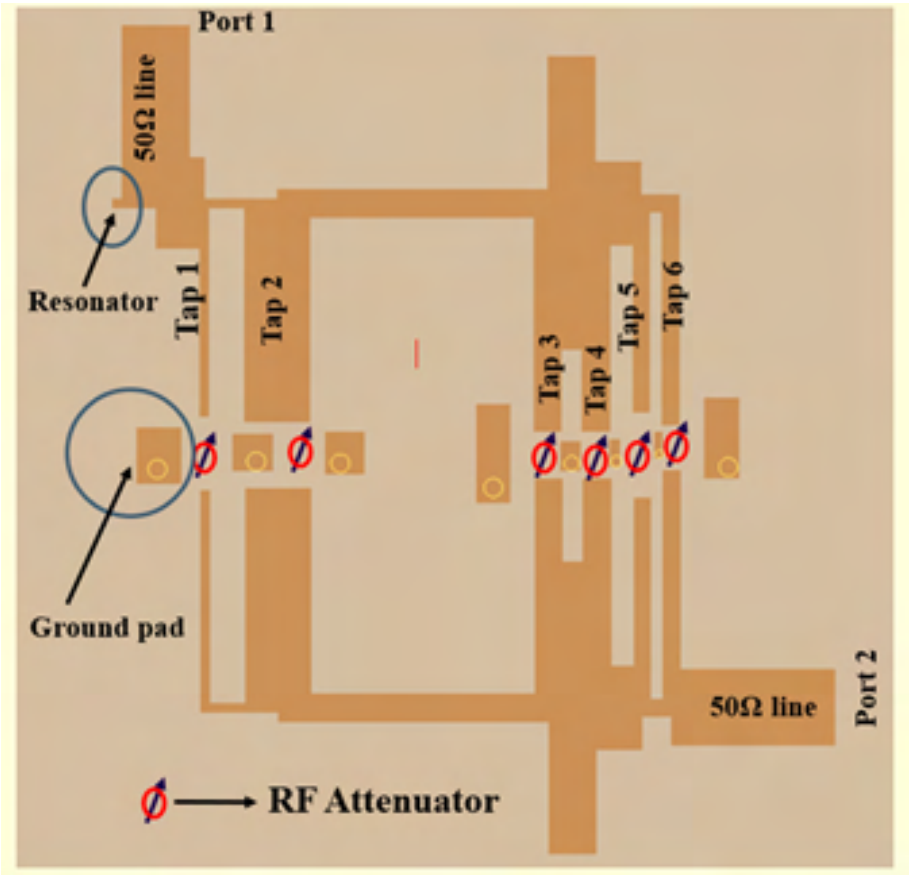


Figure 3.8: EM layout of a hybrid FIR-resonator.

at center frequency (*viz.* 1.4 GHz). Also, the resonator's parameters were found to be $r = 0$dB and $\tau_r = 4$ps. Using these values, the response of the FIR-resonator is compared against the measured antenna coupling response. As shown in Figs. 3.9 and 3.10, the FIR resonator responses (magnitude and phase) closely match the antenna coupling response. Based on the antenna and FIR-resonator response, SIC was computed using (3.19). Results are plotted in Fig. 3.11, showing an average of 22dB of SIC across 800MHz.

### 3.2.4 Electromagnetic (EM) Simulation of the FIR-Resonator

The EM layout of the FIR-resonator circuit, based on the circuit optimization, is depicted in Fig. 3.8. Microstrip transmission lines and attenuators notably replaced time delays and tap coefficients. Specifically, the minimum thickness of the trace line for the cooper layer is .5mm. A resonator is added by inserting an open stub at the beginning of the copper trace of the FIR-resonator. Six lumped attenuators representing surface mount components are inserted on each tap of the FIR-resonator. The purpose of the lumped attenuator is to adjust the gain for approximating the channel coupling. Notably, the filter is matched to 50-$\Omega$ at the input and output ports. The length of the resonator is 0.5mm$\times$0.5 mm, while the length of the FIR filter is 44 mm$\times$37mm. The area of the resonator is 0.015% of the size of the FIR filter's area. Notably, if we only consider the FIR resonator, the total size is 1628.25mm$^2$. Conversely, using a filter bank with two filters, the size is 3256mm$^2$. As such, using an FIR resonator reduces the size of the circuit by nearly half in comparison to the FIR filter bank. In addition, they are using a higher dielectric constant ($\epsilon_r = 9.2$), resulting in a lower footprint of the SIC circuit design.

We note that, in this simulation, we considered the $S$-parameters of actual components provided by vendors. Here also, the DE optimizer was used to fine-tune

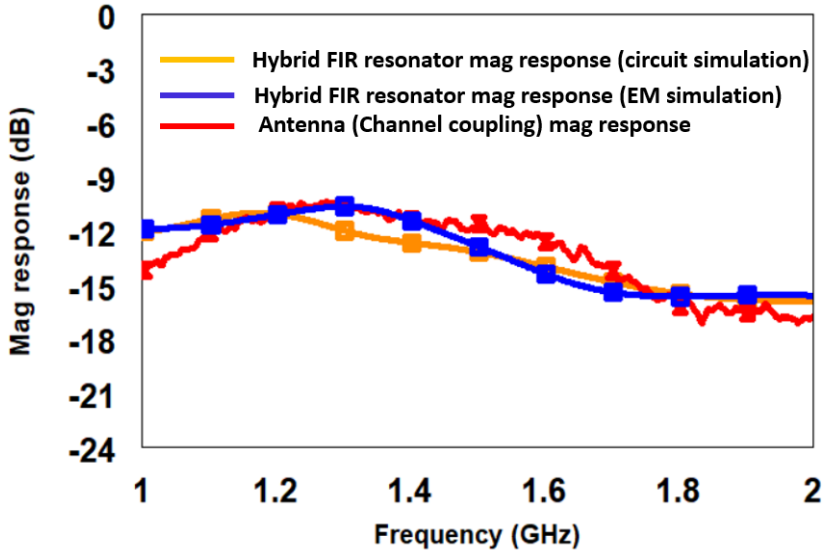


Figure 3.9: Simulation results showing the magnitude of the simulated hybrid FIR-resonator circuit vs. the channel magnitude response.

the layout to match the antenna coupling response closely. Figs. 3.9 and 3.10 show the EM layout's simulated magnitude and phase response. Fig. 3.11 shows that an average 22dB of RF coupling suppression was achieved across 800MHz in EM simulation.

## 3.3 Fabricated FIR-Resonator

The FIR-resonator was fabricated using low-cost commercial off-the-shelf (COTS) components on a $TMM10$ substrate from Rogers company with $\epsilon_r = 9.2$ and $h =$ 60mil (*viz.* 1.5mm). The total dimension of the SIC circuit is $44mm \times 37mm$. The fabricated prototype is shown in Fig. 3.12. We used Mini circuits PAT series attenuators (PAT 0dB, 12dB, 7dB, 12dB, 5dB, 3dB). A two-port vector network analyzer (VNA) measured the fabricated FIR-resonator prototype. The estimated magnitude and phase response are depicted in Fig. 3.13 and 3.14, respectively. The

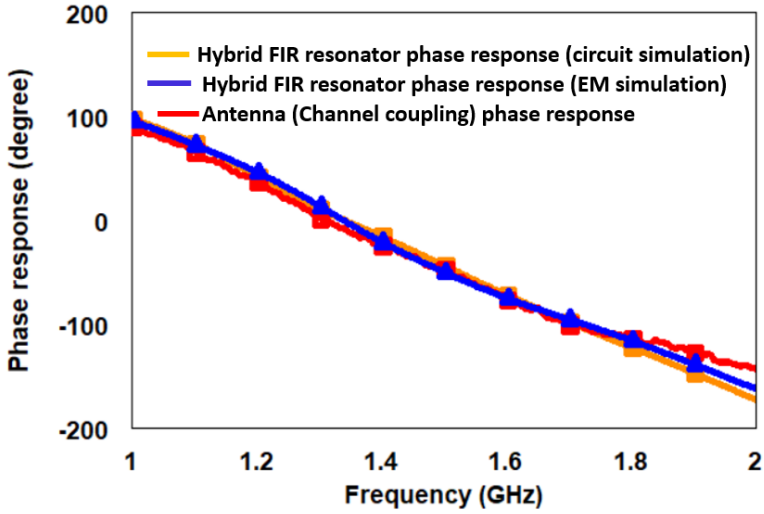


Figure 3.10: Simulation results showing the simulated hybrid FIR-resonator circuit phase of the simulated hybrid FIR-resonator circuit vs. the channel's conjugate phase.

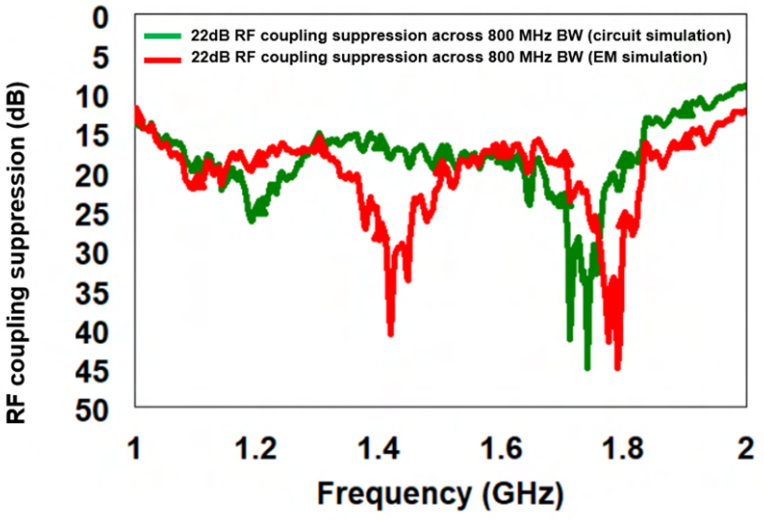


Figure 3.11: Simulation results showing an average of 22dB cancellation across 800MHz.

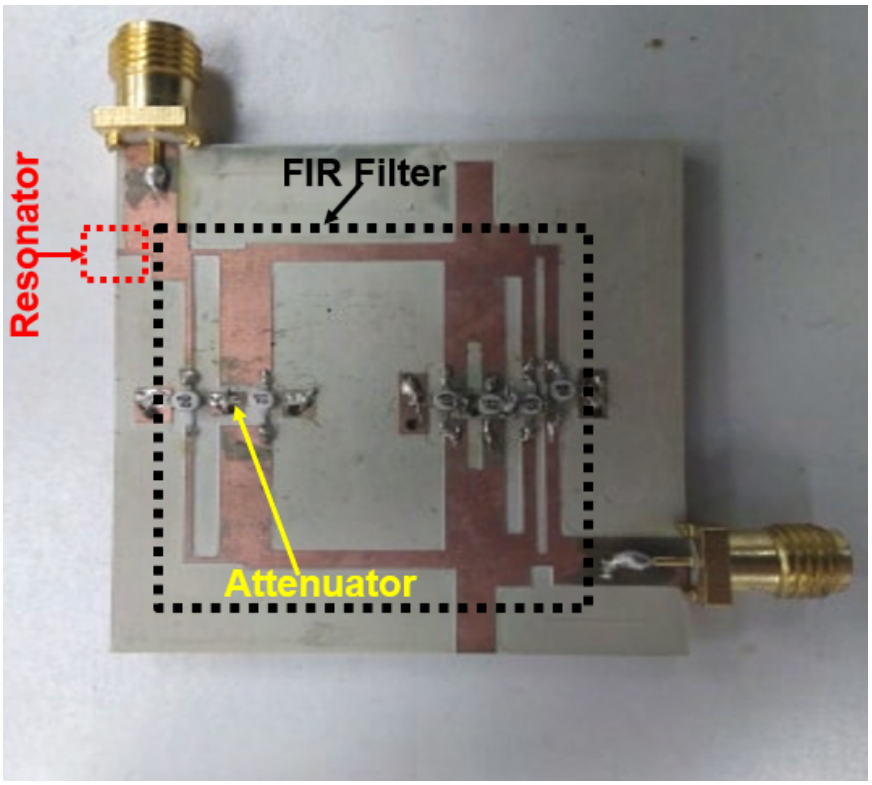


Figure 3.12: Fabricated FIR-resonator prototype.

results are in good agreement with the simulation ones. This implies 20dB SIC cancellation across 800MHz, as shown in Fig. 3.15.

## 3.4 Antenna and FIR resonator

In this study, we connected the antenna shown in Fig. 3.3 to the RF-SIC circuit. Doing so, 33dB isolation is obtained across 800 MHz, as illustrated in Fig. 3.16. As expected, the antenna isolation contributed to an additional isolation of 11 dB [THG+22].

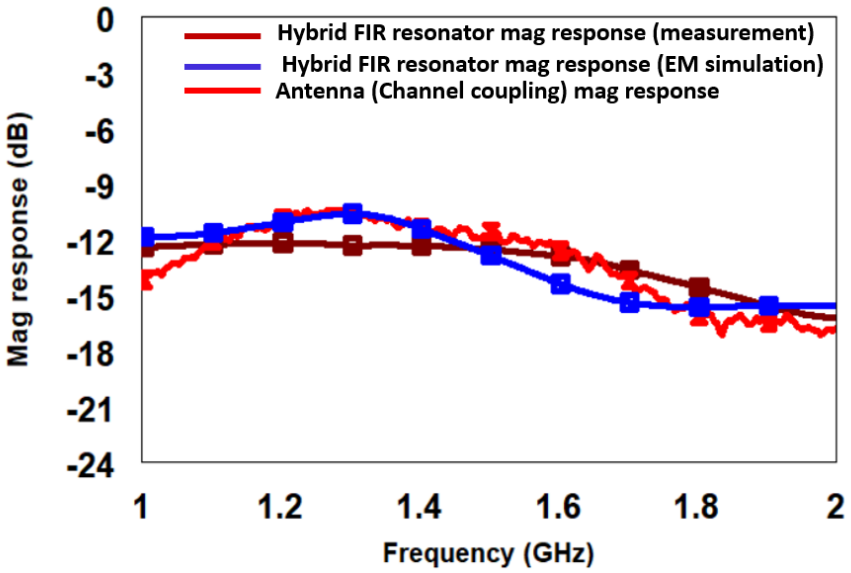


Figure 3.13: Measured results showing the magnitude of the fabricated hybrid FIR-resonator circuit and the complex conjugate of the channel.

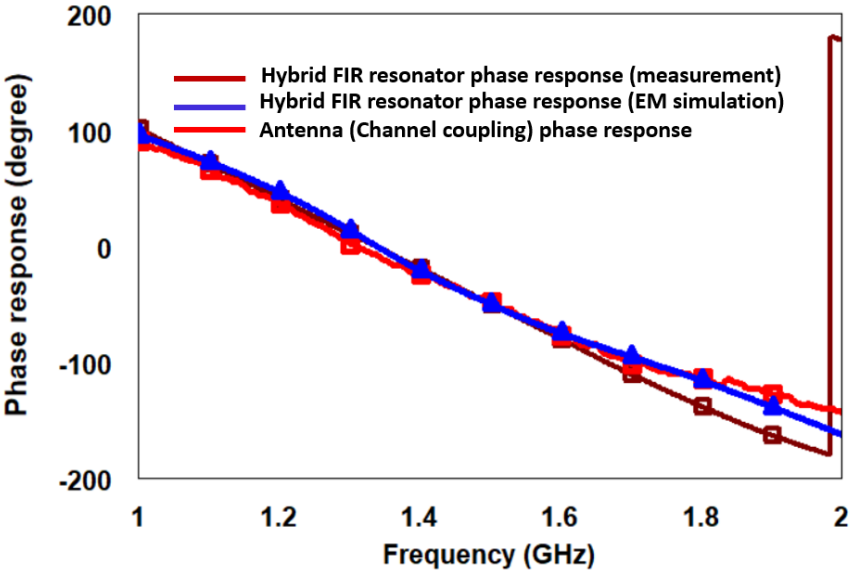


Figure 3.14: Measured results showing the phase of the fabricated hybrid FIR-resonator circuit vs. the channel's conjugate phase response.

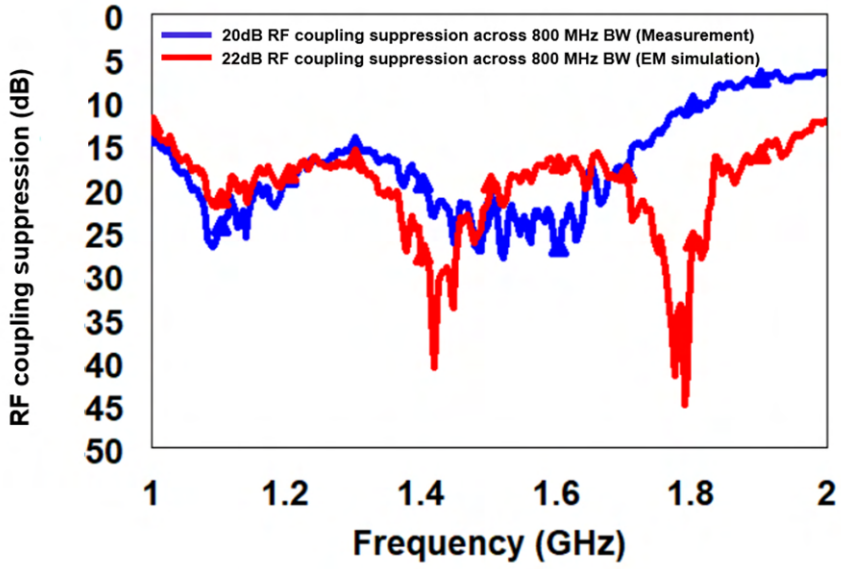


Figure 3.15: RF coupling suppression calculated using measured results vs. EM simulations, showing an average of ≈ 20dB cancellation across 800MHz.

Table 3.1: Performance comparison with the state-of-the-art STAR SIC filters in RF domain.

| Reference | Bandwidth | TX-RX isolation | Technology |
|---|---|---|---|
| [VAV18] | 500MHz | 25dB | FIR filter |
| [CJS+10] | 5MHz | 20dB | QHx220 chip |
| [BJK14] | 80MHz | 47dB | 16 tap filter |
| [KMP16] | 30MHz | 30dB | Multitap RF canceller RF canceller |
| [Weg14] | 100MHz | 30d | Near field filter |
| [VHAV19] | 1GHz | 25dB | Filter bank (Multiple FIR filters) |
| [RBVV21] | 1GHz | 20dB | 3 stage filter bank |
| This work | 800MHz | 22dB | FIR resonator (single circuit), no filter bank, and no coupling exist. |

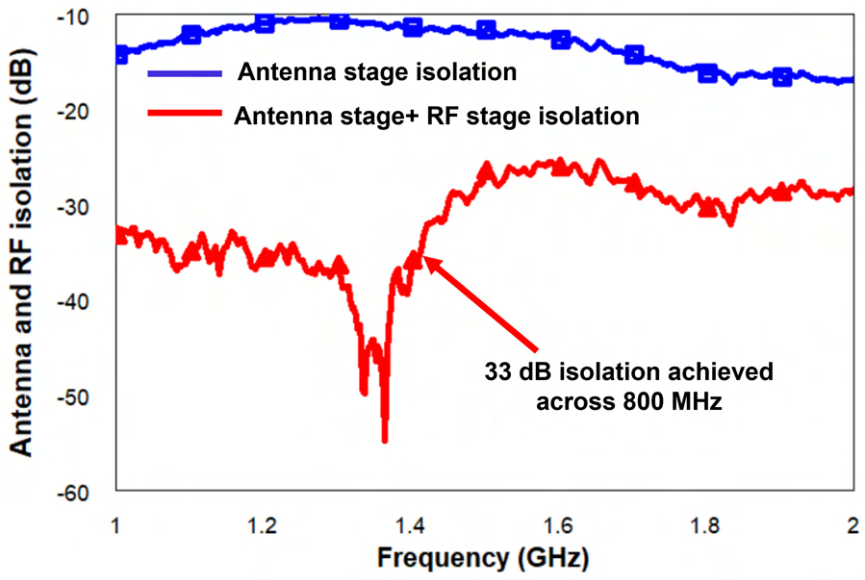


Figure 3.16: Antenna and RF isolation

## 3.5 Comparison with Other State-of-Art RF-SIC Filter

Table 1 shows a performance comparison of the RF-SIC with other state-of-art self-cancellation topologies. With the early STAR RF-SIC approaches it is possible to cancel up to 20dB for extremely narrowband signals with a bandwidth of 5MHz [CJS+10]. Other realizations of the STAR RF-SIC filter achieved the cancellation of up to 47dB over an 80MHz bandwidth [BJK14]. Undoubtedly, each of these methods was narrowband. Research on wideband RF STAR filters, on the other hand, has shown a 25dB cancellation over 500MHz by only implementing an FIR filter[VAV18]. In another research [VHAV19, RBVV21], RF isolation of up to 22dB was achieved by creating a filter bank while simultaneously increasing the bandwidth to 1GHz. However, implementing this approach results in complicated circuitry and creates coupling between the many filters. As part of our research, we have developed a simple FIR resonator that is capable of offering a cancellation of 22dB over 800MHz. In addition to the wideband cancellation, it boasts low-profile characteristics due to

using a simple resonator instead of a filter bank. The FIR resonator accomplishes a nearly 50%

## 3.6 Conclusion

We presented a simple, low-profile RF-SIC circuit for IBFD systems that achieves 20dB of interference suppression across 800MHz bandwidth. The circuit uses a hybrid multi-tap FIR filter with a resonator stub. A prototype was fabricated and tested to validate the design. To our knowledge, this simple design was the first to achieve RF-SIC cancellation across such a large bandwidth.

CHAPTER 4

# BI-STATIC STAR SYSTEM

Current electromagnetic spectrum (EM) is too congested to facilitate a continuous frequency spectrum for ultra-wideband (UWB) communication [Lar14, HBC +14, VAV18, SBL +17]. This limitation has spurred the necessity for efficient spectrum access techniques such as in-band full-duplex (IBFD) or simultaneous transmit and receive (STAR) [LYJ +15, SGE17, WAKV15]. The latter enables a cellular network to transmit and receive simultaneously over the same frequency band [Ale19]. As such, STAR enables frequency re-use. Hence, the spectral efficiency is doubled. Since the existing RF spectrum is very costly, greater spectrum efficiency in the STAR system implies significant cost reduction for spectrum licensing [HAV20].

The key challenge to realizing STAR systems is mitigating self-interference (SI) [HVAV18, EEF16b]. The latter refers to the high-power transmit a signal that couples to the receiver port, which is typically $\sim$ 100 dB stronger than the received signal, and causes receiver desensitization [HBC +14]. To circumvent this issue, typical communication systems have adopted different methods such as time-division duplexing (TDD) or frequency division duplexing (FDD) [SBL +17, PS98, Don07, ENS97, HHLT00]. However, these duplexing schemes exploit orthogonality of time/frequency resources at the expense of spectral efficiency [BVAV17]. In brief, TDD and FDD occupy double the time and frequency, respectively. In addition, TDD requires stringent time/phase synchronization to realize full-duplex, whereas FDD uses an extra guard band beyond its dedicated transmit (Tx)/Receive (Rx) frequencies.

Alternatively, doubling the spectral efficiency can be achieved using STAR systems [SSG +14]. The successful implementation of these systems requires high isolation between transmitter and receiver of as much as 100 dB [SSG +14, LSYB17,

BMK13, HVAV18, AHV16, HAV17]. To do so, we must 1) cancel the transmit signals that directly couple to the receiver chain, 2) suppress harmonics from power amplifiers (PAs), and 3) eliminate coupled noise from the Tx chain. Further, advanced STAR circuits are needed to remove multipath reflected signals. Notably, coupled interference suppression from nearby transmitters should be enacted adaptively to unlock the impact of dynamically varying environments. So far, STAR implementations have overcome unwanted SI by implementing multiple stages of coupled signal suppression techniques across the receiver chain. As such, SI cancellation was achieved in 1) propagation domain, 2) analog domain, and 3) digital domain [KPH19]. Propagation domain cancellation was accomplished by employing techniques such as cross-polarization of Tx/Rx antenna or Tx beamforming [CD12, LGL11, WJAM17, ZL19]. Notably, these techniques have shown that SI becomes even higher in the case of an antenna array. Therefore, the interfering signal must be sufficiently canceled at subsequent RF and baseband stages to realize an efficient STAR system. Analog stage cancellation incorporates an RF filter to cancel the replica of the transmit signal from the receiver chain [BVAV17, SWA$^+$15, WAKV15]. However, analog self-interference cancellation (SIC) needs to achieve enough cancellation to preserve the analog-to-digital converter (ADC) dynamic range (DR). For a linear ADC, the DR is calculated using DR=6.02n +1.76 (dB) [SO89]. Hence, assuming a 12-bit ADC (including a 2-bit margin), the dynamic range is 62 dB. Therefore, we require 48 dB of analog suppression to achieve a total of 110 dB cancellation. The digital domain involves probabilistic modeling of the propagation channel for post-processing the digitized signal to further reduce the SI in the receiver chain [GRT$^+$19].

However, most of these STAR topologies have only been applied to narrowband signals (*viz.* <100 MHz) [KGK11b, DS10b, LM15, Weg14]. Frequency selectiv-

ity at the antenna interface limits the SIC bandwidth. Conventional RF canceller mimics at a single frequency point, limiting the SIC bandwidth to achieve infinite cancellation. To extend the SIC bandwidth, we must mimic the SI signal at several frequencies for wideband SIC cancellation. In a recent work [LM15], an RF front-end for a full duplex radio system with three antennas (ATRX1, ATRX2, and ARXD) is presented. The transmitting signal is first fed to a rat race coupler with two output transmit antennas (ATRX1 and ATRX2). The transmit signals at ATRX1 and ATRX2 are summed out of phase at the differential port of the rat race coupler and fed to the receive antenna port (ARXD). Two SI reference generators are implemented at the receiver side to further reduce the residual signal by 60 dB across 80 MHz. Our work employed one TX and 2 RX antennas with one splitter, two directional couplers, one hybrid coupler, and two custom-made SIC FIR resonators. Our design achieves 52 dB across 500 MHz. Furthermore, our work uses direct coupling in the RF domain instead of residual signals in the time domain used in [LM15]. We note that direct coupling provides more cancellation across a wider bandwidth. In [Weg14], two narrowband tunable resonators were used in the antenna array near field to provide a 30 dB reduction in Tx/Rx coupling across 110 MHz.

Recently, researchers have been working on fully integrated RFIC incorporating SIC for the STAR system. In [ZCDK15], a multiple-stage bandpass filter (BPF) is implemented using nanoscale CMOS technology for SI cancellation in the RF domain. Tunability, reconfigurability, and high Q are the favorable features for this CMOS implementation. However, this technique can achieve 20 dB of SIC across a 20 MHz bandwidth (BW). A CMOS transceiver is implemented with 65 dB deep Tx SI cancellation across 80 MHz in another study [CKZ+18]. In [NGA+21], a seven-tap RF canceller with time-interleaved switched capacitor delays is designed in a 65 nm CMOS platform. However, this technique can operate in narrow BW

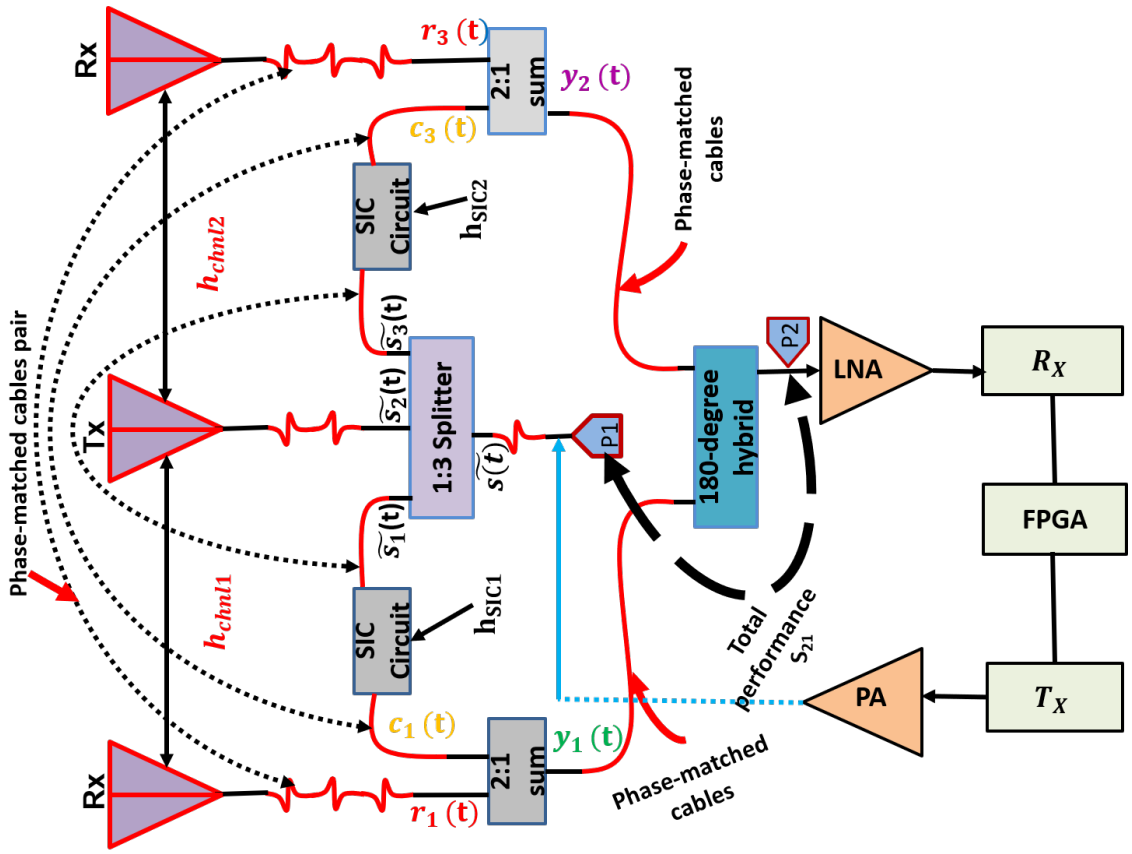


Figure 4.1: A two-stage wideband STAR system operating across 500 MHz. The architecture is based on symmetric coupling suppression at the antenna stage, followed by two SIC circuits and a hybrid coupler. The total SIC is up to 52 dB.

and provides an average of 32.5 dB cancellation across 20 MHz BW.

Multi-tap finite impulse response (FIR) filters were also implemented for SI. Notably, a 16-tap filter was implemented in [LSYB17] and demonstrated 47 dB cancellation across a narrow bandwidth of 80 MHz. This cancellation circuit used many attenuators (in this case, 16), implying additional complexity of the optimization algorithm. In [KMP16], a time-domain narrowband cancellation using a filter with four tap delay lines and attenuators demonstrated 30 dB cancellation across a BW of 30 MHz. Other multi-stage STAR implementations introduced a stage of digital baseband cancellations to achieve up to 60-80 dB cancellation [CJS+10, JCK+11].

More recently, research on wideband STAR systems abound. In [EEF16b], one pair of Tx and one pair of Rx antennas were designed with two 3 dB 180° hybrid couplers, resulting in 39.6 dB of SI cancellation across 4:1 BW. Another study showed 35 dB Tx/Rx isolation across 2-2.9 GHz using a ring array [KHFP12]. However, this approach requires an external beamformer to improve isolation to 50 dB, implying additional complexity (see Table 2.1 ). In [VAV18, BVAV17] wideband FIR filters were implemented to provide RF cancellation across 500 MHz. Indeed, a multi-tap FIR filter offers more degrees of freedom (such as tunability and attenuation) to achieve cancellation across larger bandwidths. This approach was able to achieve 25 dB RF cancellation across 500 MHz. This work was later expanded to obtain 25 dB cancellation across 1 GHz bandwidth by cascading multiple FIR filters [VHAV19, BVAV18]. However, this cascaded approach is hardware intensive.

This chapter presents a two-stage wideband STAR architecture operating across 500 MHz, as shown in Fig. 4.1. This is an extension of our previous work, published in [TNA20], based solely on simulation. This chapter brings forward several novelties, among them:

1) The passive symmetric cancellation technique is introduced in the RF domain and is achieved using two customized SIC circuits.

2) The SIC circuit is novel and based on a hybrid FIR filter and resonator topology. The resonator adds extra flexibility to approximate the SI signal.

3) The cancellation is 30 dB across a wide bandwidth of 500 MHz. Other published work showed 30 dB cancellation across 80 MHz [LM15].

4) The benefit of passive symmetric RF cancellation is that we can achieve additional SIC cancellation using a 180-degree hybrid coupler,

5) Since implementing the FIR resonator requires a highly tuned solution and no initial guess, we have chosen a differential evolution (DE) algorithm. DE is a

population-based optimizer for finding the best solution to a problem. In its most basic form, DE is the process of adding the weighted difference between two population vectors to a third vector. The differential evolution algorithm works well for no initial solution and is also effective for a high-tuned solution.

Our STAR architecture achieved 41 dB minimum to 65 dB maximum isolation (simulation) and 40 dB minimum to 50 dB maximum isolation (measurement) between the Tx and the two Rx ports across 1 to 1.5 GHz. In particular, we introduce a symmetric coupling suppression technique using a three-element antenna array. The symmetry between the Tx and each of the Rx antennas leads to 12 dB isolation. The latter can improve to 32.5 dB if a 180° hybrid coupler combines the two Rx ports. Instead, more isolation can be achieved by introducing an RF stage using a novel six-tap FIR-resonator circuit between Tx and Rx antenna. This achieves a total cancellation of 40 dB. Finally, the 180° hybrid is employed between the Rx ports to improve average cancellation to 52 dB.

Overall, the proposed architecture improved spectral efficiency across various space communication bands,s including L ban,d by providing highly coveted isolation of  52-70 dB. We anticipate that the antenna isolation triad customized SIC filter suppression and couplers will lead the way for practical, secure, and spectrally efficient space and satellite communication STAR radios. It is noted that STAR technology also provides excellent advantages for magnetic resonance imaging (MRI), where a significant amount of isolation is the crucial requirement over various loading conditions in an MRI scanner [SVL$^+$16]. The applications include next-generation (5G/6G) wireless systems, phased array radar systems, military, law enforcement, aerospace communications, pulse-Doppler radar systems, the biomedical field, etc.

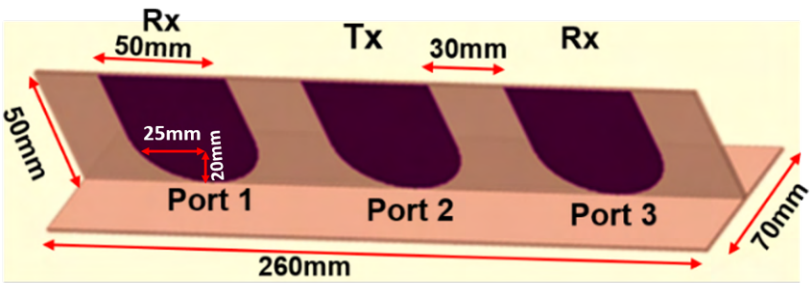


(a)

## 4.1 A Two-Stage RF Self -Interference Cancellation

In this chapter, a compact, symmetric, analog RF cancellation is developed across a wide bandwidth, *viz.* 500 MHz. The architecture consists of a three-element antenna array, one for Tx and two for Rx, two SIC circuits, three power splitters, and one power combiner, as depicted in Fig. 4.1. In bistatic STAR, one pair of Tx and Rx antennas is typical to achieve a balanced configuration and provide sufficient SIC cancellation. The design of the entire system is presented first, followed by a detailed procedure of the RF SIC circuits design and optimization from 1 to 1.5 GHz.

As mentioned, STAR systems require significantly canceling the coupled Tx signal into the Rx chains. Coupling suppression can be achieved by improving the isolation between the Tx and Rx antennas and introducing SIC circuits at the RF and analog/digital baseband. In our design, two Rx antennas are placed at an equal distance from the Tx antenna, as shown in Fig. 4.2 (a).

A prototype was fabricated as shown in Fig. 4.2 (b). The isolation between the Tx and each of the Rx antennas is 12 dB. Notably, the coupled signals at each Rx antenna are symmetric and fed to a 180° hybrid coupler to achieve >32.5 dB coupling suppression at the antenna stage, as shown in Fig. 4.2 (c). The antenna isolation alone is not enough for STAR implementation, as for high Tx power (on

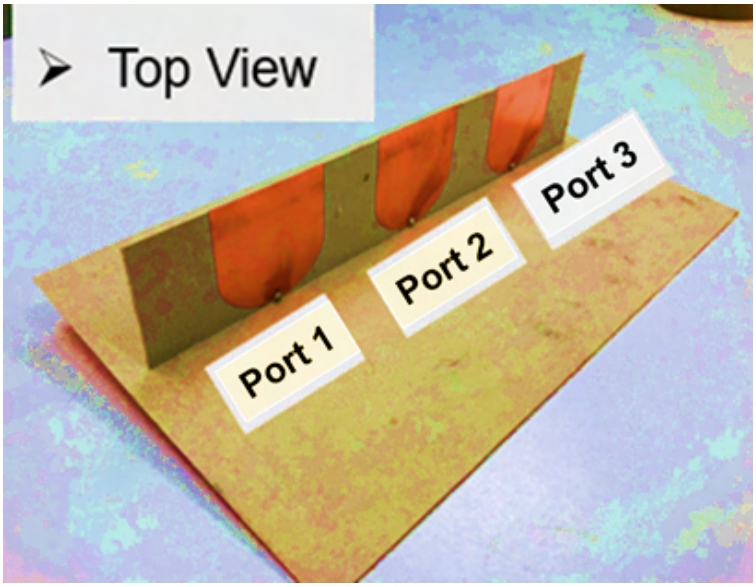


(b)

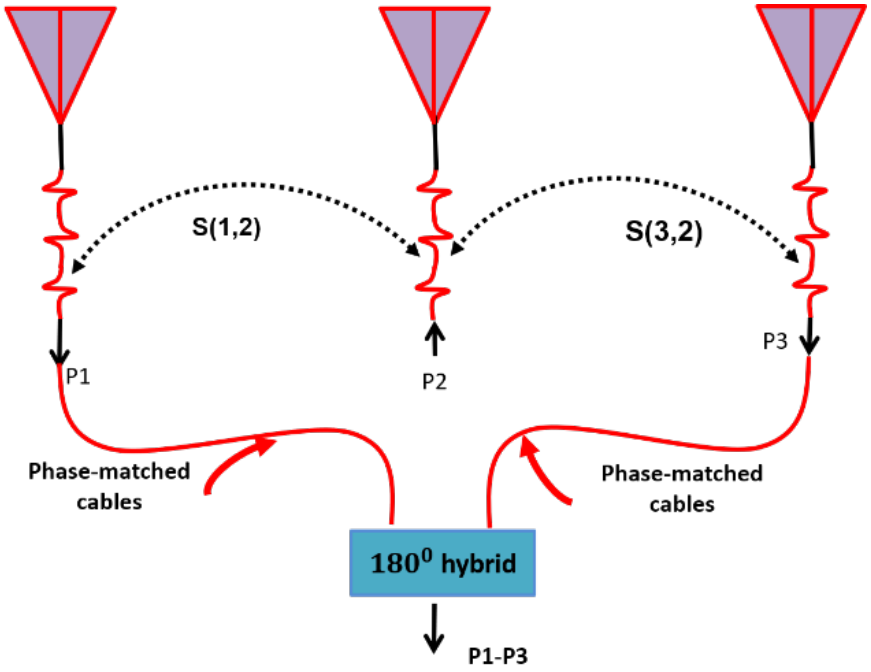


(c)

Figure 4.2: (a) Simulated three-element monopole array; (b) Fabricated prototype of 3-element monopole array; (c) Schematic of a SIC for three-element monopole array using a hybrid coupler.

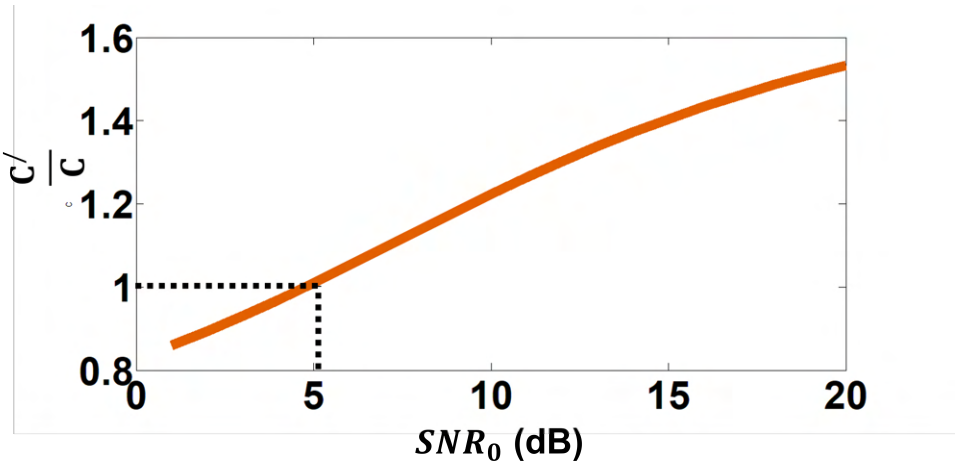


Figure 4.3: Channel capacity ratio between FD and traditional system.

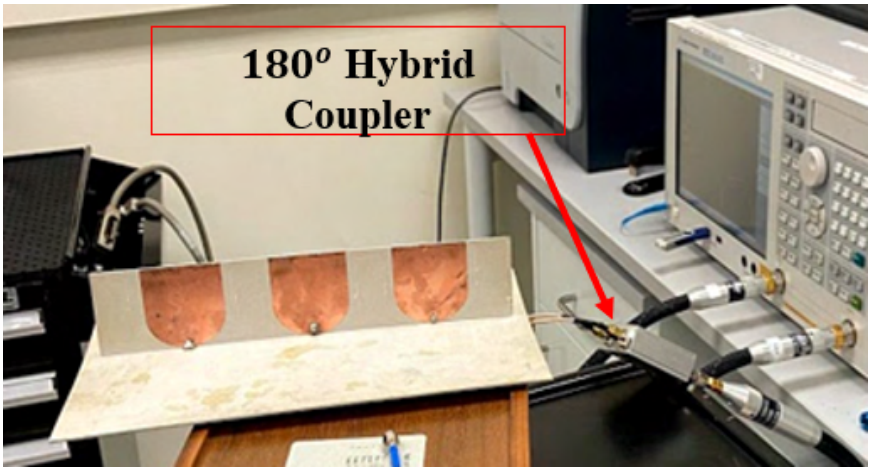


Figure 4.4: Photograph of a SIC setup for fabricated 3-element monopole array using a hybrid coupler.

the order of a few dBW), the coupled signal after the antenna stage is still very high and risks desensitizing the Rx chain. Therefore, an additional stage is introduced to improve the average cancellation to 52 dB. An SIC circuit is implemented between the Tx antenna and each Rx antenna (see Fig. 4.1). The SIC circuits are designed with a response conjugately matched to the coupling between the Tx and each Rx antenna. To do so, a 3-way power splitter is used to split the transmit signal. One output is fed to the Tx antenna. The other two outputs are provided to each SIC

circuit between the Tx and Rx ports.

At each Rx chain, the SIC circuit's output is combined with the coupled signal using a power combiner to achieve the required cancellation. The combiner's output is then fed to a 180° hybrid coupler to cancel the total coupling at both antenna elements. This approach demonstrates better symmetric cancellation in the RF stage. Finally, the output of the hybrid coupler is fed to the Rx chain. Also, note that the SIC circuits are implemented between the Tx and Rx chains and not along the Rx chains. Therefore, these circuits will not affect the Tx or the Rx signals or contribute to additional losses. However, there is a loss of 4.77 dB at the TX port. But at the same time, with this loss, we could feed the two SIC filters. Previous work [CKZ+18] has used only one SIC. In this case, a power splitter with a loss of 3 dB is needed. However, only a single SIC was used, and cancellation of 65 dB was achieved across 80 MHz. Conversely, in this work, using a 3-way power splitter, we could achieve a minimum of 41 dB and a maximum of 65 dB cancellation across 500 MHz with a loss of only 4.77 dB.

It is worth mentioning that such a loss does not greatly affect the Full Duplex (FD) capacity. This can be validated by referring to the basic transceiver's channel capacity, specified as $C{=}BW.log_2(1+10^{\frac{SNR_0}{10}})$. BW denotes the channel bandwidth, and $SNR_0$ denotes the received signal-to-noise ratio. In our FD system, the bandwidth BW increases to 2BW, however, with an $SNR_0$ reduction of 4.77 dB due to 4.77-dB losses in both Tx and Rx chains. As a result, the new channel capacity is equal to $C^{/}{=}2B.log_2(1+10^{\frac{SNR_0-4.77}{10}})$.

To achieve a higher capacity (*viz.* $C^{/}C \geq 1$) with our system, $SNR_0 \geq$ 5.01 dB is needed, as shown in Fig. 4.3. Most digital modulation schemes require a minimum $SNR_0$ of 10 to 15 dB, implying that our system will always achieve a higher capacity than traditional systems.

More details on the antenna design and SIC circuits are provided in the next section.

## 4.2 Antenna Isolation

For symmetric coupling cancellation, the geometry of the linear 3-element monopole antenna array is shown in Fig. 4.2 (a). The total antenna dimensions (L×W×h) are 260 mm×70 mm×50 mm. Fig. 4.2 (a) shows that the geometry of the designed monopole array consists of a rectangular patch with width=50 mm, length=50 mm, and an elliptical patch with a radius ratio equal to 1.25 with a major axis equal to 25 mm, and a minor axis similar to 20 mm. Adding an oval patch improves the bandwidth of the monopole antenna array. The Tx antenna (Port 2) is placed at the array's center. The two Rx antennas (Port 1 and Port 3) are placed at an equal distance away from the center element (*viz.* 80 mm). The prototype (see Fig. 4.2 (b)) is printed on a Rogers 5880 substrate with a loss tangent of 0.0009, a dielectric constant of 2.2, and a substrate thickness of 1.27 mm. The transmission coefficients S(1,2) and S(3,2) must be identical to achieve high isolation between the Tx and Rx antennas. This is realized using a perfectly symmetric configuration. As such, the coupled signals at each Rx port are similar. When combined out of phase using a 180° hybrid coupler (see Fig. 4.2 (c)), the coupled Tx signal is substantially reduced. The 3-element antenna prototype with the hybrid coupler was tested, as shown in Fig. 4.4.

A ∼36 dB isolation was measured across 1-1.5 GHz band, as shown in Fig. 4.5. We note that we have not designed the hybrid coupler. It was purchased from a vendor with ∼3.5 dB insertion loss. The part number for this item is ZAPDJ-2. Therefore, the antenna isolation without hybrid coupler insertion loss is ∼32.5

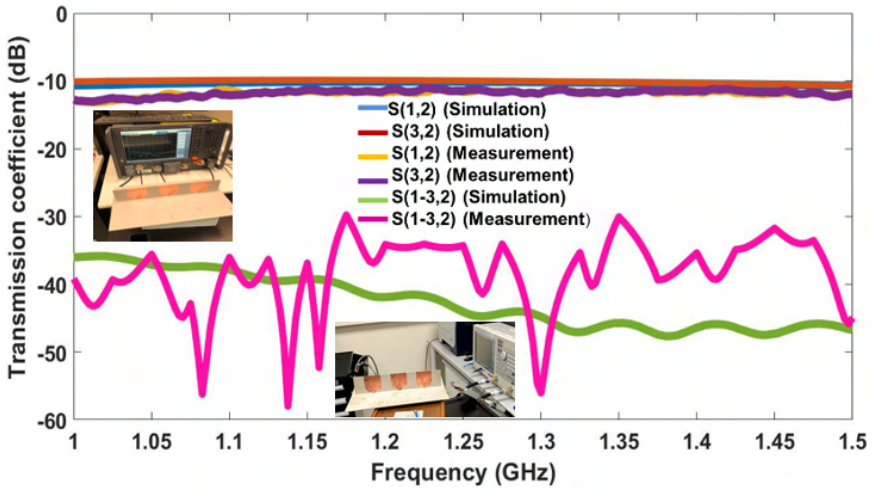


Figure 4.5: Transmission coefficient at different ports. Coupling channels from Tx to Rx antennas are nearly identical, resulting in significant cancellation when combined (pink color), showing the measured isolation of 36 dB.

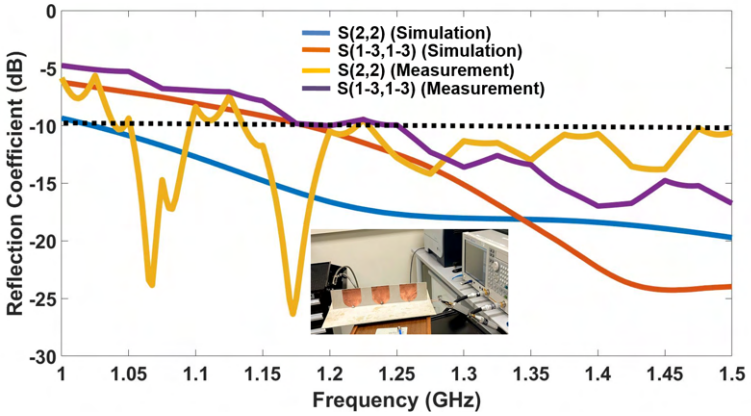


Figure 4.6: Simulation and measurement of the active reflection coefficient for the 3-element monopole array prototype.

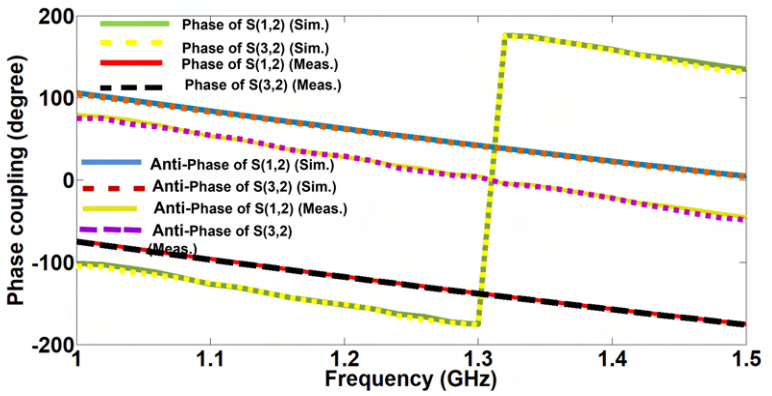


Figure 4.7: Simulation and measurement of phase and the anti-phase response of symmetric coupling path between the Tx and each Rx antenna port.

dB. Fig. 4.6 shows each port's simulated and measured reflection coefficients. The phase coupling and its corresponding antiphase response are also shown in Fig. 4.7. The antiphase coupling is required to improve isolation, as will be discussed in the following section.

## 4.3 Symmetric Coupling Cancellation in the RF Stage

The symmetric configuration of the antennas demonstrates up to 32.5 dB of isolation. Additional suppression can be achieved (>50 dB) by employing a second stage of SIC at the RF front-end, as depicted in Fig .4.1. The SIC circuit at the front end combines an FIR filter and a resonator, as depicted in Fig. 4.8. RF cancellation is achieved by tapping the transmitted signal before transmission, applying gain/delay adjustments using the SIC circuit, and subsequently inserting the modified signal into the Rx chain for cancellation. More in detail, the coupling between the Tx and each of the Rx antennas is represented by the impulse response $h_{chnl1}$ and $h_{chnl2}$ (see Fig. 4.1), respectively. Since both couplings are identical,

$$S(1,2) = S(2,3) \tag{4.1}$$

The scattering parameters are related to the channel impulse response using [VAV18]:

$$h_{chnl1} = \frac{S(1,2)(1-\Gamma_L)(1-\Gamma_S)}{(1-S(1,1)\Gamma_L)(1-S(2,2)\Gamma_S) - S(2,1)\Gamma_L S(1,2)\Gamma_S} \tag{4.2}$$

$$h_{chnl2} = \frac{S(3,2)(1-\Gamma_L)(1-\Gamma_S)}{(1-S(3,3)\Gamma_L)(1-S(2,2)\Gamma_S) - S(2,3)\Gamma_L S(3,2)\Gamma_S} \tag{4.3}$$

Where, $\Gamma_L$ and $\Gamma_S$ are the reflection at the source and load of the two-port network formed by the Tx and each of the Rx ports. Under matching conditions, $\Gamma_L = \Gamma_S = S(1,1) = S(2,2) = S(3,3) = 0$

Hence, (4.2) and (4.3) become

$$h_{chnl1} = S(1,2) \tag{4.4}$$

$$h_{chnl2} = S(3,2) \tag{4.5}$$

Referring to (4.1)

$$h_{chnl1} = h_{chnl2} \tag{4.6}$$

In Fig. 4.1, we define $s(t)$ as the power amplifier's (PA) output signal and $\widetilde{s}_2(t)$ as the output of the power splitter feeding the Tx antenna port. $\widetilde{s}_1(t)$ and $\widetilde{s}_3(t)$ are the signals at ports 1 and 3 of the power splitter, that will be fed to the each of the SIC circuits, respectively. The coupled signals $\widetilde{r}_1(t)$ and $\widetilde{r}_3(t)$ represent the SI at ports 1 and 3 of the Rx antennas, respectively, such as

$$r_1(t) = \widetilde{s}_1(t) * h_{chnl1}(t) \tag{4.7}$$

$$r_3(t) = \widetilde{s}_3(t) * h_{chnl2}(t) \tag{4.8}$$

To cancel these coupled SI signals, the outputs of the power splitter $\widetilde{s}_1(t)$ and $\widetilde{s}_3(t)$ are passed through the two designed RF SIC circuits of impulse responses $h_{sic1}(t)$ and $h_{sic2}$ (t), respectively. The filtered signals at each Rx port are then,

$$c_1(t) = \widetilde{s}_1(t) * h_{sic1}(t) \tag{4.9}$$

$$c_3(t) = \widetilde{s}_3(t) * h_{sic2}(t) \tag{4.10}$$

At the Rx ports, a 2:1 power combiner is employed. The combined Rx signals from both symmetric sides are:

$$y_1(t) = c_1(t) + r_1(t) \tag{4.11}$$

$$y_2(t) = c_3(t) + r_3(t) \tag{4.12}$$

Thus, our goal is to minimize $y_1(t)$ and $y_2(t)$. This is accomplished by designing SIC circuits with the following impulse response:

$$h_{sic1}(t) = -h_{chnl1}(t) \tag{4.13}$$

$$h_{sic2}(t) = -h_{chnl2}(t) \tag{4.14}$$

In other words, if the phases of the coupled and filtered SIC signal are 180° out-of-phase, destructive interference is achieved, leading to signal cancellation. Further reduction of SI can be achieved using a 180° degree hybrid coupler. At the output of the hybrid coupler, the total coupled signal cancels out. As such, $y_1(t)$ and $y_2(t)$ are combined out of phase, leading to additional cancellation. In other words,

$$y_1(t) + y_2(t) = 0 \tag{4.15}$$

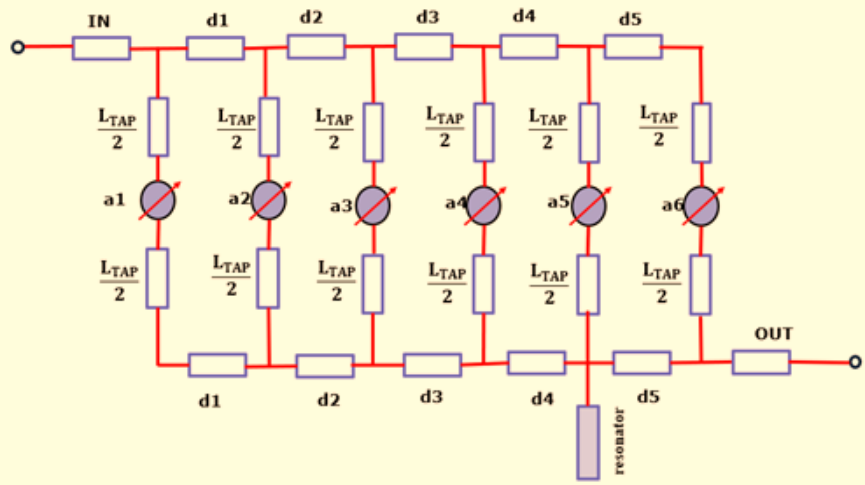


Figure 4.8: RF FIR-resonator circuit operating across 500 MHz. This circuit consists of delay lines, attenuators, and a resonator stub. The number of taps determines the order of the filter.

## 4.4 Self-Interference Cancellation Circuit

In this section, we present the design and optimization of the SIC circuit. A 6-tap FIR-resonator is considered for our design, as depicted in Fig. 4.8. The delay lines, attenuators, and resonator stub were optimized to achieve a filter response that satisfied (4.13) and (4.14). In other words, the hybrid FIR-resonator response can be matched conjugately to the antenna channel response by adjusting the gain delay of the attenuators and the transmission lines (copper trace) across the desired frequency band (1-1.5 GHz). Adding a resonator provides additional tunable parameters and hence, an extra degree of freedom to mimic the SI signal. We note that, in our SIC circuit design, we considered the measured results of the symmetric coupling of the fabricated 3-element antenna prototype, shown in Fig. 4.5 and Fig. 4.7.

For the three-element monopole array, one antenna acts as a Tx antenna, and the other is an Rx antenna (Rx1, Rx2). The coupling from Tx to Rx1 is denoted as $S(1,2)$, and coupling from Tx to Rx2 is denoted as $S(3,2)$. Let the signal transmit-

ted from antenna 2 be $\widetilde{s}_2(t)$ , hence the SI signal is at antenna Rx1 due to coupling is $\widetilde{s}_2(t)S(1,2)$. Similarly, the SI at Rx2 due to Tx is $\widetilde{s}_2(t)S(3,2)$. The coupling function can be expressed as $S(1,2)$=$S(3,2)$= $\frac{e^{-sT}}{(\alpha(s))}$ with $T$=$\frac{d}{c}$, where $d$ is the inter-antenna distance, $\alpha$ is the attenuation constant. Here SI can be suppressed using an SIC circuit (*viz.* FIR resonator) having transfer function (TF) $h_{sic}(t)$=$S(1,2)$=$S(3,2)$.

The basic network shows that the passive multiport networks corresponding to the antenna arrays with mutual coupling contain TFs with zeros and poles in their integer-order polynomial representations. The approximation of such coupling functions using an FIR resonator is possible. However, the only trade-off is the order of the FIR resonator. Here, we are using a microstrip substrate to keep the circuit low profile. To reproduce this network's unit impulse response, an FIR filter would need to sample it at close intervals of time and use the sampled values as weights (*viz.* taps) for the FIR realization.

The TF of the FIR resonator can be represented using circuit taps and a resonator. The FIR resonator designed is static. Circuit taps are implemented using tap delay lines and tap coefficients. An open stub line is used to design the resonator circuit. To realize the FIR resonator in the analog domain, the tap delays and resonator are realized by microstrip line, and attenuators discover tap coefficients. The width and length of the delay lines, attenuators, and resonator stub are optimized to achieve a transfer function conjugately matched to the channel transfer function between the Tx and Rx antennas. Adding a resonator provides additional tunable parameters and hence, extra degrees of freedom to mimic the SI signal.

More in detail, we design a $5^{th}$ order circuit (*viz.* 6 taps). This topology is passive, as it only consists of passive elements: delay lines, attenuators, and a resonator stub. The width and length of the delay lines, attenuators, and resonator stub are optimized to achieve a TF conjugately matched to the channel's TF (between the

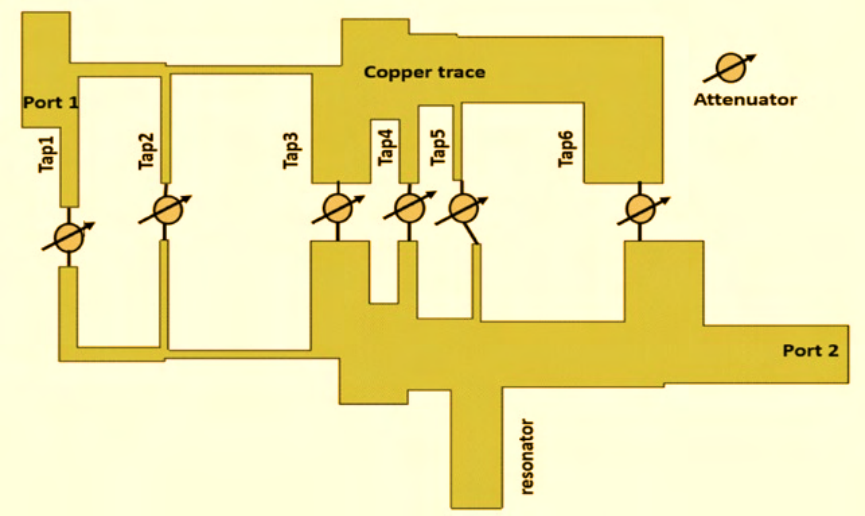


Figure 4.9: EM model of FIR- resonator circuit.

TX and Rx antennas). The delay spread, and filter coefficients are obtained using a DE algorithm. For optimization, we have considered several factors. To calculate population size, a general rule is to multiply the number of optimizable parameters by five until the maximum number of parameters is reached (60 in this case). A small population size produces faster results, but it is also more likely to stall in a local optimum. Independent of the number of parameters, population sizes greater than 60 are generally not beneficial. In our circuit tuning for mimicking the coupling response, our population size was always less than 60. We have chosen a greedy strategy in our SIC design since it produces the most rapid results. With no initial guess, the problem becomes complex. Therefore, we have chosen a higher cross-over probability. Typical values are between 0.0 and 1.0. In our case, the cross-over probability is 0.9. Using this algorithm, we first performed a circuit simulation to get the optimum weights of the circuit elements.

For fabrication purposes, more than a circuit simulation is needed to get an accurate result for SIC cancellation. Therefore, we have performed an EM simulation to get more accurate results. Here also, the DE algorithm was performed with the

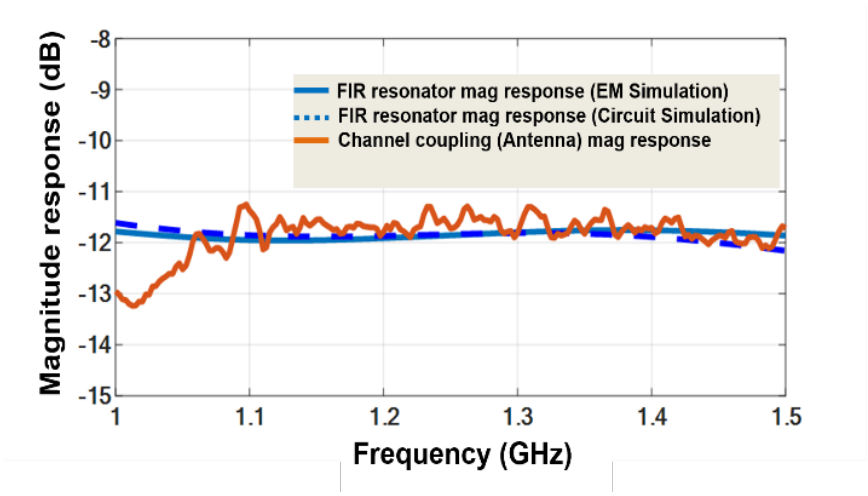


(a)

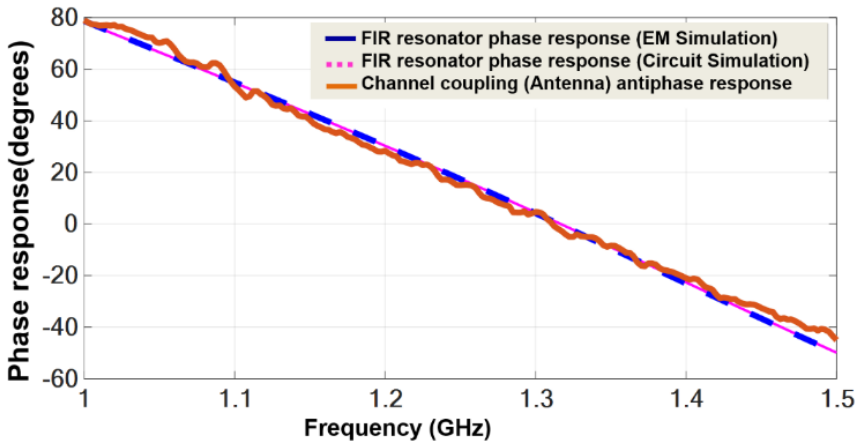


(b)

Figure 4.10: Simulation results showing the (a) magnitude and (b) phase response of the simulated hybrid FIR-resonator circuit and the complex conjugate of the channel.

EM simulation. The EM model is developed, as shown in Fig. 4.9. We considered the vendor's actual S-parameter of the circuit element so that the fabricated prototype is well-matched to the antenna coupling. In brief, EM simulation of the circuit elements' actual S parameter helps find total optimum weights. The specific filter taps (*viz.* weighted filter) coefficients are 3, 3, 5, 0, 0, 15 and delay spread are 0.02, 0.039, 0.065, 0.015, 0.017, 0.063 ns at the center frequency. Insertion loss depends

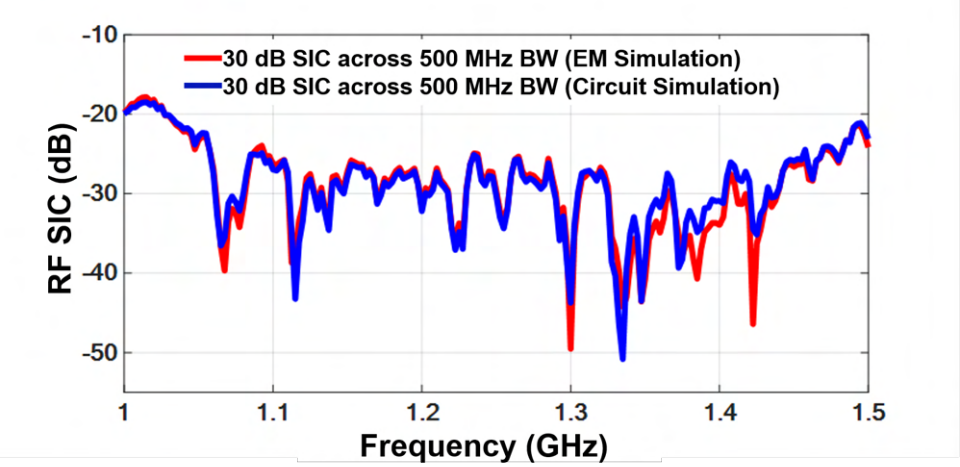


Figure 4.11: Computed SIC using the simulation results showing an average cancellation of ∼30 dB at each Rx port.

on the mutual coupling of the antenna array. The insertion loss of the FIR resonator is defined by $-20log_{10}|S(2,1)|dB$ and is shown in Fig. 4.10 (a). We note that the SIC circuit's dimension is 37 mm×31 mm. A comparison between the magnitude response and phase response of the FIR-resonator and complex conjugate of the channel is depicted in Fig. 4.10 (a) and (b). The magnitude and phase response of the FIR-resonator and the channel between Tx and Rx antennas agree well across 500 MHz bandwidth. Then, using the FIR-resonator response, SIC is computed according to the following expression [VAV18]:

$$SIC_{dB} = 20\log_{10}[\frac{1}{2 \mid H_{leakage}(j\omega) \mid^2}(\mid H_{leakage}(j\omega) \mid^2 + \mid H_{cancellation}(j\omega) \mid^2 +2 \mid H_{leakage}(j\omega) \mid \times \mid H_{cancellation}(j\omega) \mid \cos(\angle H_{cancellation}(j\omega) - \angle H_{leakage}(j\omega)))]^{\frac{1}{2}} \tag{4.16}$$

Using (4.16), an average of 30 dB suppression is obtained from 1 to 1.5 GHz, as shown in Fig. 4.11.

Since we are building the SIC circuit across a more comprehensive frequency range, the variable delay lines provide greater flexibility in achieving cancellation. A fixed delay line can also offer SI cancellation even though it operates within a

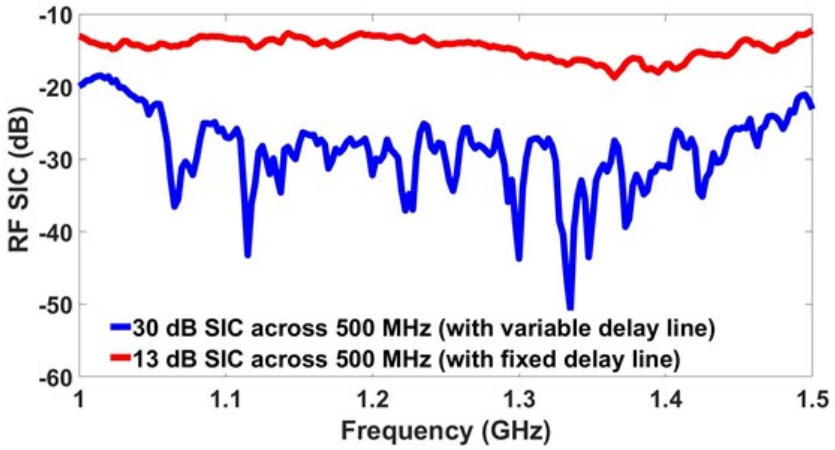


Figure 4.12: Effect of variable and fixed delay lines on SIC.

limited bandwidth. Fig. 4.12 shows the RF SIC response using the SIC circuit for fixed and variable delay lines.

For STAR, amplitude and phase matching are critical factors in achieving the desired SI cancellation across operational bandwidth. Our system has commercial off-the-shelf (COTS) components contributing to phase and magnitude imbalance. The impact of phase and amplitude imbalances on the RFSIC is shown in Fig. 4.13.

## 4.5 Fabricated Self-Interference Cancellation Circuit

Two FIR-resonator prototypes were fabricated for each symmetric channel, as shown in Fig. 4.14. Each prototype was constructed on a TMM10 substrate with a dielectric constant of 9.2, a loss tangent of 0.0027, and a substrate thickness of 1.52 mm. Fig. 4.15 shows the fabricated prototypes' measured magnitude and phase responses, excellently matching with the antenna coupling responses. Using (4.16), these results imply 26 dB and 27 dB SIC of the coupled signal at each Rx antenna,

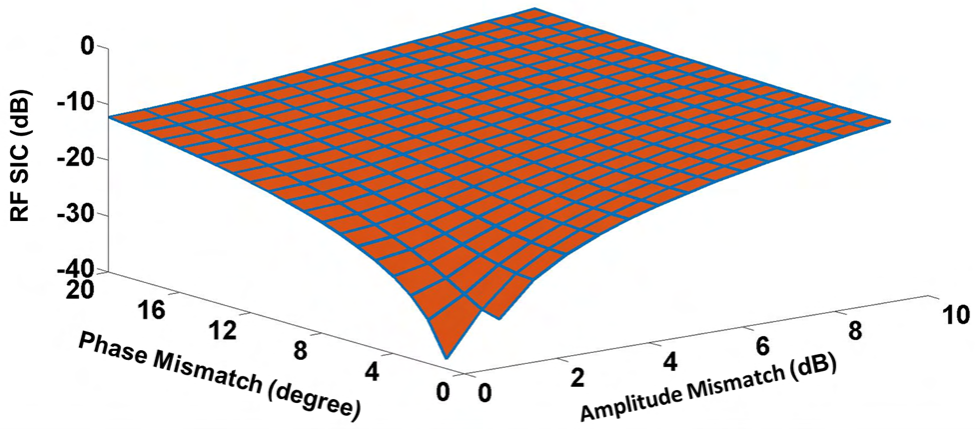


Figure 4.13: Effect of amplitude mismatch and phase mismatch on SIC.

as depicted in Fig. 4.16. The slight discrepancy between the channel coupling and measured FIR resonator results is mainly due to fabrication tolerances.

## 4.6 Overall RF Self-Interference Cancellation System

Additional cancellation is achieved using a 180° hybrid coupler to combine the canceled signals $y_1(t)$ and $y_2(t)$ at the output of the power combiner at each of the Rx sides, as depicted in Fig. 4.1. Simulation shows that up to 65 dB with an average of 52 dB of coupling suppression across 500 MHz is achieved (see Fig. 4.17). Notably, adding a hybrid coupler provides an additional 12 dB avg. Isolation between the Tx and combined Rx port, as depicted in Fig. 4.17.

We conducted a laboratory experiment using our combined RF analog cancellation topology to verify the simulation. The measurement setup is depicted in Fig. 4.18. The system was not evaluated in an isolated environment. It is worth mentioning that the measurements' accuracy is contingent on the accuracy of the attenuator values, the same phase balance of each power combiner, and hybrid coupler losses.

Fig. 4.19 shows an average measured cancellation of 44 dB with a minimum of 40 dB suppression across a BW of 500 MHz. The hybrid coupler provided an average of 8 dB of additional cancellation across 500 MHz in the measurements. However, we note that an average 11 dB cancellation was observed across 1.25 GHz to 1.45 GHz, implying a 47 dB average cancellation. We note that the insertion losses of the hybrid couplers and power combiners were subtracted from overall SIC in Fig. 4.17 and Fig. 4.19.

To evaluate the effect of reflections on neighboring objects, we have placed a reflector antenna at different distances from our setup. In particular, the reflector was set at 2 cm, 10 cm, and 100 cm. Measurements were conducted for each distance, and SIC was computed, as shown in Fig. 4.20. SIC is not significantly affected by the position of the reflector. Undoubtedly, hardware non-idealities and calibration errors are the leading cause of the slight difference between the simulated and measurement results.

We ran another experiment to test our STAR system with a modulated system. A Quadrature Phase Shift Keying (QPSK) modulated signal was generated and fed to the system with 0 dBm. Simulation results show an average isolation of 52 dB across 500 MHz, as depicted in Fig. 4.21. The result was also verified with our COTS components. An average SIC of 44 dB is achieved, which agrees with our simulated results. The measured performance is shown in Fig. 4.22.

## 4.7 Comparison with Other State-of-Art STAR System

Table 4.1 compares our 2-stage STAR implementation with other state-of-the-art systems. Early STAR architectures used two stages of interference cancellation: 1) antenna isolation and 2) analog post-processing to achieve up to 78 dB cancellation

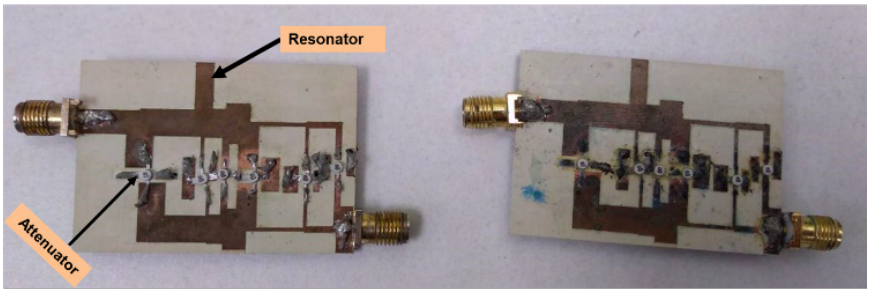


Figure 4.14: Fabricated RF FIR-resonator prototypes.

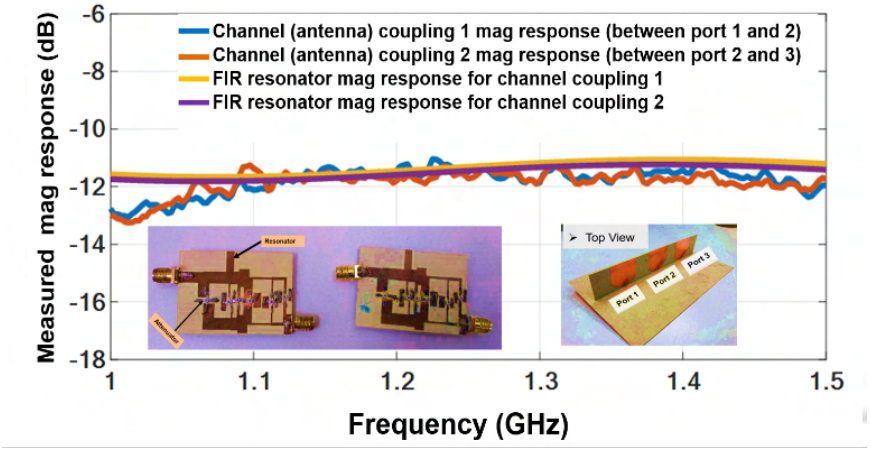


(a)

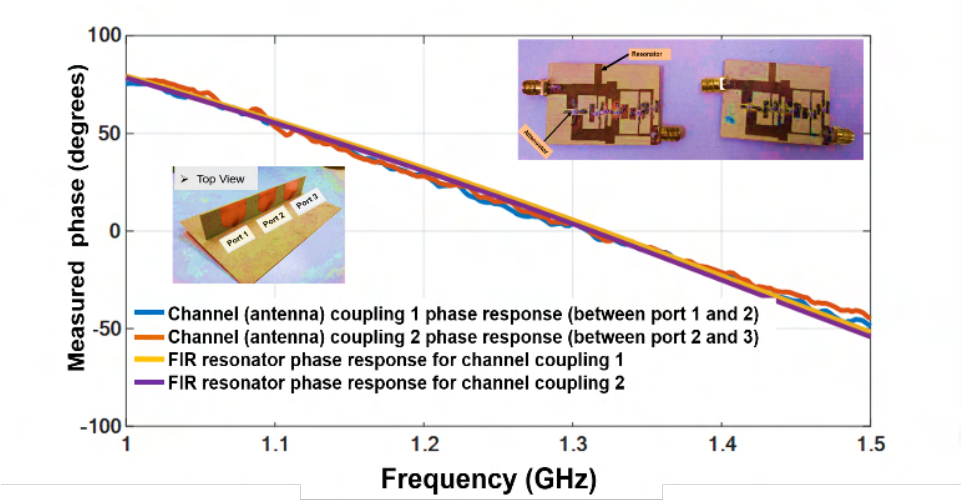


(b)

Figure 4.15: Measured results showing the (a) magnitude and (b) phase response of the fabricated hybrid FIR-resonator circuit, with the complex conjugate of the channel.

for very narrowband signals (20 MHz BW) [KMP16]. Other bi-static STAR implementations achieved up to 60 dB cancellation across 80 MHz BW [LM15]. It is clearly shown that these techniques were all narrowband. On the contrary, research on wideband STAR has shown 25 dB to 50 dB (across $>$ 500 MHz) by only designing a single stage without a comprehensive system implementation [BVAV17, VHAV19] or by introducing hardware complexity (*e.g.*, beamformer [KHFP12]). In our work, we implemented a two-stage wideband cancellation system based on the symmetric coupling cancellation technique with wideband cancellation. This is the first time a comprehensive two-stage STAR system has been implemented using a low-profile FIR resonator architecture. We have achieved an average of 52dB (a minimum of 41 dB and a maximum of 65 dB) coupling cancellation across a BW of 500 MHz. Clearly, our design shows higher isolation for the wideband application with reduced hardware complexity.

Table 4.1: Performance comparison with the state-of-the-art in STAR system implementations.

| Reference | Bandwidth | TX-RX isolation | Technology | Stages |
|---|---|---|---|---|
| [LM15] | 80 MHz | 60 dB | 3 antennas (2 Tx and 1 Rx), SI signal generator | Three stages |
| [Weg14] | 110 MHz | 30 dB | Near-field filter | Two stages |
| [ZCDK15] | 20 MHz | 20 dB | Bank of bandpass filter | RF stage |
| [CKZ+18] | 80 MHz | 65 dB | Double RF canceller | Three stages |
| [NGA+21] | 20 MHz | 32.5 dB | RF canceller and BB canceller | Two stages |
| [KMP16] | 20 MHz | 78 dB | Multitap RF canceller | Two stages |
| [CJS+10] | 5 MHz | 60 dB | 2 Tx and 1 Rx, QHx220 chip, digital cancellation | Three stages |
| [JCK+11] | 10 MHz | 73dB | Signal inversion, digital cancellation | Three stages |
| [VAV18] | 500 MHz | 25 dB | FIR filter | RF stage |
| [EEF16b] | 4:1 BW | 39.5 dB | Spiral antenna, hybrid (But it is mo-static STAR system) | Two stages |
| [KHFP12] | 900 MHz | 35 dB<br>50 dB | 8 Tx and 1 Rx, mutual coupling suppression<br>8 Tx and 1 Rx, added external beamformer | Single stage<br>Two stages |
| [BVAV18] | 1 GHz | 25 dB | FIR filter bank | RF stage |
| **This work** | **500 MHz** | **52 dB (sim.)**<br>**44 dB (meas.)** | **1 Tx and 2 Rx, 2 SIC circuits, symmetric cancellation** | **Two stages** |

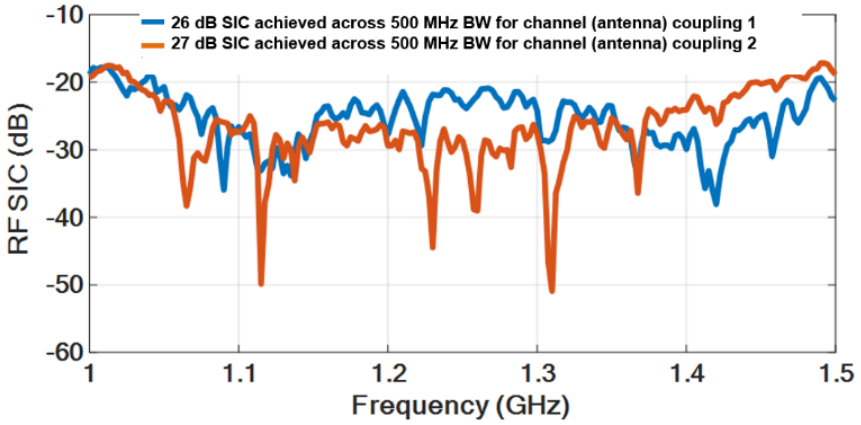


Figure 4.16: Computed SIC using the measured results showing an average ∼26.5 dB cancellation at each Rx port.

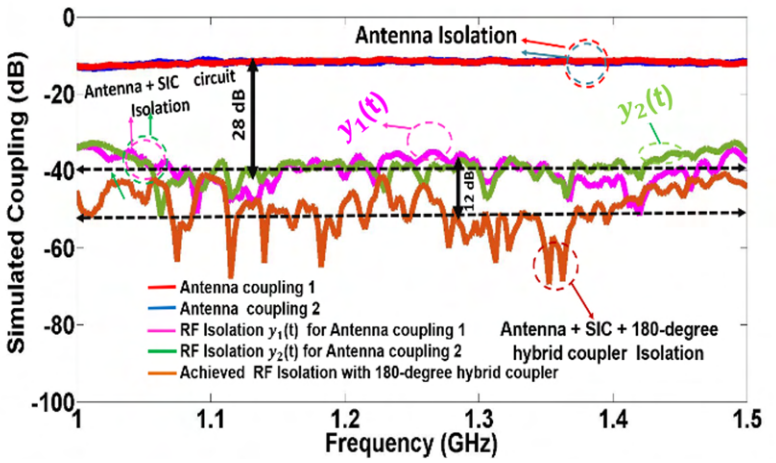


Figure 4.17: SIC of the simulated two-stage SIC system showing $\sim$ 52 dB cancellation.

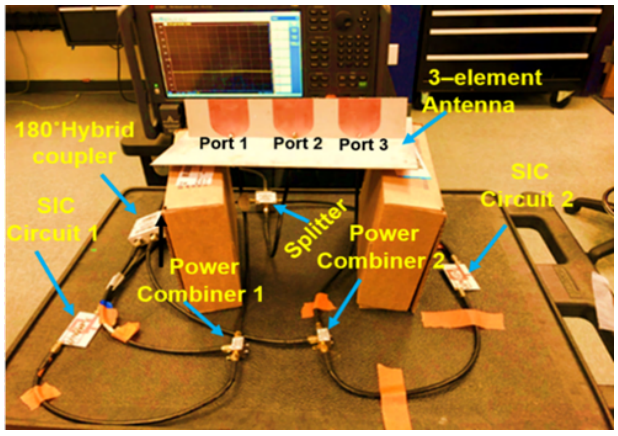


Figure 4.18: Measurement setup of the two-stage SIC system.

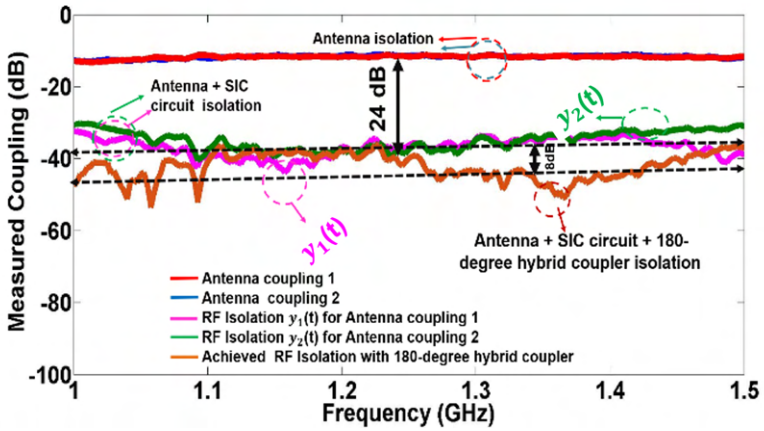


Figure 4.19: SIC of the measured two-stage SIC system showing ∼44 dB cancellation.

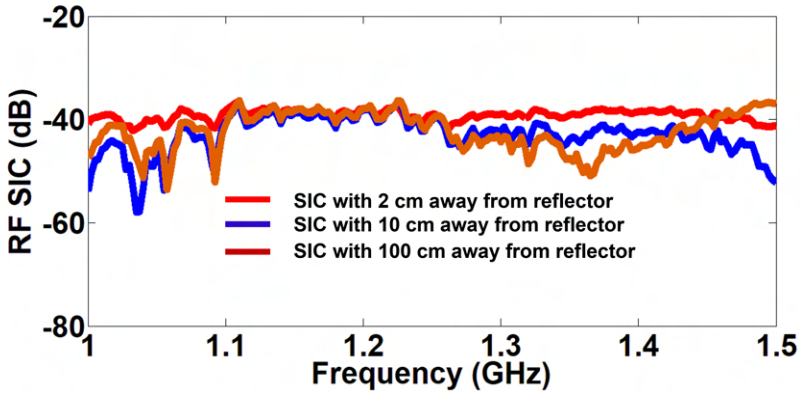


Figure 4.20: SIC performance with a reflector (antenna) placed at different distances.

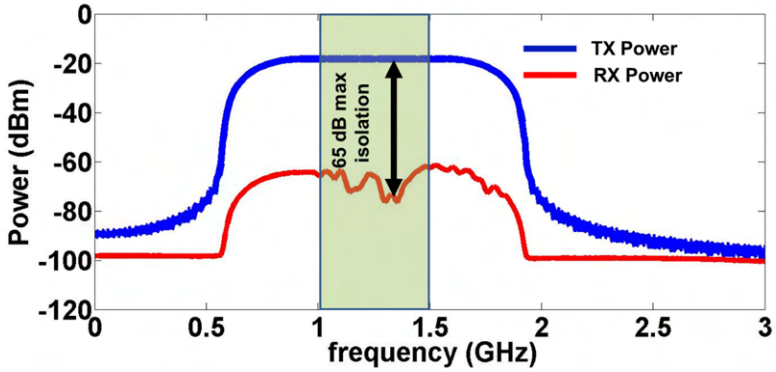


Figure 4.21: SIC with a QPSK signal. Simulated performance shows cancellation with a maximum of 65 dB and an average of 52 dB across the operational BW (1 to 1.5 GHz).

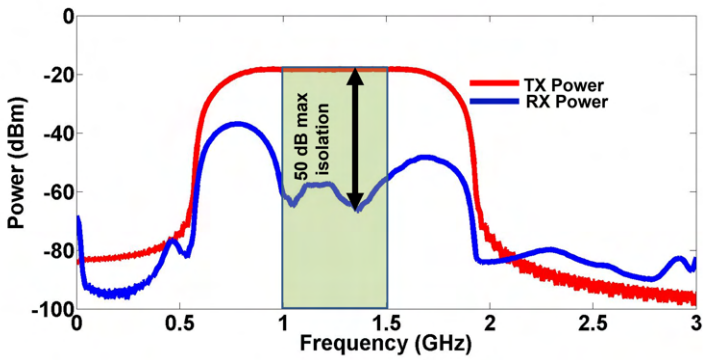


Figure 4.22: SIC with a QPSK signal. Measurements show cancellation with a maximum of 50 dB and an average of 44 dB across the operational BW (1 to 1.5 GHz).

## 4.8 Conclusion

This chapter presented a two-stage STAR architecture operating across 500 MHz that achieved 52 dB (a minimum of 41 dB and a maximum of 65 dB) coupling suppression between Tx and Rx ports. Our design consists of a three-element antenna (one Tx and two Rx) with a total isolation of 12 dB. Channel cancellation is achieved by implementing 6-tap FIR-resonator circuits between Tx and Rx antenna ports that increase the total isolation to 40 dB. The final stage combines the two Rx ports using a 180° hybrid coupler to achieve an overall average cancellation of 52 dB. Our system was fabricated and tested, showing 44 dB (a minimum of 40 dB and a maximum of 50 dB) of measured cancellation. The discrepancy between simulation and measurement is mainly due to the fabrication tolerance, exact phase balance of the power combiner, hybrid coupler, and phase-matched cables. This unprecedented wideband performance makes our STAR system a leading candidate for future 5G communication.

CHAPTER 5

# CONCLUSIONS AND FUTURE WORK

## 5.1 Summary of this Dissertation

It's crucial to enhance isolation when implementing a simultaneous transmit and receive system to support the growing number of wireless devices for new applications. In Chapter II, we proposed a unique mono-static quasi-symmetrical self-interference cancellation design at 25 MHz to enhance the separation between the transmitter and receiver. We've demonstrated using a secondary circulator and a single Finite Impulse Response (FIR) filter to develop a new quasi-passive cancellation method.

In this work, we have developed an advanced topology that addresses the challenge of interference cancellation in narrow bandwidth operation while prioritizing power efficiency. What sets our approach apart is its ability to achieve high isolation while minimizing power loss in the transmit (Tx) signal, unlike other existing designs that experience an additional 3dB loss in both the Tx and receive (Rx) signals [MDTE20, DSPV$^+$20, WSWL20, CHWC10].

Our system, known as mono-static RFSIC (Radio Frequency Self-Interference Cancellation), introduces a unique symmetry into the design architecture by incorporating a second circulator and a finite impulse response (FIR) circuit. This additional circulator, in conjunction with the FIR circuit, plays a crucial role in generating a quasi-replica of the leaked transmitted signal.

By harnessing this generated quasi-replica signal, we can passively cancel out the interference in a symmetric manner. This innovative design achieves impressive interference cancellation performance across a 25 MHz bandwidth, with average cancellation levels ranging from 40 dB to 55 dB depending on the order of the FIR filter used [TGN$^+$23].

Remarkably, our topology achieves these outstanding results with a straightforward setup, requiring two circulators, a hybrid coupler, and an FIR filter circuit. This simplicity contributes to the power efficiency of our system, making it highly suitable for future full-duplex technologies.

Furthermore, our technology holds significant potential for enhancing communication systems operating in specific frequency bands, such as the 2.395-2.42 MHz range allocated for various applications, including mobile communication, aviation, amateur radio, RF devices, and ISM (Industrial, Scientific, and Medical) equipment.

The scientific community has recognized the significance of our work. These findings were published in the prestigious IEEE Journal of Microwave [TGN+23], demonstrating the groundbreaking nature of our research. Additionally, our work was selected for a special session at the 2021 IEEE International Symposium on Antennas and Propagation and USNC-URSI Radio Science Meeting (APS/URSI), further highlighting the importance of our contributions to the field [TRA21].

We also have demonstrated the development of a bi-static STAR system, which utilizes multiple antennas.

In Chapter III, a low-profile self-interference cancellation circuit with wide bandwidth was created for the bi-static STAR system. The key feature of our SIC circuit is the integration of a hybrid FIR filter and resonator architecture topology. Incorporating resonator structures within the FIR circuit is a novel approach that enables remarkable self-interference cancellation performance. Specifically, we have achieved a significant 22 dB cancellation of self-interference at 800 MHz [TA22], which surpasses the results of previously published research on wideband STAR SIC circuits where 20 dB cancellation was achieved only at 20 MHz [ZCDK15]. Additionally, this implementation led to a 50% reduction in the size of previously the filter bank [RBVV21] while simultaneously reducing the complexity and hardware requirements of the system design.

This Wideband technology offers substantial advantages due to its ability to support large channel capacities, such as real-time high-definition video streaming and signal spreading with encryption capabilities.

Chapter IV describes the development of wideband RF cancellation for coupled transmit signals in a bistatic simultaneous transmit and receive system. The chapter covers implementing and measuring the bistatic RF Self-Interference Cancellation (RFSIC) system, which uses symmetrical passive cancellation. During simulation, this bistatic STAR architecture provided an average of 52 dB of isolation across a 500 MHz bandwidth (1-1.5 GHz). A prototype was fabricated and tested, demonstrating an average cancellation of 44 dB, consistent with the simulation results [THG+22].

With the emergence of 5G mobile networks, the focus is on advancing connectivity, throughput, and spectral efficiency while enhancing the user experience. To meet these evolving demands, ongoing research and development efforts continuously explore novel technologies. Among them, the STAR system stands out as a promising interface technique for 5G due to its ability to tackle crucial factors such as throughput, spectral efficiency, latency, and connectivity, all while operating within the designated frequency bands. Mobile device users now expect faster data speeds and a more reliable connection, which can be achieved by implementing STAR technology in 5G networks.

Notably, the 5G technology deployed in the United States primarily operates at frequencies below 6 GHz. Therefore, designing SIC circuits for frequencies below 6 GHz holds particular significance in the context of 5G's key benefits, including faster data transfers, reduced latency, and increased capacity for remote execution.

We have successfully implemented our SIC circuit and bistatic STAR system for frequencies ranging from 1 GHz to 1.5 GHz, aligning with the frequency bands

of interest for 5G applications. These advancements were presented at the 2022 National Radio Science Meeting in a session titled "Strengths and Circuits for RF Sensing, Radar, and STAR Applications," highlighting the groundbreaking nature of our research.

As a result of our contributions, two journal papers based on this research have been published in prestigious IEEE publications, namely IEEE Access [TA22] and IEEE Journal of Microwaves [THG+22]. These publications further validate the significance and impact of our research in self-interference cancellation for wideband STAR systems.

## 5.2 Future work

The dissertation proposes a solution to design RF circuits and systems that cancel out self-interference during simultaneous transmission and reception. The research explores ways to increase isolation levels to reduce self-interference. The proposed solution consists of a two-stage circuit shown in Fig. 5.1 that incorporates a band stop filter and a self-interference cancellation filter, effectively reducing the transmission signal and preventing receiver desensitization. The proposed technique achieves a high level of coupling suppression, with an 81 dB cancellation at 2.405 GHz, as displayed in Fig. 5.2. The study opens up avenues for further research in this field.

The implementation of a power-efficient tri-stage self-interference cancellation system for in-band full-duplex (IBFD) radios is discussed in another work. IBFD radios enable simultaneous transmission and reception within the same frequency band, increasing the system's spectral efficiency. The power-efficient tri-stage self-interference cancellation system includes a circulator, band stop filter, and self-interference cancellation (SIC) filter to reduce the coupled significantly transmit

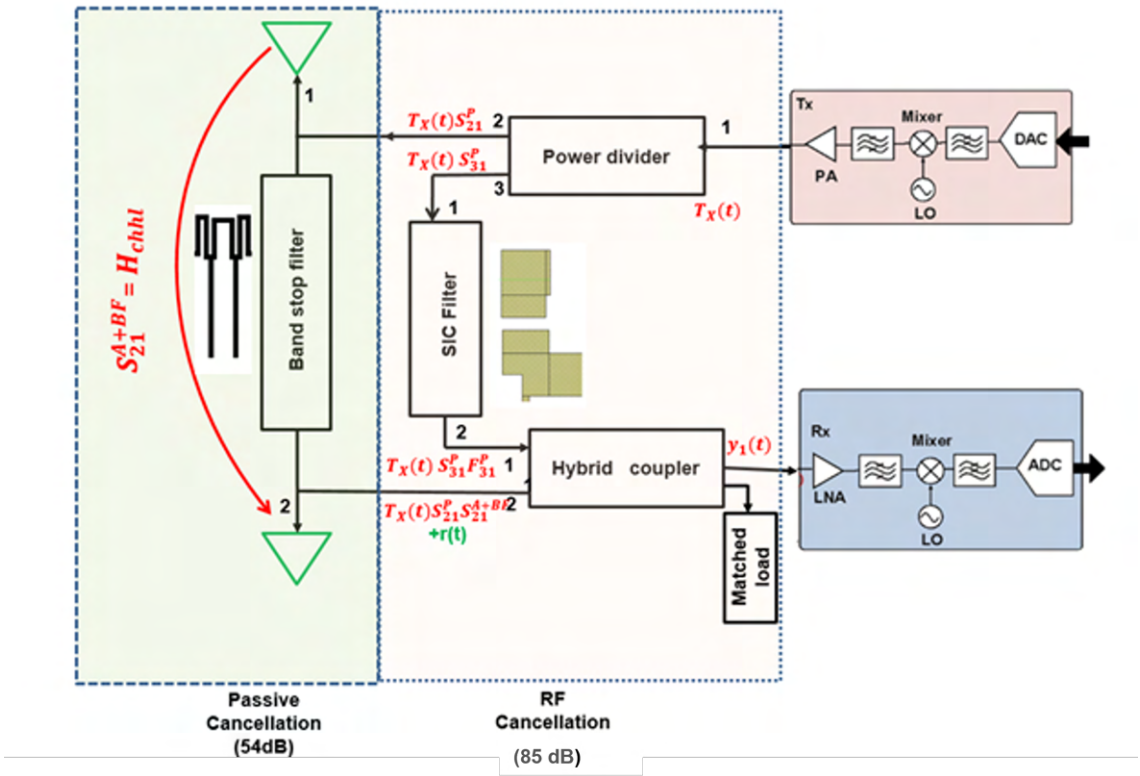


Figure 5.1: A two-stage embedded STAR system.

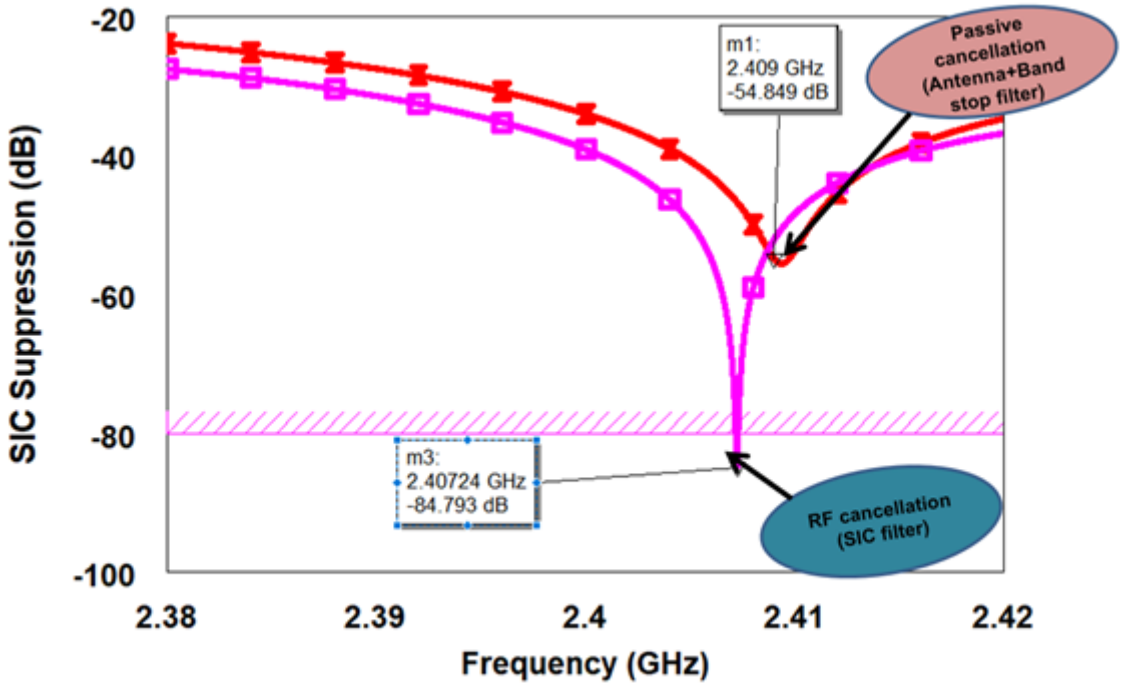


Figure 5.2: Computed SIC using the simulated results showing an average ∼85 dB cancellation at each Rx port.

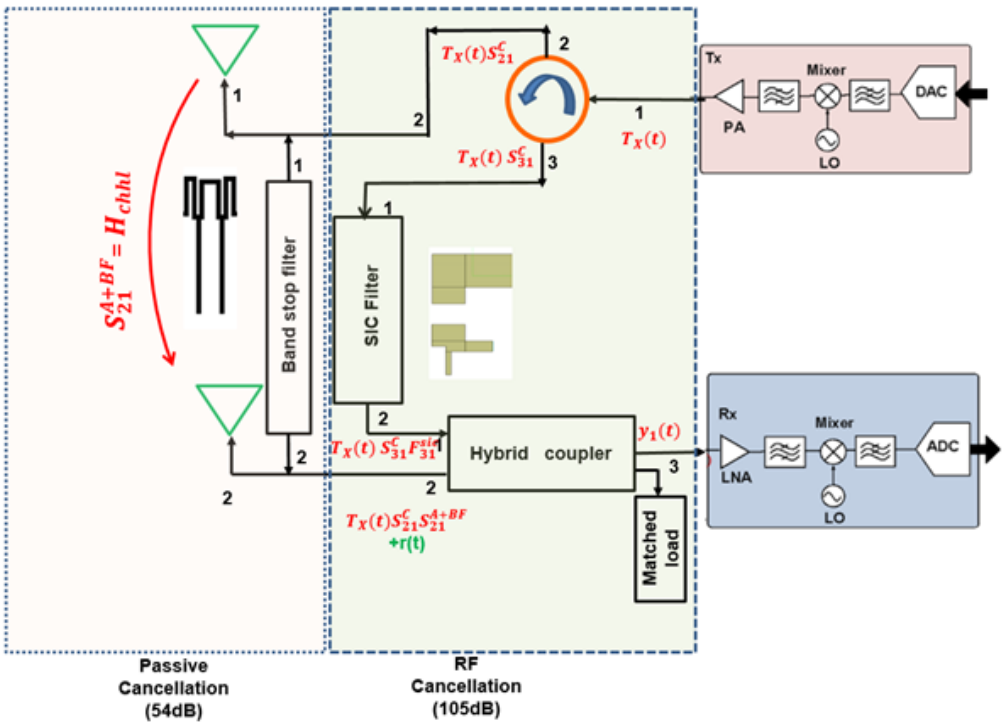


Figure 5.3: A three-stage embedded STAR system.

signal and prevent receiver desensitization, as shown in Fig. 5.3. As depicted in Fig. 5.4, this enhanced coupling suppression technique achieves 105 dB of cancellation at 2.406 GHz, making it a power-efficient solution.

Implementations of STAR systems have primarily relied on the assumption of polarization orthogonality at the antenna stage and a static environment. However, these implementations have overlooked essential factors such as array scanning mismatches, transmit noise, and multi-path reflections. Consequently, there is a pressing need to realize advanced adaptive cancellation filters that offer high tunability and reconfigurability, specifically designed to operate effectively across the frequency range of 1-6 GHz (Fig. 5.5).

To address these challenges, we will introduce tunability to reduce mutual noise coupling between adjacent elements in the array. We will incorporate tunable el-

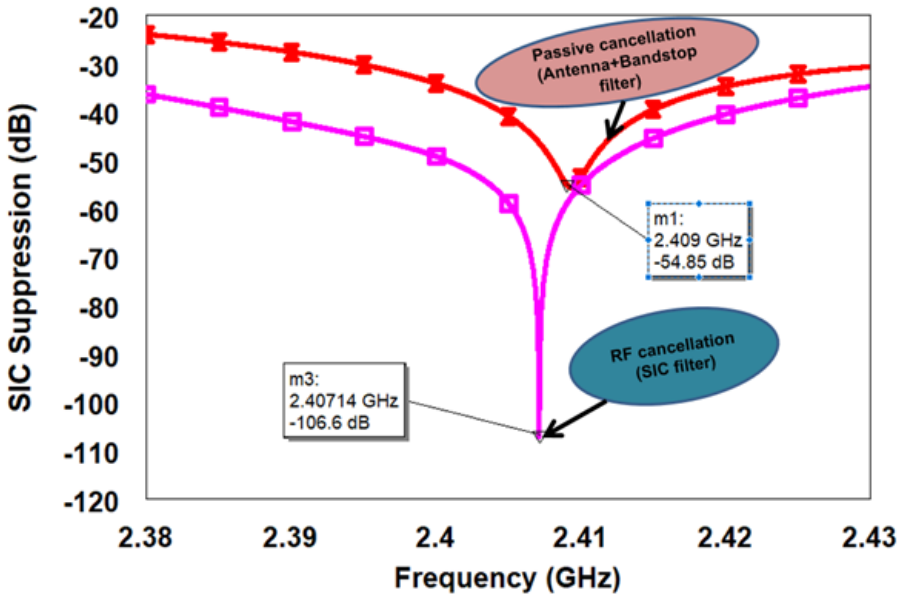


Figure 5.4: Computed SIC using the simulated results showing an average of ∼105 dB cancellation at each of Rx ports.

ements within the self-interference cancellation (SIC) filter to account for array scanning mismatches and other RF impairments. These tunable components enable dynamic adjustments to compensate for phase or amplitude mismatches that may occur in the system.

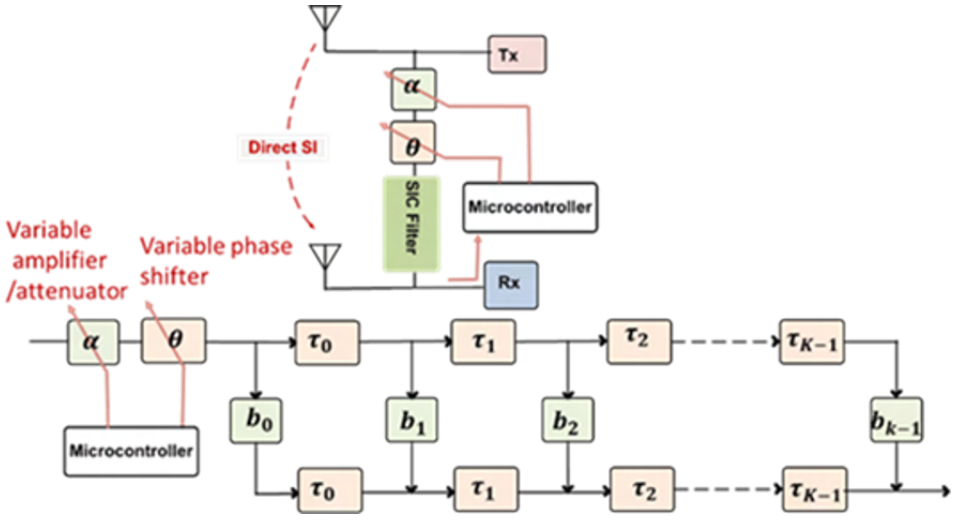


Figure 5.5: Modified RF-SIC to account for phase mismatch and amplitude scale.

# BIBLIOGRAPHY


[AHV16] Elias A Alwan, Alexander Hovsepian, and John L Volakis. Ultra-wideband dual polarization arrays with collocated elements for high isolation simultaneous transmit and receive systems. In *2016 IEEE International Symposium on Phased Array Systems and Technology (PAST)*, pages 1–3. IEEE, 2016.

[Ale19] ERNST FW Alexanderson. Simultaneous sending and receiving. *Proceedings of the Institute of Radio Engineers*, 7(4):363–378, 1919.

[BJK14] Dinesh Bharadia, Kiran Joshi, and Sachin Katti. Robust full duplex radio link. *ACM SIGCOMM Computer Communication Review*, 44(4):147–148, 2014.

[BMK13] Dinesh Bharadia, Emily McMilin, and Sachin Katti. Full duplex radios. In *Proceedings of the ACM SIGCOMM 2013 conference on SIGCOMM*, pages 375–386, 2013.

[Bra12] David Brandwood. *Fourier transforms in radar and signal processing*. Artech House, 2012.

[BVAV17] Satheesh Bojja-Venkatakrishnan, Elias A Alwan, and John L Volakis. Wideband rf and analog self-interference cancellation filter for simultaneous transmit and receive system. In *2017 IEEE International Symposium on Antennas and Propagation & USNC/URSI National Radio Science Meeting*, pages 933–934. IEEE, 2017.

[BVAV18] Satheesh Bojja-Venkatakrishnan, Elias A Alwan, and John L Volakis. Simultaneous transmit and receive system with 1 ghz rf cancellation bandwidth. In *2018 IEEE International Symposium on Antennas and Propagation & USNC/URSI National Radio Science Meeting*, pages 1241–1242. IEEE, 2018.

[CA11] Charles H Cox and Edward I Ackerman. Photonics for simultaneous transmit and receive. In *2011 IEEE MTT-S International Microwave Symposium*, pages 1–4. IEEE, 2011.

[CD12] David Carsenat and Cyril Decroze. Uwb antennas beamforming using passive time-reversal device. *IEEE Antennas and Wireless Propagation Letters*, 11:779–782, 2012.

[CHWC10] Siu K Cheung, Timothy P Halloran, William H Weedon, and Craig P Caldwell. Mmic-based quadrature hybrid quasi-circulators for simultaneous transmit and receive. *IEEE Transactions on Microwave Theory and Techniques*, 58(3):489–497, 2010.

[CJS+10] Jung Il Choi, Mayank Jain, Kannan Srinivasan, Phil Levis, and Sachin Katti. Achieving single channel, full duplex wireless communication. In *Proceedings of the sixteenth annual international conference on Mobile computing and networking*, pages 1–12, 2010.

[CKZ+18] Kun-Da Chu, Mohamad Katanbaf, Tong Zhang, Chenxin Su, and Jacques C Rudell. A broadband and deep-tx self-interference cancellation technique for full-duplex and frequency-domain-duplex transceiver applications. In *2018 IEEE International Solid-State Circuits Conference-(ISSCC)*, pages 170–172. IEEE, 2018.

[DK15] Tolga Dinc and Harish Krishnaswamy. At/r antenna pair with polarization-based reconfigurable wideband self-interference cancellation for simultaneous transmit and receive. In *2015 IEEE MTT-S International Microwave Symposium*, pages 1–4. IEEE, 2015.

[Don07] Liang Dong. Open-loop beamforming for frequency-division duplex mobile wireless access. *IEEE transactions on vehicular technology*, 56(4):1845–1849, 2007.

[DS10a] Swagatam Das and Ponnuthurai Nagaratnam Suganthan. Differential evolution: A survey of the state-of-the-art. *IEEE transactions on evolutionary computation*, 15(1):4–31, 2010.

[DS10b] Melissa Duarte and Ashutosh Sabharwal. Full-duplex wireless communications using off-the-shelf radios: Feasibility and first results. In *2010 Conference Record of the Forty Fourth Asilomar Conference on Signals, Systems and Computers*, pages 1558–1562. IEEE, 2010.

[DSPV+20] Udara De Silva, Sravan Pulipati, Satheesh Bojja Venkatakrishnan, Shubhendu Bhardwaj, and Arjuna Madanayake. A passive star microwave circuit for 1-3 ghz self-interference cancellation. In *2020 IEEE 63rd International Midwest Symposium on Circuits and Systems (MWSCAS)*, pages 105–108. IEEE, 2020.

[EEF15a] Mohamed A Elmansouri, Ehab A Etellisi, and Dejan S Filipovic. Ultra-wideband circularly-polarized simultaneous transmit and re-

ceive (star) antenna system. In *2015 IEEE International Symposium on Antennas and Propagation & USNC/URSI National Radio Science Meeting*, pages 508–509. IEEE, 2015.

[EEF15b] Ehab A Etellisi, Mohamed A Elmansouri, and Dejan S Filipovic. Wideband monostatic simultaneous transmit and receive (star) antenna. *IEEE Transactions on Antennas and Propagation*, 64(1):6–15, 2015.

[EEF16a] Ehab A. Etellisi, Mohamed A. Elmansouri, and Dejan S. Filipovic. Wideband dual-mode monostatic simultaneous transmit and receive antenna system. In *2016 IEEE International Symposium on Antennas and Propagation (APSURSI)*, pages 1821–1822, 2016.

[EEF16b] Ehab A Etellisi, Mohamed A Elmansouri, and Dejan S Filipović. Wideband simultaneous transmit and receive (star) circular array system. In *2016 IEEE International Symposium on Phased Array Systems and Technology (PAST)*, pages 1–5. IEEE, 2016.

[EEF17] Ehab A. Etellisi, Mohamed A. Elmansouri, and Dejan S. Filipović. Wideband multimode monostatic spiral antenna star subsystem. *IEEE Transactions on Antennas and Propagation*, 65(4):1845–1854, 2017.

[ENS97] Riaz Esmailzadeh, Masao Nakagawa, and Essam A Sourour. Time-division duplex cdma communications. *IEEE Personal Communications*, 4(2):51–56, 1997.

[eri] Mobile data traffic outlook. https://www.ericsson.com/en/reports-and-papers/mobility-report/dataforecasts/mobile-traffic-forecast. Accessed: 2023-01-30.

[FEB21] Dejan S Filipović, Mohamed Elmansouri, and Ljubodrag Boskovic. Full-duplex communications: Antenna story. In *2021 15th International Conference on Advanced Technologies, Systems and Services in Telecommunications (TELSIKS)*, pages 3–6. IEEE, 2021.

[GRT+19] Nimrod Ginzberg, Dror Regev, Genadiy Tsodik, Shimi Shilo, Doron Ezri, and Emanuel Cohen. A full-duplex quadrature balanced rf front end with digital pre-pa self-interference cancellation. *IEEE transactions on microwave theory and techniques*, 67(12):5257–5267, 2019.

[HAV17] Alexander Hovsepian, Elias A Alwan, and John L Volakis. Wideband scanning array of spiral antennas for simultaneous transmit and receive (star). In *2017 IEEE International Symposium on Antennas and Propagation & USNC/URSI National Radio Science Meeting*, pages 487–488. IEEE, 2017.

[HAV20] Alexander Hovsepian, Elias A Alwan, and John L Volakis. A wideband, scanning array of four-arm spiral elements for simultaneous transmit and receive. *IEEE Antennas and Wireless Propagation Letters*, 19(4):537–541, 2020.

[HBC+14] Steven Hong, Joel Brand, Jung Il Choi, Mayank Jain, Jeff Mehlman, Sachin Katti, and Philip Levis. Applications of self-interference cancellation in 5g and beyond. *IEEE Communications Magazine*, 52(2):114–121, 2014.

[HBE+21] Carlos A. Mulero Hernández, Ljubodrag B. Boskovic, Mohamed A. Elmansouri, Maxim Ignatenko, and Dejan S. Filipovic. Fixed and steerable beam dual-polarized lens antenna with high tx to rx isolation. *IEEE Transactions on Antennas and Propagation*, 69(11):7213–7221, 2021.

[HEPF17] Jaegeun Ha, Mohamed A Elmansouri, Prathap Valale Prasannakumar, and Dejan S Filipovic. Monostatic co-polarized full-duplex antenna with left-or right-hand circular polarization. *IEEE Transactions on Antennas and Propagation*, 65(10):5103–5111, 2017.

[HEVPF17] Jaegeun Ha, Mohamed A. Elmansouri, Prathap Valale Prasannakumar, and Dejan S. Filipovic. Monostatic co-polarized full-duplex antenna with left- or right-hand circular polarization. *IEEE Transactions on Antennas and Propagation*, 65(10):5103–5111, 2017.

[HHLT00] Harri Holma, Sanna Heikkinen, O-A Lehtinen, and Antti Toskala. Interference considerations for the time division duplex mode of the umts terrestrial radio access. *IEEE Journal on Selected Areas in communications*, 18(8):1386–1393, 2000.

[HSNS16] Insoo Hwang, Bongyong Song, Cong Nguyen, and Samir S Soliman. Digitally controlled analog wideband interference cancellation for indevice spectrum sharing and aggregation. *IEEE Journal on Selected Areas in Communications*, 34(11):2838–2850, 2016.

[HVAV18] Alexander Hovsepian, Satheesh Bojja Venkatakrishnan, Elias A Alwan, and John L Volakis. Wideband, scanning array for simultaneous transmit and receive. In *2018 International Applied Computational Electromagnetics Society Symposium (ACES)*, pages 1–2. IEEE, 2018.

[JCK+11] Mayank Jain, Jung Il Choi, Taemin Kim, Dinesh Bharadia, Siddharth Seth, Kannan Srinivasan, Philip Levis, Sachin Katti, and Prasun Sinha. Practical, real-time, full duplex wireless. In *Proceedings of the 17th annual international conference on Mobile computing and networking*, pages 301–312, 2011.

[JKY10] Sung-Chan Jung, Min-Su Kim, and Youngoo Yang. A reconfigurable carrier leakage canceler for uhf rfid reader front-ends. *IEEE Transactions on Circuits and Systems I: Regular Papers*, 58(1):70–76, 2010.

[KCHG00] C. Kalialakis, M.J. Cryan, P.S. Hall, and P. Gardner. Analysis and design of integrated active circulator antennas. *IEEE Transactions on Microwave Theory and Techniques*, 48(6):1017–1023, 2000.

[KFSE18] Seiran Khaledian, Farhad Farzami, Besma Smida, and Danilo Erricolo. Inherent self-interference cancellation for in-band full-duplex single-antenna systems. *IEEE Transactions on Microwave Theory and Techniques*, 66(6):2842–2850, 2018.

[KGK11a] Georg Karawas, Kavita Goverdhanam, and James Koh. Wideband active interference cancellation techniques for military applications. In *Proceedings of the 5th European Conference on Antennas and Propagation (EUCAP)*, pages 390–392, 2011.

[KGK11b] Georg Karawas, Kavita Goverdhanam, and James Koh. Wideband active interference cancellation techniques for military applications. In *Proceedings of the 5th European Conference on Antennas and Propagation (EUCAP)*, pages 390–392, 2011.

[KHFP12] KE Kolodziej, PT Hurst, AJ Fenn, and LI Parad. Ring array antenna with optimized beamformer for simultaneous transmit and receive. In *Proceedings of the 2012 IEEE International Symposium on Antennas and Propagation*, pages 1–2. IEEE, 2012.

[KMP16] Kenneth E Kolodziej, Joseph G McMichael, and Bradley T Perry. Multitap rf canceller for in-band full-duplex wireless communications.

*IEEE Transactions on Wireless Communications*, 15(6):4321–4334, 2016.

[Kno12] Michael E Knox. Single antenna full duplex communications using a common carrier. In *WAMICON 2012 IEEE Wireless & Microwave Technology Conference*, pages 1–6. IEEE, 2012.

[KPH19] Kenneth E Kolodziej, Bradley T Perry, and Jeffrey S Herd. In-band full-duplex technology: Techniques and systems survey. *IEEE Transactions on Microwave Theory and Techniques*, 67(7):3025–3041, 2019.

[Lar14] Lawrence Larson. Rf and microwave hardware challenges for future radio spectrum access. *Proceedings of the IEEE*, 102(3):321–333, 2014.

[LBMH14] Leo Laughlin, Mark A Beach, Kevin A Morris, and John L Haine. Optimum single antenna full duplex using hybrid junctions. *IEEE Journal on Selected Areas in Communications*, 32(9):1653–1661, 2014.

[LGL11] Haitao Liu, Steven Gao, and Tian Hong Loh. Compact dual-band antenna with electronic beam-steering and beamforming capability. *IEEE Antennas and Wireless Propagation Letters*, 10:1349–1352, 2011.

[LM15] Donghyun Lee and Byung-Wook Min. 1-tx and 2-rx in-band full-duplex radio front-end with 60 db self-interference cancellation. In *2015 IEEE MTT-S International Microwave Symposium*, pages 1–4. IEEE, 2015.

[LSYB17] Ruina Lian, Ting-Yen Shih, Yingzeng Yin, and Nader Behdad. A high-isolation, ultra-wideband simultaneous transmit and receive antenna with monopole-like radiation characteristics. *IEEE Transactions on Antennas and Propagation*, 66(2):1002–1007, 2017.

[LYJ+15] Gang Liu, F Richard Yu, Hong Ji, Victor CM Leung, and Xi Li. In-band full-duplex relaying: A survey, research issues and challenges. *IEEE Communications Surveys & Tutorials*, 17(2):500–524, 2015.

[MDTE20] Mohammed Mahdi, Mohammad Darwish, Hossam Tork, and Ayman A Eltager. Balun based transmitter leakage cancellation for wide-band applications. In *2020 12th International Conference on Electrical Engineering (ICEENG)*, pages 254–257. IEEE, 2020.

[MvLC+14] Mina Mikhael, Barend van Liempd, Jan Craninckx, Rafik Guindi, and Björn Debaillie. An in-band full-duplex transceiver prototype with an in-system automated tuning for rf self-interference cancellation. In *1st International conference on 5G for ubiquitous connectivity*, pages 110–115. IEEE, 2014.

[nag] Realm of wireless rf communication - all you need to know. https://www.nagarro.com/en/blog/wireless-rf-communication. Accessed: 2023-01-30.

[NGA+21] Aravind Nagulu, Aditya Gaonkar, Sohail Ahasan, Sasank Garikapati, Tingjun Chen, Gil Zussman, and Harish Krishnaswamy. A full-duplex receiver with true-time-delay cancelers based on switched-capacitor-networks operating beyond the delay–bandwidth limit. *IEEE Journal of Solid-State Circuits*, 56(5):1398–1411, 2021.

[PEF17] Prathap Valale Prasannakumar, Mohamed A Elmansouri, and Dejan S Filipovic. Wideband decoupling techniques for dual-polarized bi-static simultaneous transmit and receive antenna subsystem. *IEEE Transactions on Antennas and Propagation*, 65(10):4991–5001, 2017.

[PS98] Haralabos C Papadopoulos and C-EW Sundberg. Reduction of mixed cochannel interference in microcellular shared time-division duplexing (stdd) systems. *IEEE transactions on vehicular technology*, 47(3):842–855, 1998.

[RBVV21] Md Rakibur Rahman, Satheesh Bojja-Venkatakrishnan, and John L Volakis. Ultra-wideband rf self interference cancellation filter for star radios. In *2021 IEEE International Symposium on Antennas and Propagation and USNC-URSI Radio Science Meeting (APS/URSI)*, pages 523–524. IEEE, 2021.

[SAF17] Aman Samaiyar, Ahmed H. Abdelrahman, and Dejan S. Filipovic. Simultaneous transmit and receive reflectarray antennas on low cost uav platforms. In *2017 IEEE International Symposium on Antennas and Propagation USNC/URSI National Radio Science Meeting*, pages 2047–2048, 2017.

[sam] Next generation communications. https://research.samsung.com/next-generation-communications. Accessed: 2022-10-30.

[SBL+17] Shree Krishna Sharma, Tadilo Endeshaw Bogale, Long Bao Le, Symeon Chatzinotas, Xianbin Wang, and Björn Ottersten. Dynamic spectrum sharing in 5g wireless networks with full-duplex technology: Recent advances and research challenges. *IEEE Communications Surveys & Tutorials*, 20(1):674–707, 2017.

[SGE17] Nirmal V Shende, Özgür Gürbüz, and Elza Erkip. Half-duplex or full-duplex communications: Degrees of freedom analysis under self-interference. *IEEE Transactions on Wireless Communications*, 17(2):1081–1093, 2017.

[SO89] Ronald William Schafer and Alan V Oppenheim. *Discrete-time signal processing*, volume 5. Prentice Hall Englewood Cliffs, NJ, 1989.

[SSE+20] D-C Son, A Samaiyar, M Elmansouri, D Filipovic, and P Valale Prasannakumar. Phased array antenna for bi-static simultaneous transmit and receive (star) system. In *2020 IEEE International Symposium on Antennas and Propagation and North American Radio Science Meeting*, pages 173–174. IEEE, 2020.

[SSG+14] Ashutosh Sabharwal, Philip Schniter, Dongning Guo, Daniel W Bliss, Sampath Rangarajan, and Risto Wichman. In-band full-duplex wireless: Challenges and opportunities. *IEEE Journal on selected areas in communications*, 32(9):1637–1652, 2014.

[sta] Mobile communications - statistics facts. https://www.statista.com/topics/1147/mobile-communications/topicOverview. Accessed: 2023-01-30.

[SVL+16] Sung-Min Sohn, J Thomas Vaughan, Russell L Lagore, Michael Garwood, and Djaudat Idiyatullin. In vivo mr imaging with simultaneous rf transmission and reception. *Magnetic resonance in medicine*, 76(6):1932–1938, 2016.

[SWA+15] Kevin L Scherer, Stephen J Watt, Elias A Alwan, Abe A Akhiyat, Brian Dupaix, Waleed Khalil, and John L Volakis. Simultaneous transmit and receive system architecture with four stages of cancellation. In *2015 IEEE International Symposium on Antennas and Propagation & USNC/URSI National Radio Science Meeting*, pages 520–521. IEEE, 2015.

[TA22] Md Nurul A. Tarek and Elias A. Alwan. Wideband, low profile coupling suppression circuit for simultaneous transmit and receive system based on hybrid finite impulse response and resonator topology. *IEEE Access*, 10:126508–126515, 2022.

[TGN+23] Md Nurul Anwar Tarek, Marisol Roman Guerra, Anthony Nunez, MD Nazim Uddin, and Elias A. Alwan. Improving isolation in monostatic simultaneous transmit and receive systems using a quasi-symmetrical self-interference cancellation architecture. *IEEE Journal of Microwaves*, 3(2):655–664, 2023.

[THG+22] Md Nurul Anwar Tarek, Rimon Hokayem, Sandhiya Reddy Govindarajulu, Markus H Novak, and Elias A Alwan. A two-stage wideband rf cancellation of coupled transmit signal for bi-static simultaneous transmit and receive system. *IEEE Journal of Microwaves*, 2(3):429–441, 2022.

[TNA20] Md Nurul Anwar Tarek, Markus Novak, and Elias A Alwan. Rf coupling suppression circuit for simultaneous transmit and receive systems. In *2020 IEEE International Symposium on Antennas and Propagation and North American Radio Science Meeting*, pages 1833–1834. IEEE, 2020.

[TRA21] Md Nurul Anwar Tarek, Marisol Roman, and Elias A Alwan. Power efficient rf self-interference cancellation system for simultaneous transmit and receive. In *2021 IEEE International Symposium on Antennas and Propagation and USNC-URSI Radio Science Meeting (APS/URSI)*, pages 113–114. IEEE, 2021.

[UC20] Md Nazim Uddin and Sangjo Choi. Non-uniformly powered and spaced corporate feeding power divider for high-gain beam with low sll in millimeter-wave antenna array. *Sensors*, 20(17):4753, 2020.

[VAV18] Satheesh Bojja Venkatakrishnan, Elias A Alwan, and John L Volakis. Wideband rf self-interference cancellation circuit for phased array simultaneous transmit and receive systems. *IEEE Access*, 6:3425–3432, 2018.

[VHAV19] Satheesh Bojja Venkatakrishnan, Alexander Hovsepian, Elias A Alwan, and John L Volakis. Rf cancellation of coupled transmit signal and noise in star across 1 ghz bandwidth. In *2019 URSI International*

*Symposium on Electromagnetic Theory (EMTS)*, pages 1–4. IEEE, 2019.

[vNDRB+03] Line van Nieuwstadt, Roger De Roo, David Boprie, Ron Rizor, Peter Hansen, Anthony W England, Hanh Pham, and Boon Lim. A compact direct detection receiver for l-band star radiometry. In *IEEE MTT-S International Microwave Symposium Digest, 2003*, volume 1, pages 563–566. IEEE, 2003.

[WAKV15] Stephen J Watt, Elias A Alwan, Waleed Khalil, and John L Volakis. Wideband self-interference cancellation filter for simultaneous transmit and receive systems. In *2015 IEEE International Symposium on Antennas and Propagation & USNC/URSI National Radio Science Meeting*, pages 129–130. IEEE, 2015.

[WC12] Andrew T. Wegener and William J. Chappell. Simultaneous transmit and receive with a small planar array. In *2012 IEEE/MTT-S International Microwave Symposium Digest*, pages 1–3, 2012.

[Weg14] Andrew T Wegener. Broadband near-field filters for simultaneous transmit and receive in a small two-dimensional array. In *2014 IEEE MTT-S International Microwave Symposium (IMS2014)*, pages 1–3. IEEE, 2014.

[WJAM17] Wang Wei, Wang Jing, Liu Aimeng, and Guo Meng. Design of 2 by 2 dual-polarized antenna array with high isolation, wideband and low cross polarization. In *2017 IEEE International Symposium on Antennas and Propagation & USNC/URSI National Radio Science Meeting*, pages 2161–2162. IEEE, 2017.

[WLK11] Lu Wang, Yee Hui Lee, and Wee Jin Koh. Generic prediction equation of both the in-band and out-of-band resonant frequencies of l-band and s band blade antennae. In *10th International Symposium on Electromagnetic Compatibility*, pages 824–828. IEEE, 2011.

[WLX+22] Di Wu, Ruina Lian, Bing Xiao, Bo Wang, Min Li, Yujiang Wu, and Kwan Lawrence Yeung. Wideband co-polarized antenna system for in-band full-duplex applications. In *2022 16th European Conference on Antennas and Propagation (EuCAP)*, pages 1–4. IEEE, 2022.

[WSWL20] Di Wu, Yu-Xiang Sun, Bo Wang, and Ruina Lian. A compact, monostatic, co-circularly polarized simultaneous transmit and receive (star)

antenna with high isolation. *IEEE Antennas and Wireless Propagation Letters*, 19(7):1127–1131, 2020.

[YF21] Songyi Yen and Dejan S. Filipović. Design of helical antennas for full-duplex communication systems. In *2021 IEEE-APS Topical Conference on Antennas and Propagation in Wireless Communications (APWC)*, pages 062–062, 2021.

[ZCDK15] Jin Zhou, Tsung-Hao Chuang, Tolga Dinc, and Harish Krishnaswamy. Integrated wideband self-interference cancellation in the rf domain for fdd and full-duplex wireless. *IEEE Journal of solid-state circuits*, 50(12):3015–3031, 2015.

[ZL19] Yi-Ming Zhang and Jia-Lin Li. Differential-series-fed dual-polarized traveling-wave array for full-duplex applications. *IEEE Transactions on Antennas and Propagation*, 68(5):4097–4102, 2019.

[ZNSR17] Tong Zhang, Ali Najafi, Chenxin Su, and Jacques C Rudell. 18.1 a 1.7-to-2.2 ghz full-duplex transceiver system with¿ 50db self-interference cancellation over 42mhz bandwidth. In *2017 IEEE International Solid-State Circuits Conference (ISSCC)*, pages 314–315. IEEE, 2017.

# VITA

## MD NURUL ANWAR TAREK

| | |
|---|---|
| September 25, 1989 | Chandpur, Bangladesh |
| 2002 | Junior School Certificate Scholarship, Bangladesh |
| 2007 | Higher Secondary School Certificate Scholarship, Bangladesh |
| 2013 | B.S., Electrical and Electronic Engineering<br>Chittagong University of Engineering and Technology Chittagong, Bangladesh |
| March 2013 - Aug 2016 | Lecturer<br>Department of Electrical<br>and Electronics Engineering<br>International Islamic University Chittagong<br>Chattogram, Bangladesh |
| Aug 2016 - May 2018 | Graduate Assistant<br>Georgia Southern University<br>Statesboro, Gerogia |
| Aug 2017 - May 2018 | Lead Instructor (Teaching Assistant 2)<br>Department of Electrical<br>and Computer Engineering<br>Georgia Southern University<br>Statesboro, Gerogia |
| 2018 | M.S., Applied Engineering (Electrical)<br>Georgia Southern University<br>Statesboro, Georgia |
| August 2018-December 2020 | Project Title: Same Frequency Simultaneous Transmit and Receive Radio (PI: Dr. Markus Novak, Co-PI: Dr. Elias Alwan) Funding Source: Novaa Ltd. |
| Aug 2018- June 2023 | Graduate Research Assistant<br>Smart millimeter Wave and RF Technologies (SmARTech) Lab<br>Florida International University<br>Miami, Florida |

| | |
|---|---|
| October 2018 - September 2021 | Project Title: A Multi-Stage Wideband RF Cancellation of Coupled Transmit Signal for Simultaneous Transmit and Receive System (PI: Dr. Markus Novak) Funding Source: U.S. Army Research Laboratory and the Army SBIR Program Office under Contract No. W911QX-18P-0186 |
| 2019 | Graduate Professional Student Committee (GPSC) travel fund, Florida International University, 2020 Bangladesh-Sweden Trust Fund |
| March 2020 - February 2025 | Project Title: Next Generation Universal Radio Platform with On-Demand Operation across UHF to Sub-Terahertz Bands (PI: Dr. Elias Alwan) Funding Source: National Science Foundation (NSF), USA. |
| 2022 | M.S., Electrical Engineering Florida International University Miami, Florida |
| 2022 | National Radio Science meeting travel fund, USA |
| May 2022 - Aug 2022 | Antenna Engineer Intern Garmin International Olathe, Kansas |
| 2023 | Student life award, Top five Finalist, Florida International University |

## AREA OF INTEREST

| | | |
|---|---|---|
| Antenna Design | RF circuit Design | RF system Design |
| Bulk Acoustic Filter | Full Duplex System | Electrical Impedance Myography |

## TECHNICAL SKILL

| | | |
|---|---|---|
| HFSS | Cadence AWR | ADS |
| Vector Network Analyser | Spectrum Analyser | COMSOL |

## PUBLICATIONS AND PRESENTATIONS

M. N. A. Tarek, R. Hokayem, S. R. Govindarajulu, M. H. Novak and E. A. Alwan, (2022). *A Two-Stage Wideband RF Cancellation of Coupled Transmit Signal for Bi-Static Simultaneous Transmit and Receive System.* IEEE Journal of Microwaves, vol. 2, no. 3, pp. 429-441.